CR 86311

SCR 290 I

FINAL REPORT
FOR THE STUDY OF
SIMPLIFIED NAVIGATION
and
GUIDANCE SCHEMES

CONTRACT NAS 12-40

VOLUME I - TECHNICAL ANALYSIS

N70-16787
(ACCESSION NUMBER)
139
(PAGES)
NASA-CR-86311
(NASA CR OR TMX OR AD NUMBER)
(THRU)
1
(CODE)
(CATEGORY)
21
FACILITY FORM 602

JAN 1970
RECEIVED
NASA STI FACILITY
INPUT BRANCH

United Aircraft Corporate Systems Center
DIVISION OF UNITED AIRCRAFT CORPORATION
FARMINGTON, CONNECTICUT 06032

Reproduced by the
CLEARINGHOUSE
for Federal Scientific & Technical
Information Springfield Va. 22151

SCR 290-I

FINAL REPORT

STUDY OF SIMPLIFIED NAVIGATION AND GUIDANCE SCHEMES

VOLUME I - TECHNICAL ANALYSIS

Reported by:
G. K. White

Approved by:
R. M. Grose
Chief, Systems Studies

Manoni
L. R. Manoni
Manager, Advanced Programs

UNITED AIRCRAFT
CORPORATE SYSTEMS CENTER
Division of United Aircraft Corporation
Farmington, Connecticut
October 31, 1966

FOREWORD

The work described in this report was performed by United Aircraft Corporate Systems Center for NASA Electronics Research Center as partial fulfillment of Contract No. NAS 12-40.

TABLE OF CONTENTS

Section Page

I SUMMARY 1

II INTRODUCTION 4

III REFERENCE TRAJECTORY 6

IV NAVIGATION 15

A. Navigation Schemes 15
B. Performance Evaluation 25
C. Navigation Requirements 43

V GUIDANCE 46

A. Guidance Schemes 46
B. Comparison 49

VI COST FACTOR STUDIES 51

A. Summary of Example System 52
B. Operational Description 53
C. Functional Description 54
D. System Accuracy 59
E. System Reliability 59
F. System Mechanization 63
G. System Trade-Off and Areas for Further Investigation . . . 78

APPENDICES:

A Trajectory Analysis and Selection for Jupiter Swing-by Mission; Scientific Report No. 1 . . . . ff 81

B Navigation Analysis

C Guidance Analysis

LIST OF ILLUSTRATIONS

Figure		Page
1	Planetary Coordinate Frames	9
2	Integration Analysis, Effect of Integration Step Size on Time History of Semi-Major Axis, Earth's Sphere of Influence	13
3	Integration Analysis, Effect of Integration Step Size on Time History of Semi-Major Axis, Sun's Sphere of Influence	14
4	ISN Coordinate Systems	16
5	Interplanetary Space Navigation Scheme	18
6	Linear Optimum Filter Navigation Scheme	21
7	Interplanetary Space Navigation Scheme Control Loops . . .	27
8	ISN Performance, Two-Body Simulation, Position Errors vs Time	29
9	ISN Performance, Two-Body Simulation, Velocity Errors vs Time	30
10	ISN Performance, N-Body Simulation, Position Errors vs Time	31
11	ISN Performance, N-Body Simulation, Velocity Errors vs Time	32
12	LOF Navigation Scheme, σ_X Position Accuracy as a Function of Time	34
13	LOF Navigation Scheme, σ_Y Position Accuracy as a Function of Time	35
14	LOF Navigation Scheme, σ_Z Position Accuracy as a Function of Time	36
15	LOF Navigation Scheme, σ_{V_X} Velocity Accuracy as a Function of Time	37
16	LOF Navigation Scheme, σ_{V_Y} Velocity Accuracy as a Function of Time	38
17	LOF Navigation Scheme, σ_{V_Z} Velocity Accuracy as a Function of Time	39
18	LOF Navigation Performance, N-Body, Position Accuracy as a Function of Time	41
19	LOF Navigation Performance, N-Body, Velocity Accuracy as a Function of Time	42
20	Error in Inclination of Final Heliocentric Orbit as a Function of Observation Accuracy	44
21	Error in Semi-Latus Rectum of Final Heliocentric Orbit as a Function of Observation Accuracy	45

LIST OF ILLUSTRATIONS (Cont'd)

Figure Page

22 Guidance Schemes, Explicit and Self-Contained 47
23 Deep Space Navigation Scheme, Functional Flow Diagram . . . 58
24 Deep Space Navigation Scheme, Probability of Survival, Continuous Operation 62
25 Deep Space Navigation Scheme, Probability of Survival, Intermittent Operation 64
26 Star/Planet Sensor Measurement Accuracy vs Subtended Angle of Planet 68
27 100-500-Watt Electric Power System, Weight vs Mission Time . 75
28 Jupiter Swing-by Vehicle Temperature 77

LIST OF TABLES

Table Page

I Trajectory Characteristics 8
II Transition Matrices Relating State Errors at t_i to State Errors at t_j 10
III Final Orbital Elements, Sensitivity Coefficients 11
IV Computer Word Count 22
V Injection Conditions 24
VI Planet Observation Schedule 26
VII Comparison of Guidance Correction Schemes 50
VIII Schedule of Operational Counts 55
IX Deep Space Navigation Scheme (DSNS) Error Budget 60
X Deep Space Navigation Scheme (DSNS) Instrument Reliability . . 61
XI Physical Characteristics 66
XII Jupiter Swing-by Spacecraft Characteristics 72
XIII Total On-Board Propellant Requirements 74

I. SUMMARY

A study of the Navigation and Guidance requirements associated with a Jupiter Swing-by Mission has been conducted by the United Aircraft Corporate Systems Center. The specific mission studied is that of a solar probe injected into a final heliocentric orbit normal to the ecliptic and having a semi-latus rectum of one astronomical unit (AU). This is representative of a Saturn IB/Kick Stage Mission. It is accomplished by a close encounter with Jupiter in which Jupiter's gravitational potential deflects the vehicle into the desired post-encounter heliocentric orbit. To inject a solar probe directly from the Earth into a similar position over the Sun would require almost three times the energy of that of the Jupiter Swing-by Mission.

The results of this study show that there are no fundamental restrictions to this type of mission. Energy constraints of presently envisioned boosters do, however, impose limitations on the eccentricity or semi-major axis of the post-encounter heliocentric orbit. The selected orbit having a semi-latus rectum of one astronomical unit is in the region of the highest energy orbit presently obtainable for the assumed payload weight typical of the Kick Stage vehicle of 2000 pounds at Earth injection.

Two navigation schemes were investigated employing on-board, optical-inertial guidance systems. Radio command systems were not considered in this study; however, they may have application to the boost and injection and midcourse phases close to the Earth. The optical inertial system will have advantages in the vicinity of Jupiter. The optical inertial system is considered to be operated intermittently. The assumed schedule specifies operation every 6 days for the initial 86 days and every 10 days thereafter until entry into Jupiter's sphere of influence at 437 days. During each period of operation the inertial reference is established and a pair of planet sightings are taken to provide information to bound the on-board navigational computations. The two navigation schemes consisted of a simplified space navigation scheme and the linear optimum filter scheme of NASA TR R-135. The simplified space navigation scheme studied was an extension of a navigation scheme developed for precise self-contained orbital navigation. As extended in this program for interplanetary space navigation, it is designated the ISN.

The primary advantage envisioned of the simplified space navigation scheme over that of the linear optimum filter (LOF) is simplicity of computation with comparable performance. As mechanized for these studies, the ISN requires 3,296 words of computer storage versus 4,106 words for the LOF. When all navigational functions including erection from a dormant state, sensor compensation and data processing, attitude computation, etc. are considered, the relative comparison between the ISN and the LOF is 6,162 words versus 6,972 words. Thus the gross difference is a little more than 10 percent.

Computer simulations of these navigation schemes were formulated (see SCR 290, Volume II - Simulation Documentation) and used to evaluate their relative performance. ISN mechanization yielded relatively poor performance due to the dynamic characteristics of the fundamental ISN filter loops. In practice, it is an oscillator tuned to orbital

frequency with compensation for eccentricity and other anomalies of the gravitational potential incorporated into the forward loop of the filters. No set of ISN loop gains provided good stable performance; however, the linear optimum filters provided bounded performance proportional to the magnitude of the observational error. The basic sensitivity of the final orbital elements to observational accuracy as established for a typical observational schedule are:

Parameter	Error Sensitivity
Inclination	1.05×10^{-4} rad/arc sec
Semi-latus Rectum	0.36×10^{-4} AU/arc sec

With the inclination in radians, a direct comparison between cross-range and altitude errors is possible for a point in the vicinity of the semi-latus rectum equal to unity. This indicates that the inclination is approximately three times more sensitive to observational errors than is the semi-latus rectum.

Explicit on-board guidance schemes were also evaluated as part of this work to determine the feasibility of such techniques. Much of the mathematical logic employed for navigation may also be used to implement explicit guidance, thus there is only a small increase in computer storage requirements. The most significant effect of including the explicit guidance is the increase in computer utilization to perform the guidance computations; however, this is in the order of an additional hour of computer operation for the typical mission. A midcourse guidance scheme as well as a scheme having a terminal guidance correction at entry into Jupiter's sphere of influence were simulated.

The results summarized below indicate that both guidance schemes are effective in guiding the vehicle to the desired orbit (90-degree inclination, 1 AU semi-latus rectum). With no corrections the final heliocentric orbital elements would have an inclination of 44.8 degrees and semi-latus rectum of 0.22 AU.

	Errors		
Guidance Correction	Inclination, Rad	Semi-Latus, AU	V Req m/s
4 Midcourse	2.63 deg	- .280	122.518
4 Midcourse plus Terminal	4.19 deg	.366	174.134
Terminal	1.63 deg	.105	384.752

In these studies it was found that the performance of the guidance scheme appears to be dependent on the magnitude of perijove. This dependence explains the fact that the performance of the midcourse plus terminal correction case is worse than that of the midcourse case, and why the case with only terminal correction yields the best performance. The relative effectiveness appears to be overshadowed by the effects of the variations of perijove for the various trajectories. Development of both of these schemes warrants further study.

A preliminary operational study was conducted to formulate the operational procedures and a guidance system configuration that would demonstrate the feasibility of mechanizing an on-board optical-inertial guidance system with present technology and hardware. The guidance system consisted of the strapdown inertial measurement unit being developed by United Aircraft Corporate Systems Center, and the flight computer design based on current technology of integrated circuits. The following is a summary of the characteristics of this system:

Weight = 34.7 kilograms

Power = 163 watts

Probability of Mission Success = 0.976

The probability of mission success is based on an operational time of 100 hours in the intermittent operation previously described. Consideration of the total energy requirements including electrical power and propellant for guidance and control of this mission was conservatively estimated to increase the weight of the system by 103.2 and 344.7 kilograms, respectively. It is obvious that the weight of the guidance system components is small and that optimization of the system should consider all possible means of reducing the total energy requirements. The observational accuracy of this equipment is estimated to be 28 arc seconds, which results in a terminal mission accuracy at one AU over the Sun of 0.00296 radians in inclination and 0.00102 AU in semi-latus rectum.

This study has shown that on-board navigation and guidance systems that employ present technology and hardware are feasible for such missions as the Jupiter Swingby. However, only a single example case has been studied along with some of the system trade-offs possible. Further study is necessary to optimize the operational procedure and to specify the guidance system hardware requirement for the Kick Stage vehicle for this mission.

II. INTRODUCTION

As man plans more extensive missions that penetrate deeper into space, the concepts of navigation and guidance must be reevaluated. The current radio command system is presently adequate for launches in which the guidance and control functions are performed relatively close to Earth. However, for missions in which the guidance and control functions must be performed at several astronomical units away from Earth, and where a close encounter with a planet is involved, an on-board guidance and control system may have specific advantages with regard to accuracy, response time, and communication requirements.

As an initial step in evaluating the navigation and guidance requirements for the Advanced Kick Stage, an analytical study of self-contained on-board navigation and guidance schemes was undertaken. This study was conducted by the United Aircraft Corporate Systems Center (UACSC) for NASA/ERC under contract NAS 12-40. The objectives of this study were to evaluate explicit on-board navigation and guidance schemes and to establish the feasibility of mechanizing these schemes with existing hardware and technology.

For this study, a typical Jupiter Swing-by Mission was assumed. The mission profile consists of injection of the vehicle from an Earth orbit into a heliocentric transfer orbit providing a close encounter with Jupiter. The entry into the sphere of influence of Jupiter is such that the vehicle is deflected by Jupiter's gravity potential into a final heliocentric orbit whose plane is normal to the ecliptic. The characteristics of the orbit within this plane are dependent on the velocity vector relative to the Sun at exit from Jupiter's sphere of influence.

The navigation and guidance concepts and hardware technology employed in this study are based on simplified navigation and guidance concepts for advanced satellite vehicles and strapdown optical inertial guidance systems developed by UACSC. The simplified satellite navigation concept developed previously has been shown to provide performance equal to that of the linear optimum filter mechanization such as the Kalman filter, yet provides relative simplicity of computer mechanization. The most advanced strapdown hardware technology of both inertial and optical sensors as developed at UACSC over the past seven years has been employed in this study. This includes the application of the inertial sensor package being delivered to NASA under the LEM/ASA Apollo program and a star and planet sensor of a type that UACSC has built and tested three models of in the laboratory under simulated space environments. Advanced design and packaging techniques of integrated circuits as developed at UACSC as part of its guidance program were employed to evaluate the computer characteristics. These techniques are compatible with present state of the art computer technology.

This study effort extended and developed the simplified satellite navigation scheme for application to interplanetary space navigation. In this scheme, line of sight observational data relative to inertial space is acquired and processed in a scheduled manner to bound the navigational computation. The linear optimum filter was also mechanized to process the same observational data, thus providing a means of evaluating the relative complexity and performance of the two data processing schemes. Both schemes were mechanized in the computer simulations described in SCR 290, Volume II - Simulation Documentation, and their relative performance evaluated for a given reference trajectory and observational schedule.

Current guidance schemes are generally mechanized with perturbative techniques that require precomputation of reference trajectories and storage of considerable data in the flight computer. This technique limits operational flexibility. With navigational logic on-board, the mechanization of explicit guidance concepts becomes relatively simple. Thus the reference trajectory can be computed as required each time a guidance computation is to be made. This increases the computer utilization by a relatively small amount for the long duration mission, which employs only several guidance corrections. In this study, an explicit guidance concept was evaluated to determine if further study of explicit guidance appears warranted.

A cost study in terms of the trade-offs in operational procedures and hardware mechanization for the navigation and guidance scheme evaluated was conducted on the basis of existing technology and hardware. Weight, power, and reliability estimates were estimated and design trade-offs were evaluated. From these studies, the feasibility of employing a self-contained on-board optical-inertial guidance system has been established without consideration of the optimization of the design.

This report presents the results of these studies. The reference trajectory is described in Section III and the navigation and guidance studies are described in Sections IV and V, respectively. Section VI presents the results of the cost studies in terms of operational and hardware trade-offs. Supporting analytical data is presented in Appendices A, B, and C. Volume II of this report presents information for use with the computer simulation program delivered to NASA/ERC as part of this contract. The information in Volume II provides a complete description of these programs as well as the basic input-output format and operational procedures.

III. REFERENCE TRAJECTORY

The primary objectives of the study were the determination of the navigation and guidance requirements for the kick stage vehicle and the evaluation of a simplified navigation and guidance scheme applied to a given interplanetary mission. The first task conducted under the contract was a preliminary mission analysis. The objective of this initial task was to define the mission spectrum and the selection of a typical trajectory for the navigation study on the basis of nominal propulsion limitations and navigation sensitivities. The mission proposed by NASA was an out-of-the-ecliptic solar probe achieved by a swing-by of Jupiter. The desired results are obtained by injecting the vehicle into a trajectory, approximately in the ecliptic plane which enters Jupiter's sphere of influence with its position and velocity relative to Jupiter such that the post-encounter heliocentric portion of the trajectory lies in a plane with an inclination to the ecliptic plane of ninety degrees and has a semi-latus rectum of one astronomical unit.

The analysis that led to the selection of the reference trajectory was reported in Scientific Report No. 1 and is included in this report as Appendix A. The preliminary analysis used a patched conic approach using two-body Keplerian equations within the various spheres of influence of the Earth, Sun, and Jupiter. Once the launch date, approximate initial conditions, and the general characteristics of the trajectory were determined using the data reported in Appendix A, a definitive reference trajectory was computed using the UACSC N-Body program.

The N-Body program is a double precision Cowell integration written in FORTRAN IV for use on the IBM 7094. The N-Body model is a three-dimensional system with the planets in elliptic, non-coplanar orbits. The bodies included are the Sun, Earth, Moon, Mars, and Jupiter and its four major satellites. The user has a choice of two numerical integration techniques, fourth order Runge-Kutta or an Adams four-point with a variable step size and automatic error control. A transition matrix subroutine is also included in the program for use in determining sensitivity coefficients. As there are no closed form solutions for the N-Body program, the definitive trajectory was obtained by an iterative procedure. The initial conditions from the patched conic solution were perturbed until the desired post-encounter trajectory was obtained. For the purposes of the study it was not felt necessary to carry the iteration to the point of getting exactly a 90-degree angle of inclination and a semi-latus rectum of 1 astronomical unit.

The result of the trajectory analysis was the selection of a reference trajectory with a launch date of April 3, 1972 and with a final heliocentric portion which has an angle of inclination of 89.66 degrees to the ecliptic plane and a semi-latus rectum of 1.05 astronomical units. The flight time from injection through Jupiter's sphere of influence is 511.6 days while the total flight time from injection to semi-latus rectum is 1306.3 days (3.58 years). The magnitude of the injection velocity relative to the

Earth is 15,935 meters per second. If it is assumed that the vehicle is injected from a 185.2-km circular orbit, then the velocity increment needed for injection is 8092 m/s. Table I summarizes the pertinent trajectory characteristics for the points of entry and exit from the various spheres of influence.

The position and velocity are given relative to both coordinate systems when passing from one sphere of influence to another. The particular coordinate frame in use at any given time is a function of the computed vehicle position relative to the existing planetary configuration at the time, i.e., the particular sphere of influence through which the vehicle is passing. Thus, a planetocentric, equatorial reference system is used whenever the vehicle is within the sphere of influence of a planet; otherwise, a heliocentric, ecliptic system is used. In general a planetary equatorial system is defined such that the X_c axis is located along the intersection of the planet's equator and its orbit plane, the Y_c axis is perpendicular to the X_c axis and lies in the planet's equatorial plane, and the Z_c axis is orthogonal to both the X_c and Y_c axes. The quantities needed to specify this system are (1) i', the inclination of the planet's equator with respect to its orbit plane, and (2) Ω', the angle measured in the plane of the planet's orbit from the planetary ascending mode to the intersection of the planet's equator with its orbit plane. Figure 1 summarizes the pertinent planetary systems used herein.

The transition matrices $\phi(t_j, t_i)$ evaluated for key times along the trajectory are given in Table II. These matrices give the relationship between the deviations in position and velocity from the reference trajectory at time t_i to the deviations at time t_j. In matrix form the relationship is given by the following equation:

$$X t_j = \phi\ (t_j, t_i)\ X t_i$$

Where Xt_j and Xt_i are column matrices whose elements are the deviations in position and velocity at times t_j and t_i.

The final orbital element sensitivity coefficients are presented in Table III. The final time t_f was set at 8.5 days after exit from Jupiter's sphere of influence to further reduce the perturbation by Jupiter. These sensitivity coefficients can be used to determine the effects of the deviations in position and velocity at injection into the Earth reference hyperbolic orbit and injection into Jupiter's sphere of influence on the elements of the post encounter heliocentric orbit. For example, the deviation in the angle of inclination due to deviations in position and velocity at Earth injection is given by the following expression

$$\begin{aligned}\Delta_i = {} & 1.6475817\ \Delta X_o - 0.046266298\ \Delta Y_o + 0.27416168\ \Delta Z_o \\ & + 1.7392806\ \Delta V_{x_o} + 1.1800427\ \Delta V_{y_o} + 0.25182205\ \Delta V_{z_o}\end{aligned}$$

TABLE I
TRAJECTORY CHARACTERISTICS

Time (Days)	Condition	Position (km*)			Velocity (m/s)		
		X	Y	Z	V_X	V_Y	V_Z
0	Injection into Earth-referenced hyperbolic orbit	-6092.7121	2215.7729	1009.8828	-5911.4132	-13273.619	-6540.5716
0.921	Exit from Earth's sphere of influence	-64506.530	-832107.77	-406418.23	-687.96927	-10350.367	-5054.0216
	Entrance into Sun's sphere of influence	-.89023867 AU	.43142410 AU	-.00027909574 AU	-14325.232	-38251.861	-517.80507
436.921	Exit from Sun's sphere of influence	2.5375832 AU	-4.0940917 AU	-.031516197 AU	14054.858	-6914.6397	7.2887450
	Entrance into Jupiter's sphere of influence	-39012976	28032026	-1247247.9	11892.554	-8220.6214	494.40230
511.621	Exit from Jupiter's sphere of influence	-6736188.6	-43938536	-18737534	-2268.3571	-13053.428	-5647.9709
	Entrance into Sun's sphere of influence	2.8238002 AU	-4.2506033 AU	-.16587633 AU	-388.04795	648.03931	-5955.0861

*Except when otherwise noted, as AU while in the Sun's sphere of influence.

CENTER OF COORDINATES	ANGLE IN RADIANS			
	Ω'	i'	Ω	i
EARTH	0	-0.40926918	0	0
JUPITER	2.7751466	0.05436699	1.7472157	0.022793967

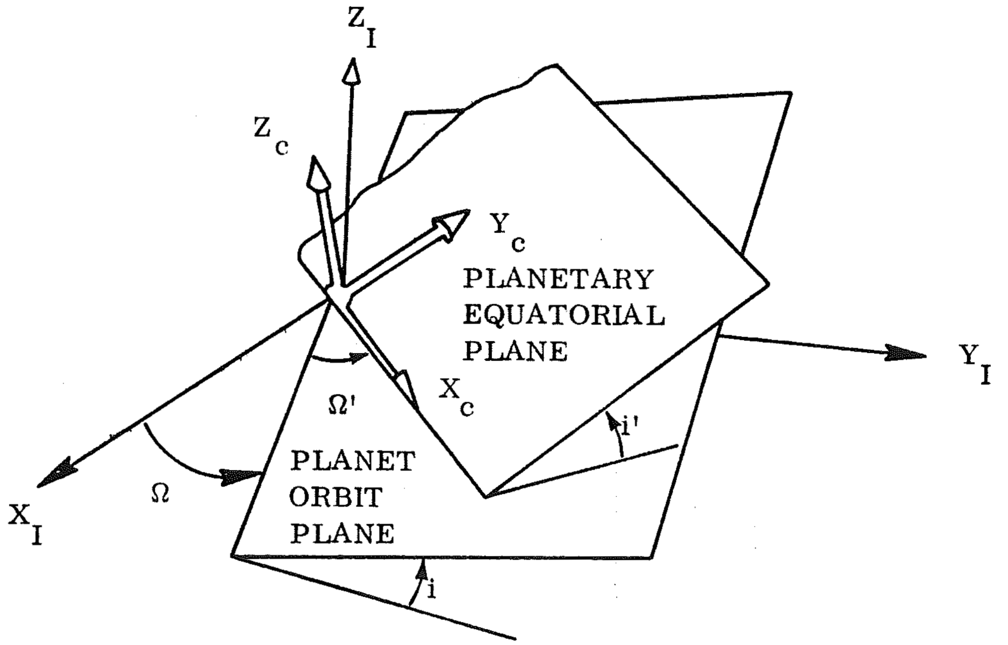
Z_I
Z_c
Y_c
PLANETARY EQUATORIAL PLANE
Y_I
X_c
Ω'
i'
PLANET ORBIT PLANE
X_I
Ω
i

66-2878

Figure 1 Planetary Coordinate Frames

TABLE II
TRANSITION MATRICES RELATING STATE ERRORS AT t_i TO STATE ERRORS AT t_j

Symbol	Time	Comments
t_o	0.000 days	Injection into Earth-referenced hyperbolic orbit
t_1	0.921 days	Entry into Sun's sphere of influence from Earth's sphere
t_2	436.921 days	Entry into Jupiter's sphere of influence from Sun's sphere
t_f	520.921 days	Arbitrary termination time in Sun's sphere of influence

UNITS Pure position and velocity elements are dimensionless: $\frac{\text{Units}}{\text{Units}}$

Mixed elements have the following: $\frac{\text{Units}}{\text{Units/Day}}$ and $\frac{\text{Units/Day}}{\text{Units}}$

$$\phi = \left[\begin{array}{c|c} \text{Position Elements} & \frac{\text{Units}}{\text{Units/Day}} \\ \hline \frac{\text{Units/Day}}{\text{Units}} & \text{Velocity Elements} \end{array}\right]$$

$$\phi(t_f, t_o) = \left[\begin{array}{rrr|rrr}
1496582.1 & 69827.463 & -137134.15 & 17529.231 & 11495.297 & 8506.1915 \\
-3187802.9 & -88545.730 & -15188.242 & -38181.554 & -24520.830 & -13324.857 \\
2172731.9 & -44629.642 & 266503.51 & 26267.429 & 18053.771 & 5336.5293 \\
\hline
27487.983 & 1649.0581 & -2844.2527 & 323.60595 & 203.85313 & 159.92778 \\
-69018.708 & -1715.4652 & -270.17319 & -8247.1729 & -535.99083 & -290.38454 \\
43910.958 & -858.60504 & 5696.3100 & 532.58931 & 362.41054 & 102.53493
\end{array}\right]$$

$$\phi(t_2, t_o) = \left[\begin{array}{rrr|rrr}
-39308.196 & 11292.376 & 4194.9959 & -347.82916 & -618.77605 & -293.22858 \\
107103.94 & -6715.8534 & -525.39301 & 1197.0879 & 1060.5009 & 509.08771 \\
724.12456 & 2191.3806 & -4526.4996 & 6.9988661 & -25.679208 & 67.830370 \\
\hline
-250.88121 & 41.382957 & 12.695049 & -2.5388626 & -3.1503508 & -1.4988668 \\
265.83400 & 27.961344 & -6.4168773 & 2.8541697 & 2.9258464 & 1.3995652 \\
-1.4833961 & -.19149673 & 1.2351619 & -.013594347 & -.013411787 & -.026187271
\end{array}\right]$$

$$\phi(t_1, t_o) = \left[\begin{array}{rrr|rrr}
77.926435 & 14.557606 & 8.5040477 & 1.0648971 & .24975369 & .12682298 \\
52.832778 & -22.164049 & -8.0905832 & .39274637 & 1.0332054 & .47666764 \\
3.6323156 & 18.145076 & -39.231762 & .022005675 & -.23304088 & .59997655 \\
\hline
83.107702 & 15.824739 & 9.2358348 & 1.1475676 & .27546181 & .13979704 \\
59.228706 & -25.285739 & -9.3148227 & .44170225 & 1.1441568 & .52910791 \\
4.0201356 & 20.041535 & -43.428861 & .024576273 & -.24769761 & .64318056
\end{array}\right]$$

TYPICAL

$$\phi(t_2, t_1) = \left[\begin{array}{rrr|rrr}
-4.3332942 & 1.2341188 & -.065775612 & -99.716668 & -518.63020 & -7.5818028 \\
14.439685 & 1.6418356 & .27495923 & 741.65644 & 746.34925 & 12.015603 \\
.091116311 & .090931164 & -4.0508908 & 4.0218104 & -.76196027 & 108.90690 \\
\hline
-.033411333 & .0038888474 & -.00055462477 & -1.2351935 & -2.4597774 & -.034183136 \\
.032951416 & .0020562436 & .00070908818 & 1.6217589 & 2.1651479 & .033686545 \\
-.00015031663 & .00014904892 & -.0085110988 & -.0048907592 & -.016350755 & -.018342815
\end{array}\right]$$

$$\phi(t_f, t_2) = \left[\begin{array}{rrr|rrr}
8.9058838 & 16.290990 & 37.184110 & 370.83188 & 639.75791 & 1438.0543 \\
-26.683781 & -38.459717 & -18.195116 & -1124.7649 & -1458.0034 & -723.32840 \\
20.290059 & 27.222051 & -42.978586 & 780.79844 & 1050.6088 & -1638.7369 \\
\hline
.18106008 & .30572787 & .77259259 & 7.4607503 & 12.101945 & 29.882860 \\
-.55805031 & -.82466739 & -.38798913 & -23.625939 & -31.217845 & -15.423263 \\
.42700429 & .55731810 & -.93160057 & 16.379873 & 21.552412 & -35.160278
\end{array}\right]$$

FOLDOUT FRAME #1

TABLE III
FINAL ORBITAL ELEMENTS, SENSITIVITY COEFFICIENTS

Relative to Earth Injection			Units
Inclination			
$\frac{\partial i_f}{\partial x_o} = 1.6475817$	$\frac{\partial i_f}{\partial y_o} = -.046266298$	$\frac{\partial i_f}{\partial z_o} = .27416168$	$\frac{\text{deg}}{\text{km}}$
$\frac{\partial i_f}{\partial V_{x_o}} = 1.7392806$	$\frac{\partial i_f}{\partial V_{y_o}} = 1.1800427$	$\frac{\partial i_f}{\partial V_{z_o}} = .25182205$	$\frac{\text{deg}}{\text{m/s}}$
Semi-Major Axis			
$\frac{\partial a_f}{\partial x_o} = -.055471525$	$\frac{\partial a_f}{\partial y_o} = .0011021360$	$\frac{\partial a_f}{\partial z_o} = -.0072368501$	$\frac{\text{AU}}{\text{km}}$
$\frac{\partial a_f}{\partial V_{x_o}} = -.058133231$	$\frac{\partial a_f}{\partial V_{y_o}} = -.039575952$	$\frac{\partial a_f}{\partial V_{z_o}} = -.011140035$	$\frac{\text{AU}}{\text{m/s}}$
Eccentricity			
$\frac{\partial e_f}{\partial x_o} = .035564333$	$\frac{\partial e_f}{\partial y_o} = -.00067526501$	$\frac{\partial e_f}{\partial z_o} = .0045551816$	$\frac{\text{units}}{\text{km}}$
$\frac{\partial e_f}{\partial V_{x_o}} = .037261477$	$\frac{\partial e_f}{\partial V_{y_o}} = .025341841$	$\frac{\partial e_f}{\partial V_{z_o}} = .0072503256$	$\frac{\text{units}}{\text{m/s}}$
Semi-Latus Rectum			
$\frac{\partial p_f}{\partial x_o} = -.18145064$	$\frac{\partial p_f}{\partial y_o} = .0034631955$	$\frac{\partial p_f}{\partial z_o} = -.023289187$	$\frac{\text{AU}}{\text{km}}$
$\frac{\partial p_f}{\partial V_{x_o}} = -.19011490$	$\frac{\partial p_f}{\partial V_{y_o}} = -.12931308$	$\frac{\partial p_f}{\partial V_{z_o}} = -.036929469$	$\frac{\text{AU}}{\text{m/s}}$
Relative to the Sun at Entrance Into Jupiter's Sphere of Influence			
Inclination			
$\frac{\partial i_f}{\partial x_2} = .000017081075$	$\frac{\partial i_f}{\partial y_2} = .000021764911$	$\frac{\partial i_f}{\partial z_2} = -.000046761383$	$\frac{\text{deg}}{\text{km}}$
$\frac{\partial i_f}{\partial V_{x_2}} = .064298767$	$\frac{\partial i_f}{\partial V_{y_2}} = .066894867$	$\frac{\partial i_f}{\partial V_{z_2}} = -.15410037$	$\frac{\text{deg}}{\text{m/s}}$
Semi-Major Axis			
$\frac{\partial a_f}{\partial x_2} = -.00000053962831$	$\frac{\partial a_f}{\partial y_2} = -.00000070422454$	$\frac{\partial a_f}{\partial z_2} = .0000011731270$	$\frac{\text{AU}}{\text{km}}$
$\frac{\partial a_f}{\partial V_{x_2}} = -.0017894153$	$\frac{\partial a_f}{\partial V_{y_2}} = -.0023521872$	$\frac{\partial a_f}{\partial V_{z_2}} = .0038669827$	$\frac{\text{AU}}{\text{m/s}}$
Eccentricity			
$\frac{\partial e_f}{\partial x_2} = .00000034502286$	$\frac{\partial e_f}{\partial y_2} = .00000045103281$	$\frac{\partial e_f}{\partial z_2} = -.00000073411518$	$\frac{\text{units}}{\text{km}}$
$\frac{\partial e_f}{\partial V_{x_2}} = .0011452225$	$\frac{\partial e_f}{\partial V_{y_2}} = .0015063217$	$\frac{\partial e_f}{\partial V_{z_2}} = -.0024194567$	$\frac{\text{units}}{\text{m/s}}$
Semi-Latus Rectum			
$\frac{\partial p_f}{\partial x_2} = -.0000017608636$	$\frac{\partial p_f}{\partial y_2} = -.0000023014540$	$\frac{\partial p_f}{\partial z_2} = .0000037558074$	$\frac{\text{AU}}{\text{km}}$
$\frac{\partial p_f}{\partial V_{x_2}} = -.0058441295$	$\frac{\partial p_f}{\partial V_{y_2}} = -.0076863052$	$\frac{\partial p_f}{\partial V_{z_2}} = .012378425$	$\frac{\text{AU}}{\text{m/s}}$

Subscripts:
f refers to t = 520.121 days (final time)
0 refers to t = 0 days (injection into Earth-referenced hyperbolic orbit)
2 refers to t = 436.921 days (injection into Jupiter's sphere of influence)

FOLDOUT FRAME #2

Prior to the generation of the reference trajectory a study was made of the accuracy of the numerical integration of the equations of motion. The equivalent two-body trajectories were integrated using different integration step sizes. The amount of change in the semi-major axis for different step sizes is shown in Figures 2 and 3. Based on this study, a step size schedule of 0.00025, 0.0025, and 0.01 day was used within the Earth's sphere of influence and one of 0.5 day in the Sun's sphere. The reference trajectory was computed using a IBM 7094 in double precision giving a word length of sixteen decimal digits or 54 binary bits.

The semi-major axis in two-body motion is a function of R, the magnitude of the position vector, and V, the magnitude of the velocity vector. The gradient of these quantities is large at perigee of the Earth-centered hyperbolic orbit. The curves of Figure 2 reflect these gradients showing an initial growth in $\Delta\alpha$ followed by a leveling off as the gradients decrease. The initial growth in Δa is due to truncation error. The integration step size used results in an error of approximately 1 ppm. Figure 3 indicates similar results, the first part of the trajectory being near perihelion. The integration step size used in the heliocentric orbit resulted in an error in the semi-major axis of approximately 0.03 ppm.

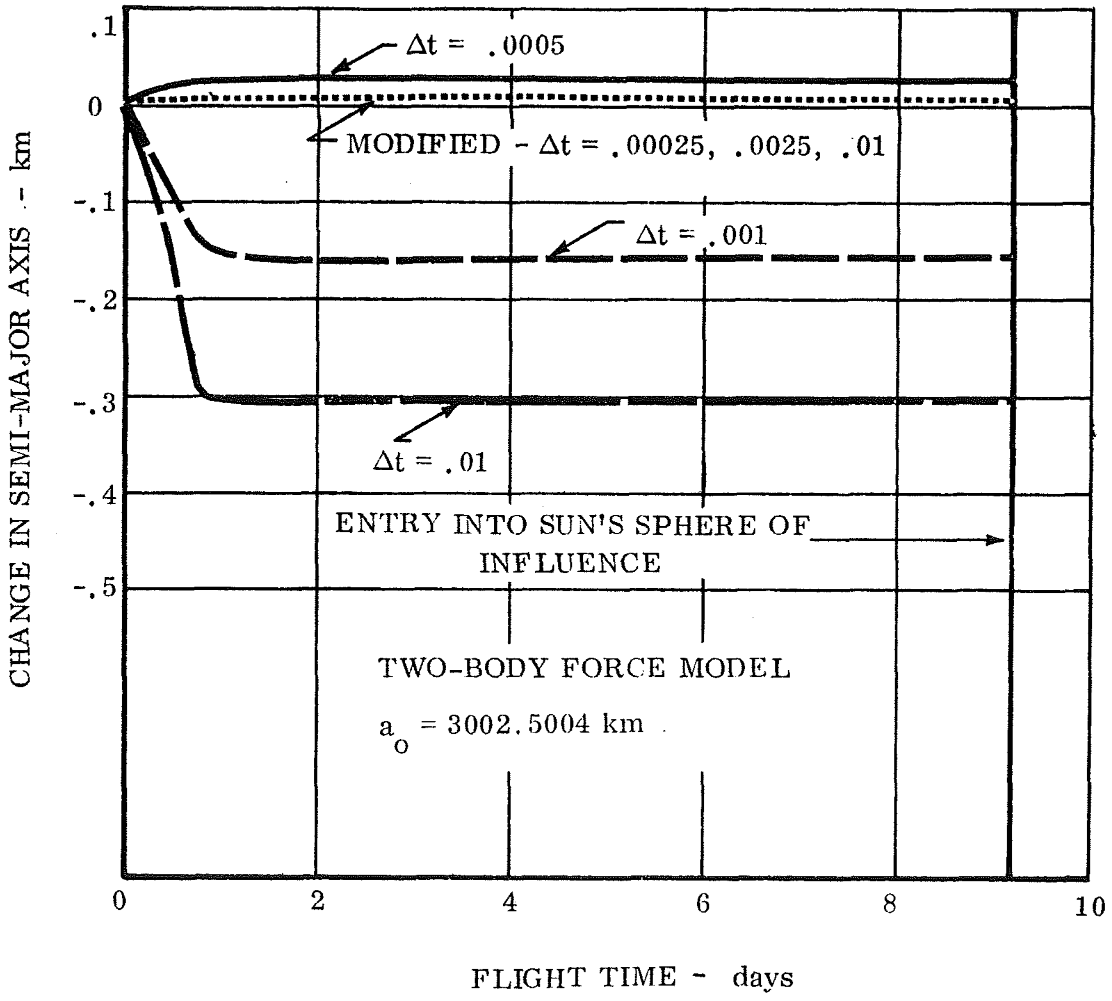

66-2863

Figure 2 Integration Analysis, Effect of Integration Step Size on Time History of Semi-Major Axis, Earth's Sphere of Influence

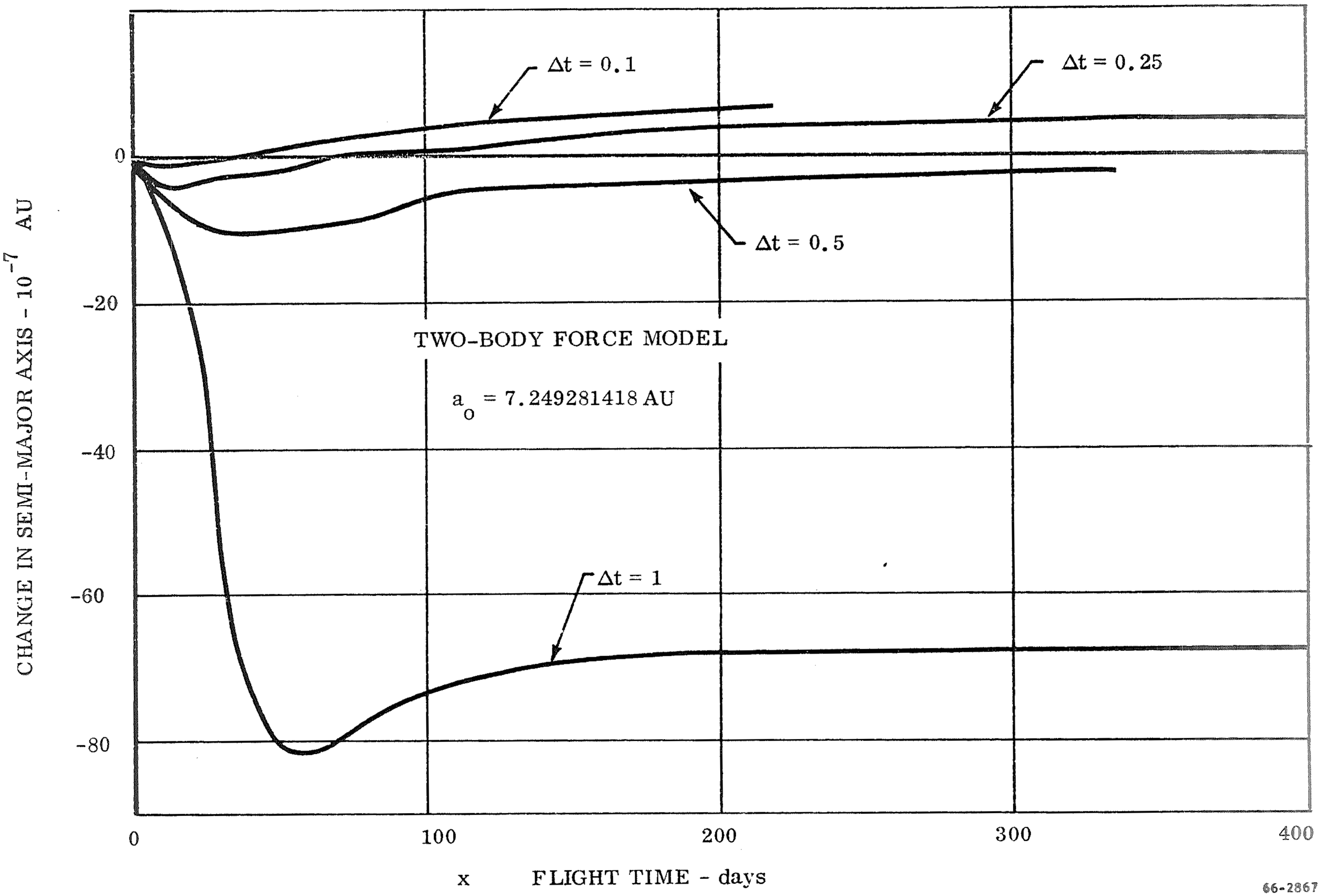

Figure 3 Integration Analysis, Effect of Integration Step Size on Time History of Semi-Major Axis, Sun's Sphere of Influence

IV. NAVIGATION

Simple explicit orbital navigation concepts were extended and developed for interplanetary missions. The results of this work, designated the Interplanetary Space Navigation (ISN) scheme, are presented below with a comparison of the ISN with a Linear Optimum Filter (LOF) navigation scheme.

A. Navigation Schemes

1. Interplanetary Space Navigation

The Interplanetary Space Navigation (ISN) scheme is an explicit, nonlinear, celestial inertial navigation scheme that uses the difference between the actually observed and the predicted based on computed position to bound the downrange and crossrange error and computes the magnitude of the position vector from the angular momentum relationship. A general description of the scheme is presented in the following paragraphs; a more detailed mathematical discussion is presented in Appendix B.

The ISN mechanizes the position tracking loops in a specific coordinate system referred to as the R-Θ-ψ spherical coordinate frame. It consists of the magnitude of the radius or position (R) from the center of the central body to the vehicle, the range angle (Θ) measured in a reference orbital plane from a line in that plane to the projection of R on the plane, and the crossrange angle (ψ) measured from said projection to R. The reference orbital plane is chosen to be closely aligned with the actual orbital plane so that the Θ and ψ computations behave in an uncoupled manner.

A typical coordinate system is depicted in Figure 4. The vehicle is depicted as a point mass at R that can be described by the spherical coordinates R, Θ, ψ in an orbit-oriented frame O_1, O_2, O_3. The latter coordinate frame is in turn described by the angles Ω and i relative to the inertial frame I_1, I_2, I_3. The initial values of Θ, Ω, and i are computed from the injection conditions. The angle Ω should be updated when ψ becomes large to eliminate coupling terms between the Θ and ψ computations. In missions such as the Jupiter swing-by the coordinate system is changed when passing from one sphere of influence to the next. For example, while within the Earth's sphere of influence the orbital plane is defined relative to an Earth-centered coordinate system. However, when the vehicle passes into the Sun's sphere of influence a new orbital plane is defined relative to the Sun.

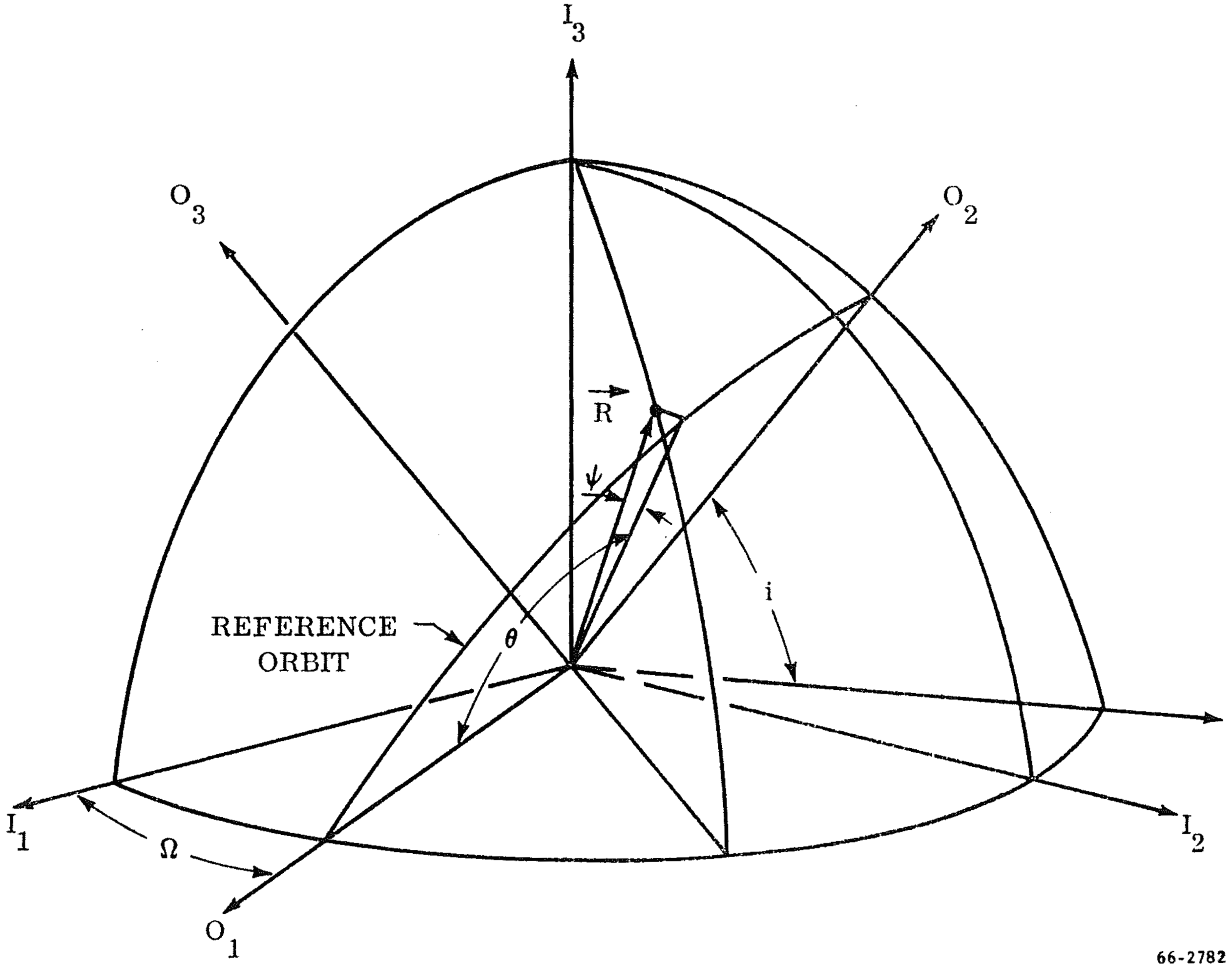
I_3
O_3
O_2
$\vec{R}$
ψ
i
REFERENCE ORBIT
θ
I_1
Ω
I_2
O_1
66-2782

Figure 4 ISN Coordinate Systems

At the time of injection, the assumed position and velocity vector are used to determine the relationship between the inertial coordinate systems and the spherical coordinate system and to specify the initial conditions used in the integration of the equations of motion. The equations of motion of a point mass in spherical coordinates are then integrated numerically until the time of an observation. The equations for $\ddot{\Theta}$ and $\ddot{\psi}$ are integrated twice to give Θ and ψ while the equation for $\ddot{R}$ is integrated once to give $\dot{R}$. $\ddot{\Theta}$ is equal to the sum of the tangential gravity and specific forces and the Coriolis force; $\ddot{\psi}$ is equal to the sum of the normal gravity and specific forces; and $\ddot{R}$ is equal to the sum of the radial gravity and specific forces and the centrifugal force. The value of R is obtained from the principle of constant angular momentum. It should be noted that the use of the angular momentum does not imply that the equations of motion need be two-body equations. Internally computed corrections in this parameter are used to compensate for perturbations of the other planetary bodies.

Prior to taking an observation of a planet, stellar observations are used to determine the orientation of the vehicle coordinate systems relative to the inertial coordinate frame. In the simulations of the navigation schemes the errors associated with the alignment and with the calculation of the orientation of the vehicle were combined with the errors of the optical sensor and called the total observational error. The trade-offs involved in these operations are discussed in Section VI. The difference between what is observed and what should have been observed based on the calculated position is used with a known geometric relationship to determine an estimate of the error in Θ and ψ. These values of $\Delta\Theta$ and $\Delta\psi$ are filtered and then multiplied by preselected gains and fed into the equations of motions as shown in Figure 5. The equations of motion are then integrated forward to the time of the next observations. The filter, the details of which are given in Appendix B, attenuates measurement noise above orbital frequency without affecting transient performance. Figure 5 also shows the calculation of R and the corrections to the momentum M_o. R is calculated by taking the square root of the quotient of the momentum M and the total angular rate ω_s. In order to correct for initial errors in M_o, the feedback of the integral of range angle error on M_o is introduced. It is based on the principle that when M is in error a corresponding lead or lag in computed range results for positive or negative values, respectively, of $M - M_{true}$. The feedback on M_o or the integral of the range angle error $\Delta\Theta_R$ is multiplied by a gain, K_m. The range angle error $\Delta\Theta_R$ is found by resolving $\Delta\Theta$ and $\Delta\psi$ into their components along the velocity direction. In the presence of lateral perturbing forces or noncentral gravity components, the simple angular momentum relationship does not hold; therefore, a momentum compensation term $\Delta\dot{M}_c$ is introduced. The analytical details of the momentum updating and compensation are presented in Appendix B. Although the integration of the equations of motion is performed in the R-Θ-ψ coordinate systems, the position and velocity are transformed into the inertial rectangular coordinate systems for comparison with the LOF data.

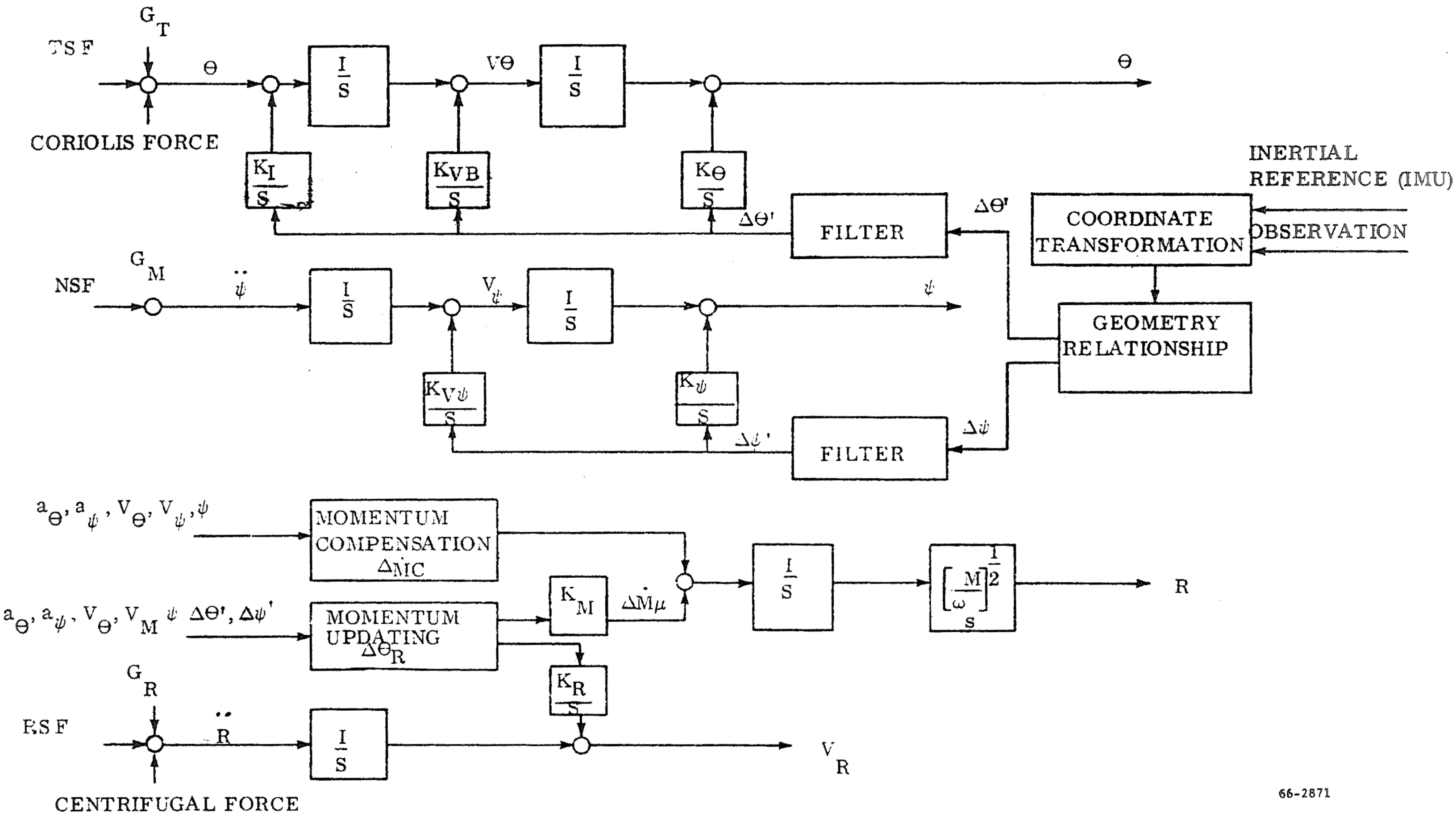
G_T
TSF
Θ
I/S
VΘ
I/S
Θ
CORIOLIS FORCE
K_I/S
K_VB/S
K_Θ/S
ΔΘ'
FILTER
ΔΘ'
INERTIAL REFERENCE (IMU)
COORDINATE TRANSFORMATION
OBSERVATION
G_M
NSF
ψ̈
I/S
V_ψ
I/S
ψ
GEOMETRY RELATIONSHIP
K_Vψ/S
K_ψ/S
Δψ'
FILTER
Δψ
a_Θ, a_ψ, V_Θ, V_ψ, ψ
MOMENTUM COMPENSATION ΔṀC
a_Θ, a_ψ, V_Θ, V_M ψ ΔΘ', Δψ'
MOMENTUM UPDATING ΔΘ_R
K_M
ΔṀμ
I/S
[M/ω]^1/2 / s
R
G_R
RSF
R̈
I/S
K_R/S
V_R
CENTRIFUGAL FORCE
66-2871

Figure 5 Interplanetary Space Navigation Scheme

The extension of the UAC orbital navigation scheme has resulted in a simplified navigation scheme for interplanetary applications which has the following features:

1) The law of conservation of angular momentum is used to calculate the magnitude of the position vector.

2) The state correction process uses constant feedback gains.

3) The feedback error quantity, which consists of the difference between the actual and predicted measurement, is processed by a filter prior to multiplication by the gains and corrections of the state parameters. This has the effect of attenuating measurement noise above a given frequency.

2. Linear Optimum Filter

The Linear Optimum Filter (LOF) navigation scheme is an explicit celestial, linear, inertial navigation scheme that uses the difference between the actual and estimated measurements processed through a Kalman filter to statistically estimate the position and velocity of a vehicle. The scheme is based on the assumption that the best estimate of the state X_n (a column matrix whose elements are the position and velocity components of the vehicle) after the nth observation is given by the following expression:

$$X_n = X'_n + K\delta A$$

Where X'_n is the state integrated forward from the time of the n-1 observation, δA is a column matrix whose elements are the difference between observed angles and calculated angles, and K is a weighting factor that is chosen to minimize the mean-square error in the estimate. The observation is related to the state by a geometry matrix that is a function of the geometrical configuration of the relevant celestial object. The weighting factor K is a function of the covariance matrix of the error in estimating the state, the geometry matrix, and the estimated standard deviation of the observational errors.

A covariance matrix is a matrix whose elements are the mean of the product of the errors of the elements of a given vector. For example, for the vector X = (X_1, X_2, . . . X_6) the elements of the covariance matrix are of the form

$$\sum_{i,j=1}^{N} \frac{\xi_i \xi_j}{N}$$

where ξ_i is the error in X_{ki}. The weighting factor K is a function of the a priori knowledge of injection and observation statistics and does not directly reflect the results of the actual observations. The actual observations affect the factor K indirectly through the transition matrices as shown in Figure 6.

The LOF simulation is mechanized using a rectangular inertial coordinate system centered on the primary body. The scheme could have been mechanized using the same coordinate system as was used with the ISN but there is no particular advantage to be gained so the more conventional system was used. A simplified flow diagram of the scheme is given in Figure 6; the details of the equations are presented in Appendix B.

As shown in Figure 6, the expressions for the acceleration in the inertial coordinates X, Y, and Z are integrated to obtain the position and velocity in inertial space. At the time of an observation the transition matrix is calculated and the gain matrix K is computed. The right ascension and declination of a planet are observed in body coordinates and transformed into the inertial systems. The right ascension and declination of the planet are then calculated based on the estimate of position of the vehicle and subtracted from the transformed observed values. The resulting Δa and $\Delta\delta$ are multiplied by the appropriate elements of the K matrix and fed into the integration of the equations of motion. Thus, the results of taking an observation appear as step changes in the estimate of position and velocity.

The main features of the LOF navigation scheme are:

1) The generation of time varying gains by the Kalman filter.

2) The use of a covariance matrix based on predetermined injection statistics.

3) The use of the transition matrix to propagate the covariance matrix. The transition matrix is obtained from integration of the equations of motion linearized with respect to the calculated trajectory.

A computer word count of the two navigation schemes was made to determine their relative computational complexity. A large part of the work load of the computer, such as the integration of the equations of rotational motion, the taking of observations, and the alignment and calibration of the sensor package, is common to both systems. The word count associated with these functions is 2866. A word count of those calculations that are different in the two navigation schemes was made and the results are presented in Table IV. The total word count for the LOF and ISN are 6972 and 6162, respectively, giving a difference of 810 words.

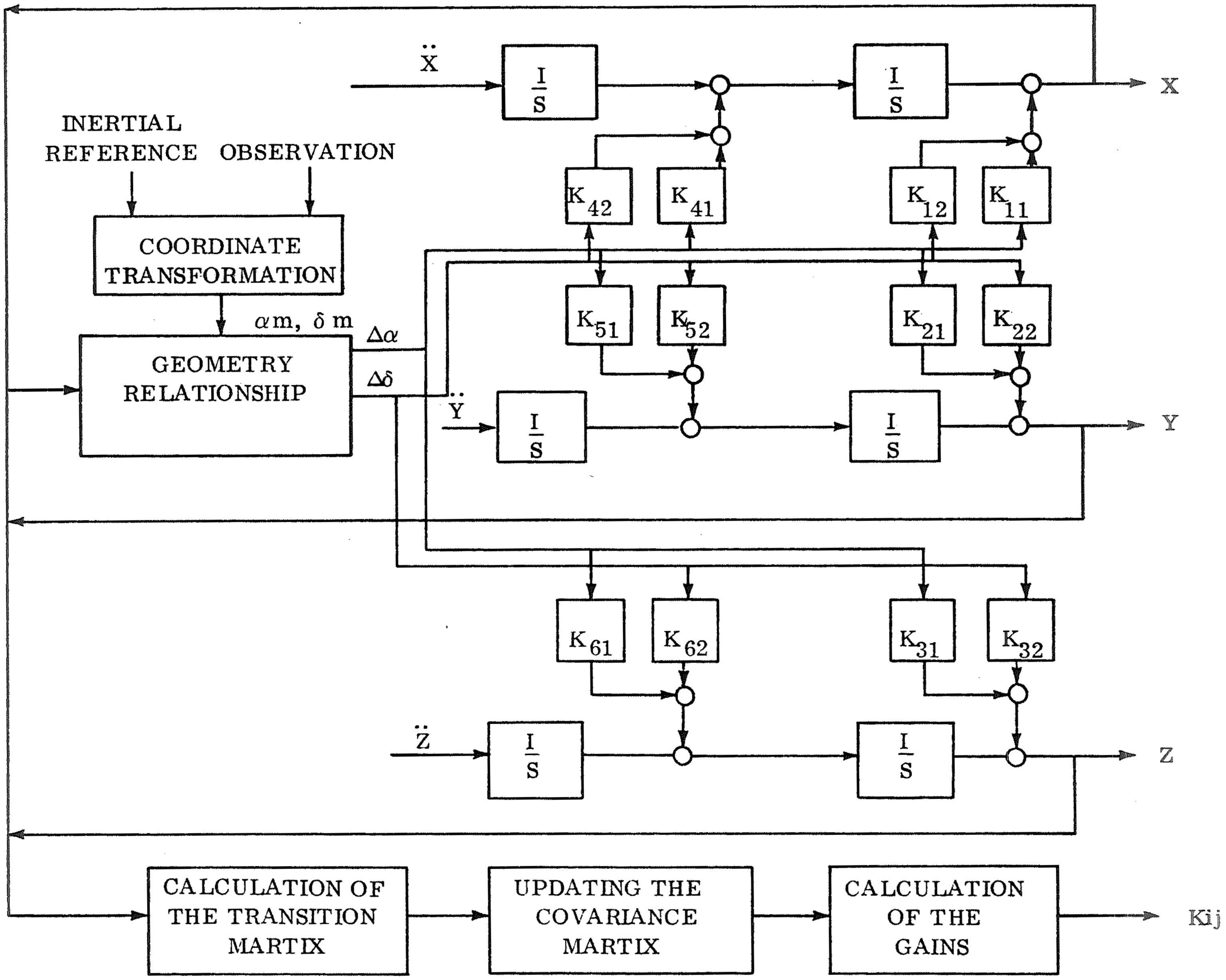
Ẍ
I/S
I/S
X
INERTIAL REFERENCE
OBSERVATION
COORDINATE TRANSFORMATION
αm, δm
Δα
Δδ
GEOMETRY RELATIONSHIP
K42
K41
K12
K11
K51
K52
K21
K22
Ÿ
I/S
I/S
Y
K61
K62
K31
K32
Z̈
I/S
I/S
Z
CALCULATION OF THE TRANSITION MARTIX
UPDATING THE COVARIANCE MARTIX
CALCULATION OF THE GAINS
Kij

66-2881

Figure 6 Linear Optimum Filter Navigation Scheme

TABLE IV
COMPUTER WORD COUNT

Linear Optimum Filter Scheme	
Integration of the Equations of Motion	1789
Calculation of the Transition Matrix and the Predicted Measurements	1074
Calculation of the Geometry and Covariance Matrices and the Weighting Function	211
Updating the State Variables	55
Updating the Covariance Matrix	80
Storage	897
TOTAL	4106

Interplanetary Space Navigation Scheme	
Calculation of the Transformation from Inertial to the R-Θ, ψ Frame	380
Calculation of Initial Conditions	191
Integration of the Equations of Motion	1821
Calculation of $\Delta\Theta$ and $\Delta\psi$	420
Calculation of $\Delta\Theta'$ and $\Delta\psi'$	103
Storage	481
TOTAL	3296

3. Navigation Parameters

Computer simulation programs were written for both the Linear Optimum Filter (LOF) and Interplanetary Space Navigation (ISN) schemes. These programs are described in detail in Volume II of this report. For the purpose of comparison, the injection error statistics, the observation schedule, and the observation error statistics were the same for both programs.

The injection error statistics are those for a Saturn IB being injected into an interplanetary trajectory from a 185.2-km circular orbit. The one sigma downrange, crossrange, and altitude errors are given in Table V with the initial conditions and inertial measuring unit characteristics. In the simulation program, the one sigma injection errors are used with a random number generator to select injection errors for each run of the program.

The observation schedule selected employs pairs of observations made a tenth of a day apart every six days for the first 86 days and ten days apart for the remainder of the time to entry into Jupiter's sphere of influence; a total of 100 observations were made. The selection of the observables is described in detail in the following paragraphs. As long as the errors in observation are assumed to be uncorrelated, this schedule favors the LOF scheme. Because of the filter in the ISN scheme and the taking of observations a tenth of a day apart, the first of the two observations has little effect on the ISN navigation. The one sigma observational error is an input item in the programs and is used with a random number generator to compute the error for each observation.

The observation schedule was selected on the basis of taking one hundred observations at equally spaced intervals. The operation of taking an observation requires that star sights be taken to determine the vehicle orientations in inertial space. As this requires an expenditure of energy, it was felt that at least two observations should be made each time the equipment is activated. It was also felt that the observations should be more frequent at the beginning to bring the injection errors under control; after the 86th day observations were made at 10-day, rather than 6-day, intervals.

The selection of the observables was optimized for the observation schedule given above. An analysis of the covariance and geometry matrices associated with the Kalman filter shows that when two planets are observed the navigation errors are minimized when the planets selected are as close as possible to the observer and are separated from each other by an angle as close to 90 degrees as possible. Based on this criterion and using the N-Body program, a study was conducted to determine a physically feasible planet sighting schedule. In addition to the distance and angular separation there are other parameters that must be considered in selecting the observables. They are the Sun-planet angle, the subtended angle, and the illumination

TABLE V
INJECTION CONDITIONS

A. Injection Performance

Position Errors (m, 1σ)			Velocity Errors (m/s 1σ)		
D.R.	C.R.	A	D.R.	C.R.	A
986	1910	1144	1.51	9.57	5.81

B. Error Sources

	1σ, 30-day values
Gyro/PTSA	
Gyro/PTSA Non-g-Sensitive Drift Stability	
Roll Gyro	0.18 deg/hr
Pitch or Yaw Gyro	0.09 deg/hr
Gyro g-Sensitive Drift Stability	
Roll Gyro	0.2 deg/hr/g
Pitch or Yaw Gyro	0.1 deg/hr/g
Gyro Minor Anisoelasticity	0.001 deg/hr/g^2
Gyro/PTSA Scale Factor Stability	100 ppm
Gyro Input Axis Alignment Stability	20 arc sec
Gyro/PTSA Equivalent Drift due to Vibration	0.02 deg/hr
Accelerometer/PTSA	
Accelerometer/PTSA Bias Stability	50 μg
Accelerometer/PTSA Scale Factor Stability	50 ppm
Accelerometer Non-linearity	10 $\mu g/g^2$
Accelerometer Input Axis Alignment Stability	15 arc sec
Accelerometer/PTSA Equivalent Bias due to Vibration	50 μg
Computational Process	
Attitude Matrix Computation Equivalent Drift	0.01 deg/hr
Position Computation Equivalent Bias	5 μg
Initial Conditions	
Launch Altitude, Range and Track Uncertainties	30.5 m
Azimuth Alignment (optical)	10 arc sec
Vertical Alignment (self)	23 arc sec

angle. The Sun-planet angle defines the angular separation of the potential observable from the Sun as observed from the vehicle. A minimum value of twenty degrees was selected in order to eliminate the problem of locating planets in the vicinity of the Sun. This criterion was violated when observations of the Earth were used near Jupiter's sphere of influence. This does not significantly effect the results of the navigation study because the Earth observations could be replaced by Sun observations. The angle subtended by the planet and the angle subtended by the illuminated portion of the planet as viewed from the vehicle were considered. A minimum illumination angle of fifty percent of the subtended angle was used as a criterion. The results of this study are presented in Table VI. Two planet combinations are shown; the observables used in the navigation studies were selected from Planet Combination 1.

B. Performance Evaluation

Computer simulations were formulated for both the ISN and LOF navigation schemes as described in SCR 290, Volume II - Simulation Documentation. These simulations were used to generate performance data for purposes of comparison. Copies of these simulations were given to NASA/ERC in partial fulfillment of this contract. A summary of the performance data for both schemes is presented in the following paragraphs.

1. Interplanetary Space Navigation

The values of the loop feedback gains for the ISN were selected using the linear analysis technique described in Appendix B. These gains have been verified through computer simulation runs, and there is good correlation between predicted time constants and natural frequencies and those of the nonlinear simulation. This correlation was obtained using a two-body case with measurements made directly to the central body (the Sun). The simulation covered the portion of the trajectory between the Earth's sphere of influence and that of Jupiter. This corresponds to approximately one-eighteenth of the orbital period of the total transfer orbit. Over this fractional portion of the orbit, it was found that the angular momentum correction paths through the gains, K_m and K_R of Figure 7, were ineffective. Figure 7 presents the ISN mechanization from a control theory viewpoint as discussed in Appendix B. However, the performance could be improved by setting K_m and K_R to zero and feeding the integral path directly to the angular acceleration summation point through the gain K_I. The design parameters selected in addition to K_I were the gains K_Θ and K_{V_Θ}. A series of cases were simulated, and a set of gains selected which yielded the best performance obtained. These gains nondimensionalized by the reference circular orbit angular velocity are:

$$\frac{K_\Theta}{V_\Theta} = 100, \quad \frac{K_{V_\Theta}}{V_\Theta^{\ 2}} = 6000, \quad \frac{K_I}{V_{\Theta_o}^{\ 3}} = 111,000$$

TABLE VI
PLANET OBSERVATION SCHEDULE

Time (day)	2	8	14	20	30	90	121	150	170	200	230	260	290	320	350	400	430
Planet Combination 1																	
Planet A	Moon	Earth	Earth	Earth	Earth	Earth	Earth	Jupiter	Jupiter	Jupiter	Jupiter	Jupiter	Jupiter	Jupiter	Jupiter	Jupiter	Jupiter
Vehicle-Planet Distance (km)	1.629×10^{6}	7.885×10^{6}	1.377×10^{7}	1.951×10^{7}	2.860×10^{7}	3.698×10^{7}	1.401×10^{8}	4.551×10^{8}	4.187×10^{8}	3.682×10^{8}	3.216×10^{8}	2.778×10^{8}	2.361×10^{8}	1.960×10^{8}	1.570×10^{8}	9.353×10^{7}	5.593×10^{7}
Planet Subtended Angle (arc sec)	440.13	333.68	191.08	134.85	92.01	71.15	18.78	63.46	68.98	78.43	89.80	103.95	122.30	147.34	183.95	308.73	516.31
Planet Illuminated Angle (arc sec)	327.04	119.25	86.25	73.06	41.83	26.00	8.82	63.26	68.85	78.39	89.79	103.86	121.97	146.50	182.14	302.80	502.56
Planet-Sun Angle (deg)	118.50	70.48	79.07	87.28	74.19	61.82	13.04	164.81	169.67	175.53	178.28	174.88	171.44	168.41	165.72	161.84	159.69
Planet B	Venus	Mars	Mars	Venus	Venus	Venus	Mars	Mars	Earth	Mars	Mars	Mars	Mars	Mars	Mars	Earth	Earth
Vehicle-Planet Distance (km)	1.270×10^{8}	2.546×10^{8}	2.677×10^{8}	1.196×10^{8}	1.177×10^{8}	1.160×10^{8}	4.685×10^{8}	5.036×10^{8}	2.780×10^{8}	5.427×10^{8}	5.534×10^{8}	5.550×10^{8}	5.486×10^{8}	5.362×10^{8}	5.212×10^{8}	7.471×10^{8}	7.150×10^{8}
Planet Subtended Angle (arc sec)	19.72	5.53	5.26	20.95	21.29	21.60	3.00	2.80	9.46	2.59	2.54	2.53	2.56	2.63	2.70	3.52	3.68
Planet Illuminated Angle (arc sec)	12.01	5.14	4.85	12.03	11.25	10.00	2.79	2.54	2.91	2.15	2.01	1.83	1.61	1.35	1.02	2.72	2.06
Planet-Sun Angle (deg)	45.41	31.85	44.59	45.90	43.86	40.83	26.26	25.48	22.55	42.76	25.98	25.95	25.32	23.77	20.99	10.69	12.13
Angle between A and B (deg)	73.09	38.69	34.55	41.41	30.34	20.99	39.26	169.41	147.18	133.00	153.18	149.10	146.20	144.68	144.76	151.17	147.58
Planet Combination 2																	
Planet A	Earth	Earth	Earth	Earth	Earth	Earth				Jupiter						Jupiter	
Vehicle-Planet Distance (km)	1.926×10^{6}	7.885×10^{6}	1.377×10^{7}	1.951×10^{7}	2.860×10^{7}	3.698×10^{7}				3.682×10^{8}						9.353×10^{7}	
Planet Subtended Angle (arc sec)	1366.3	333.68	191.08	134.85	92.01	71.15				78.43						308.73	
Planet Illuminated Angle (arc sec)	934.23	119.25	86.25	73.06	51.42	26.00				78.39						302.80	
Planet-Sun Angle (deg)	110.80	70.48	79.07	87.28	86.18	61.82				175.53						161.84	
Planet B	Venus	Venus	Venus	Mars	Mars	Mars				Earth						Mars	
Vehicle-Planet Distance (km)	1.270×10^{8}	1.236×10^{8}	1.213×10^{8}	2.811×10^{8}	3.033×10^{8}	3.251×10^{8}				3.802×10^{8}						5.045×10^{8}	
Planet Subtended Angle (arc sec)	19.72	20.26	20.66	5.01	4.46	4.33				6.92						2.79	
Planet Illuminated Angle (arc sec)	12.01	5.34	9.54	4.63	4.33	4.06				3.42						0.40	
Planet-Sun Angle (deg)	45.41	13.75	30.25	56.75	50.14	44.50				21.47						13.00	
Angle between A and B (deg)	65.40	56.94	48.88	30.60	24.13	17.40				154.30						148.86	
COMMENTS																	
Earth-Moon Angle (deg)	7.74	1.95	1.52	0.19	0.36	0.619	0.159		0.044	0.053							0.02
Venus-Mars Angle (deg)			14.72	11.23	6.67	3.99											
Sun Subtended Angle (arc sec)	1945.4	1959.1	1953.9	1930.2	1856.3	1753.5	1006.8	864.01	788.7	699.8	631.3	577.07	532.98	496.43	465.62	423.70	402.80

#1

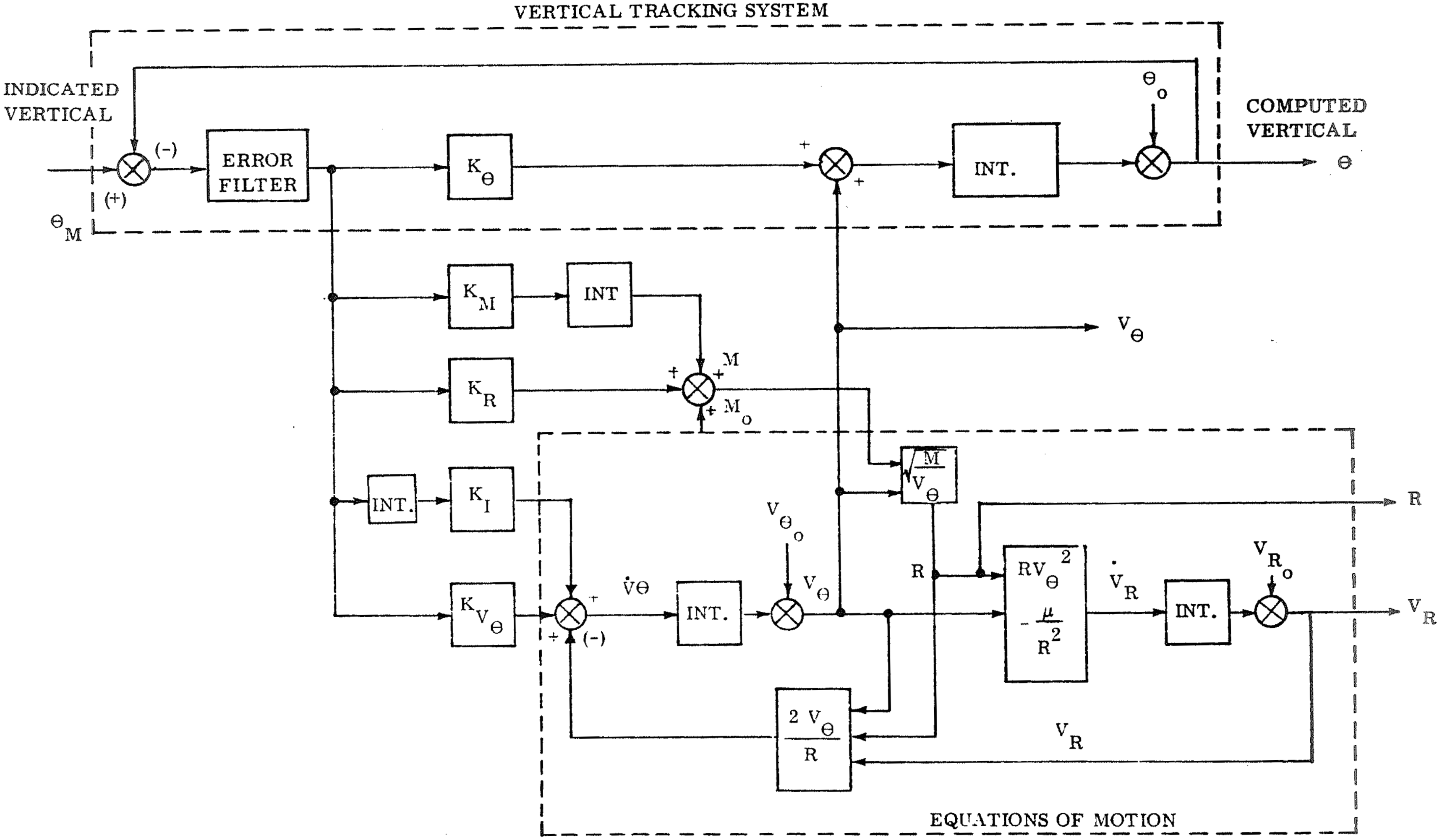
VERTICAL TRACKING SYSTEM
INDICATED VERTICAL
(-)
(+)
ΘM
ERROR FILTER
KΘ
+
+
INT.
Θo
COMPUTED VERTICAL
Θ
KM
INT
VΘ
KR
+
+ M
+ Mo
√M/VΘ
R
INT.
KI
VΘo
VΘ
R
RVΘ² − μ/R²
V̇R
INT.
VRo
VR
KVΘ
+
+
(-)
V̇Θ
INT.
2 VΘ/R
VR
EQUATIONS OF MOTION
66-2776

Figure 7   Interplanetary Space Navigation Scheme Control Loops

These gains and a typical set of initial condition errors, as defined in Table V, were simulated and the time responses of the errors in position and velocity are presented in Figures 8 and 9, respectively. These errors are in terms of the navigated values minus that of the truth value $\Theta_N - \Theta_T$. These errors are in spherical coordinate parameters, i.e., Θ and R positions and V_Θ and V_R velocities. The time scale ranges from zero at injection from Earth orbit to 437 days at entry into Jupiter's sphere of influence (JSOI). The linear analysis for this choice of gains yields one real and a pair of complex closed loop poles. The real pole is at p = -28 and the complex poles have a natural frequency of 63 and damping ratio of 0.6. Frequencies are nondimensionalized by dividing by mean orbital frequency V_Θ. For the reference orbit, $V_{\Theta_0} = 0.7 \times 10^{-3}$ rad/day and $R_o = 4.75$ AU.

The time constant associated with the first order mode accordingly is approximately 50 days and that of the second order mode is 65 days. Figures 8 and 9 show the transient behavior of the system errors. The combination of initial conditions is such as to cause the angular velocity error to overshoot appreciably, which in turn yields a large peak error in radius. This error is decreasing as Jupiter is approached, but is still of the order of 25,000 km at that time.

Further attempts to improve the speed of response of the system and to optimize the gains for measurement noise do not appear warranted. The performance attained is considered to be representative, however, since relative to the orbital period, the ISN system response time needs to be short, or, equivalently, the frequency response needs to be high. To obtain this response requires high gains, and the listed gains already are approaching values at which the system sampling ripple diverges. There also was difficulty encountered in using measurements on other than the central body since the observations are not deterministic measurements of position. To compute the error in angle to the central body from planet observations required the use of the present knowledge of vehicle position, which resulted in a noisy signal. The inaccuracies introduced by this further limit the gains that can be used.

Alternative schemes for correcting both of these difficulties were considered but results of these studies indicate that the improvement to be expected will not approach that of the linear optimum filter without adding more complexity.

To provide a computer program check run, the same gains used in the two-body simulation data of Figures 8 and 9 were used in the ISN three-dimensional computer simulation. However, a measurement accuracy of 5 arc seconds was assured rather than zero. The results of this single case are presented in Figures 10 and 11. A

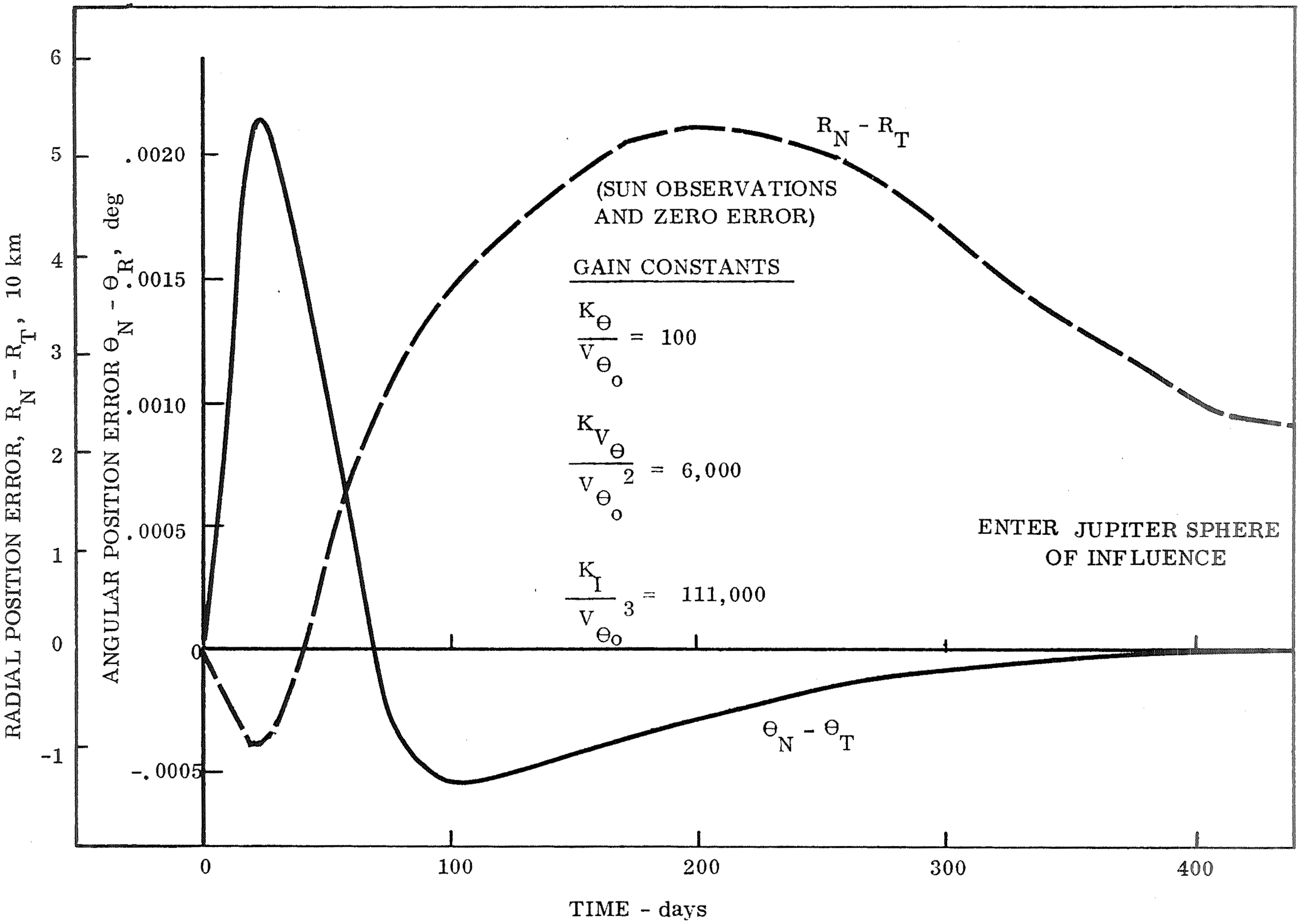

66-2873

Figure 8 ISN Performance, Two-Body Simulation, Position Errors vs Time

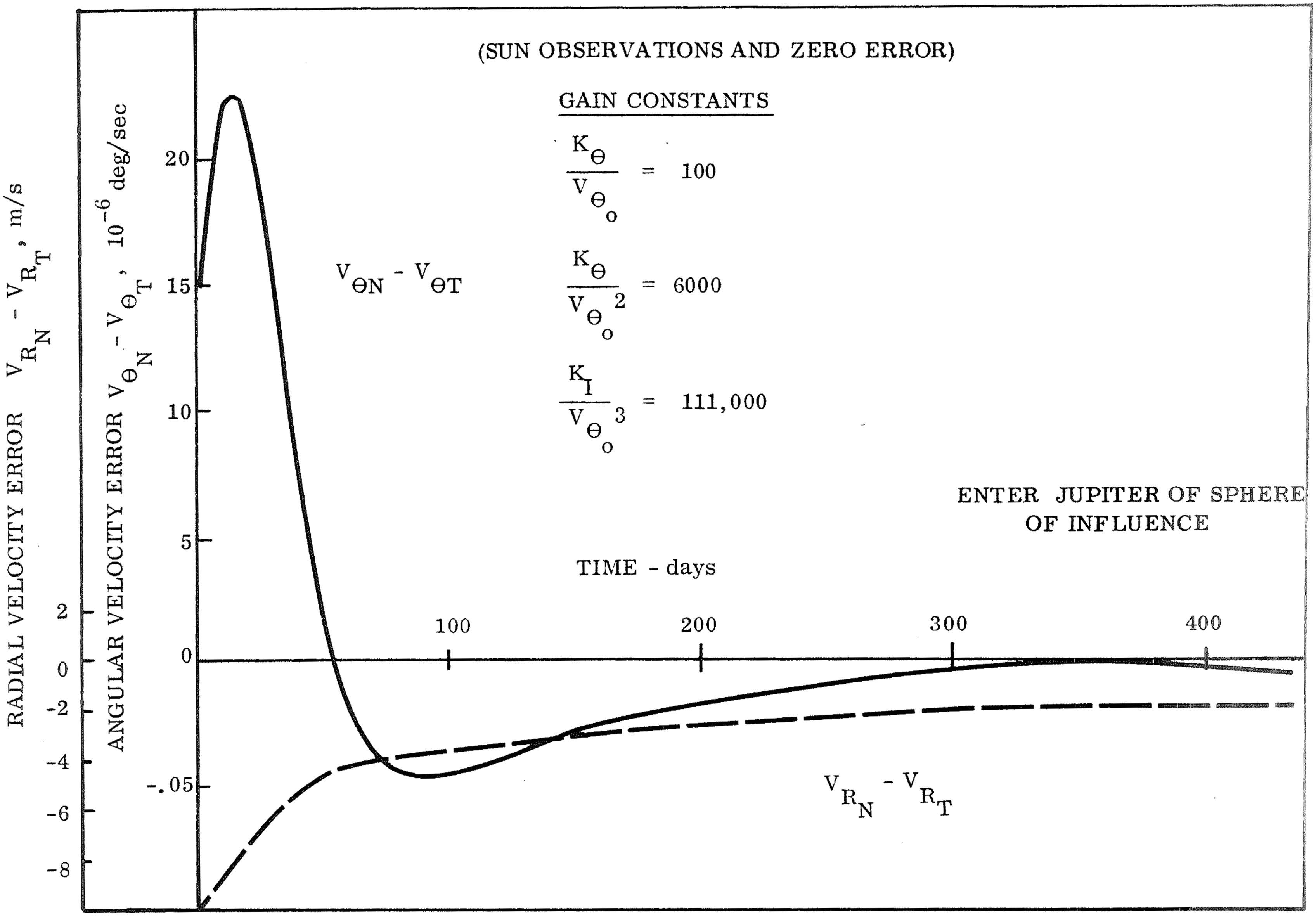

66-2874

Figure 9 ISN Performance, Two-Body Simulation, Velocity Errors vs Time

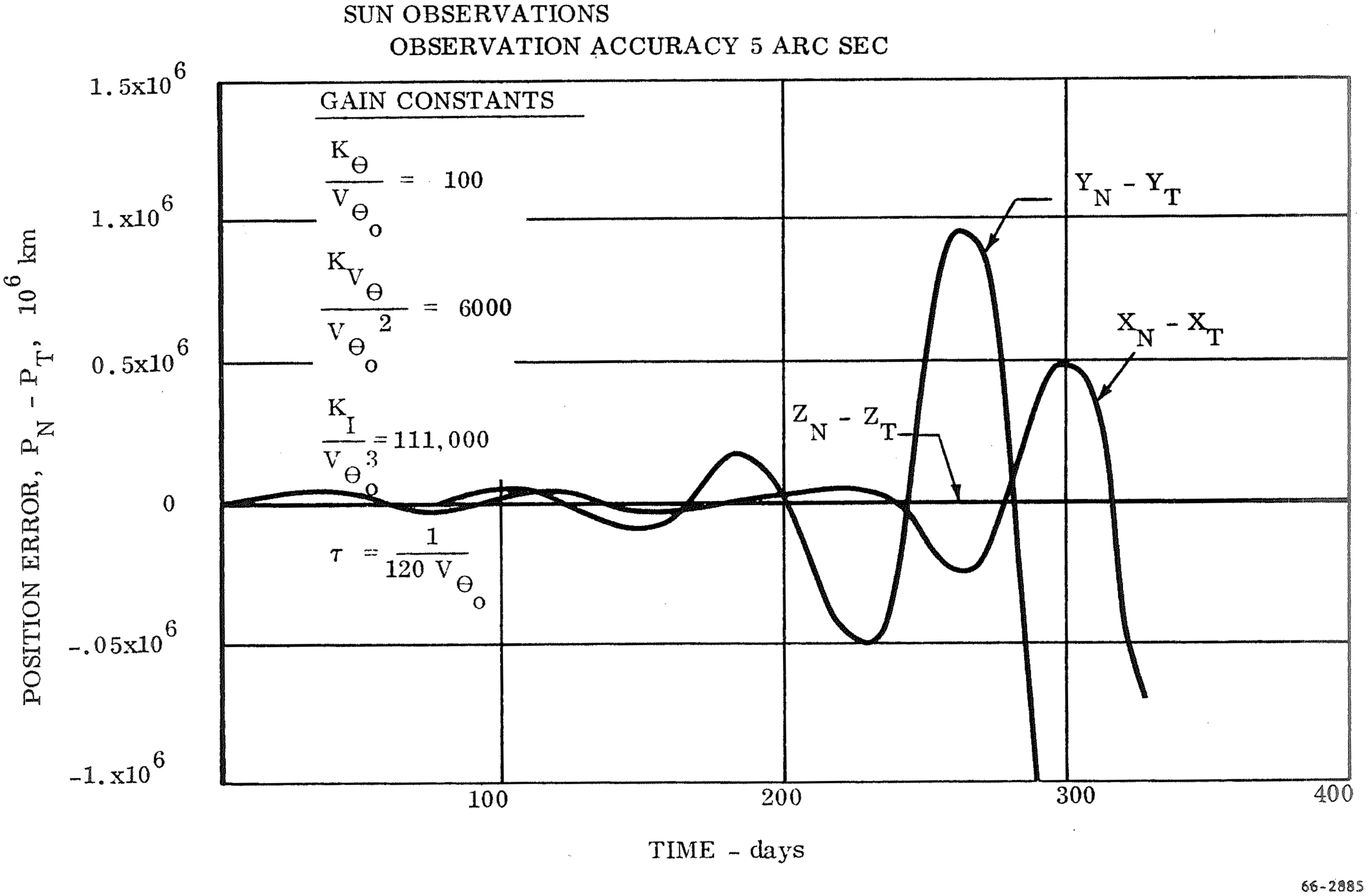

Figure 10 ISN Performance, N-Body Simulation, Position Errors vs Time

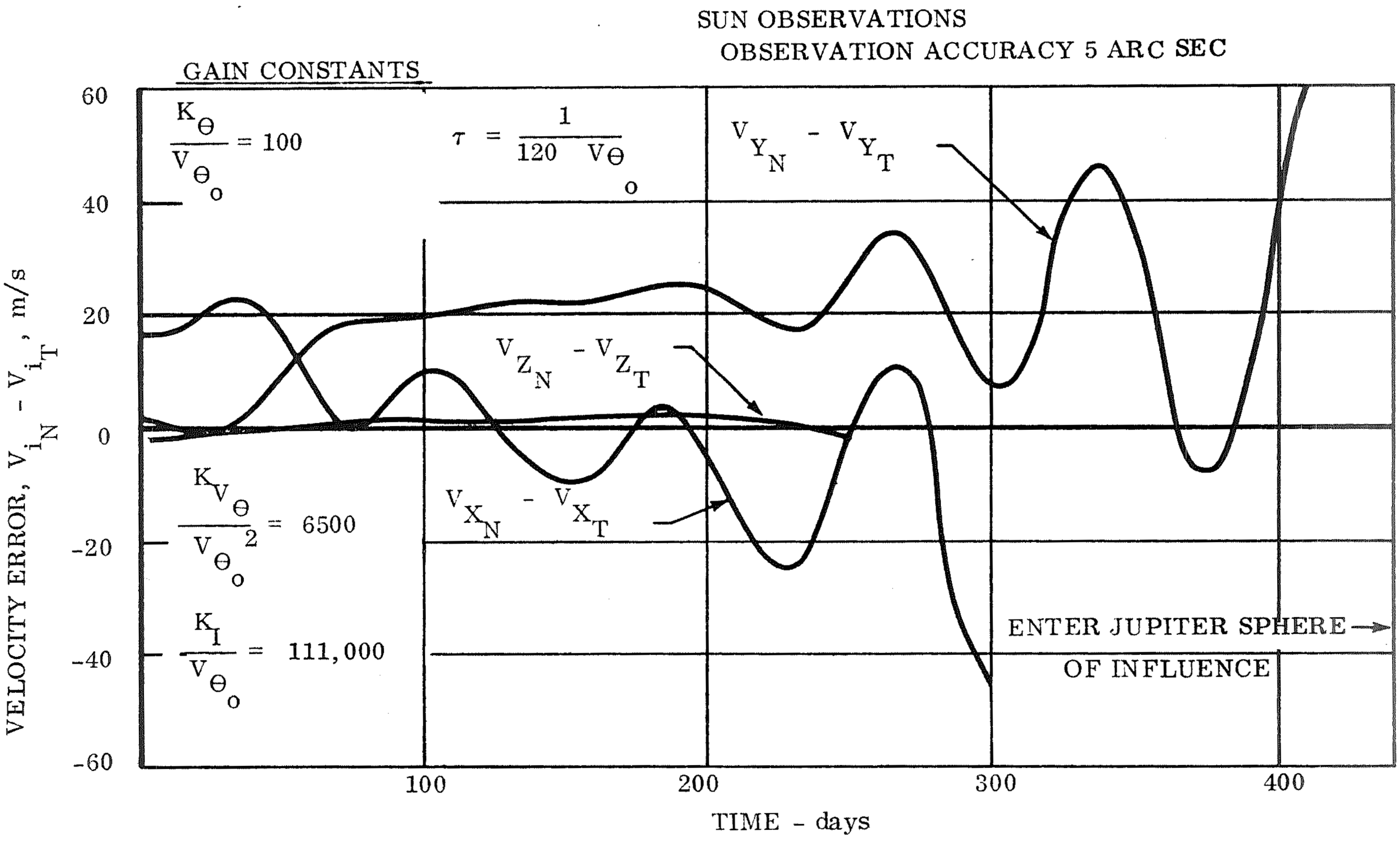

Figure 11 ISN Performance, N-Body Simulation, Velocity Errors vs Time

nominal first order filter with time constant of

$$\tau = \left(\frac{1}{120 \, V_{\Theta_o}}\right)$$

was used to smooth the error signal. These data show the divergent characters of the ISN performance in the nonlinear system. The oscillatory frequencies agree with that predicted by the linear analysis.

2. Linear Optimum Filter

The performance of the LOF navigation scheme was evaluated using the LOF simulation program which is described in detail in Volume II of this report. Using the initial conditions and the observation schedule discussed in Section IV.A.3., runs were made for one sigma total observation errors of 10, 15, and 20 arc seconds. The results of these runs are presented in Figures 12 through 17, where the standard deviations in the inertial position and velocity components are presented as a function of time. The portion of the trajectory that was simulated was from exit from the Earth's sphere of influence to entry into Jupiter's sphere. The data presented consists of the standard deviations of the LOF covariance matrix.

Two sources of error were considered, initial condition errors and observational errors. The integration scheme, integration step size, word length, and the physical model used in the truth and navigated trajectories were the same. The results shown in Figures 12 through 17 reflect the effects of these two error sources. A curve is shown on each of the figures presenting position data to indicate the rate of divergence of the navigation data if no observations were taken. This divergence is primarily due to errors in the injection velocity. In all cases it is seen that the observational data is needed primarily to bound the velocity error, thus decreasing the rate of divergence of position.

The observational schedule is defined along the ordinate of each of the curves. As previously noted, the observational frequency decreases from once every 6 days to once every 10 days after the 86th day. This is denoted by an X mark. The points where the planet observations change are indicated and a code is used to define the observable in each region. For example, during the first 20 days the Earth and Mars are observed, as indicated by E/M, whereas from 20 days to 56 days Earth and Venus (E/V) are observed; after 130 days Jupiter (J) is used as one of the observables.

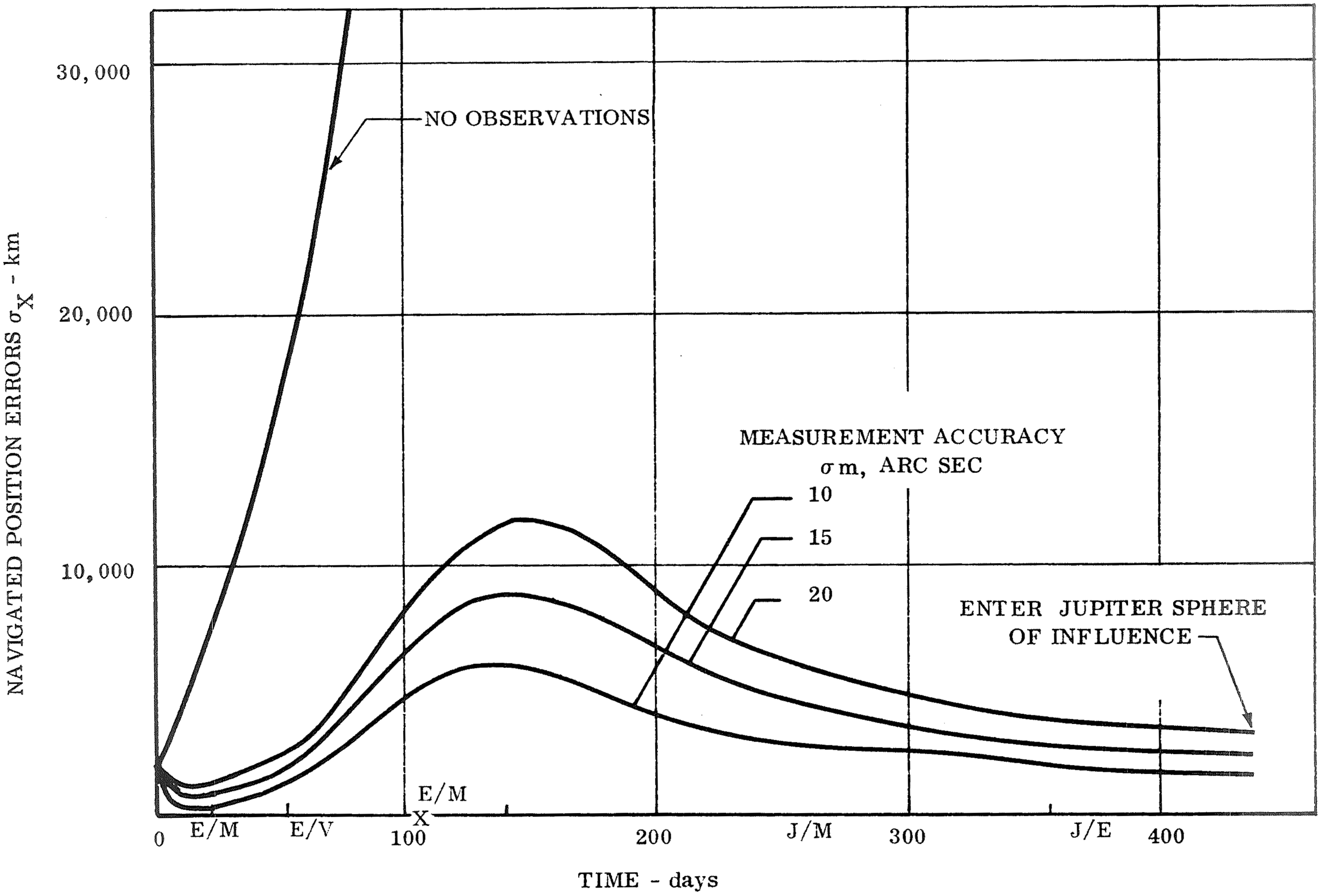

66-2880

Figure 12 LOF Navigation Scheme, σ_X Position Accuracy as a Function of Time

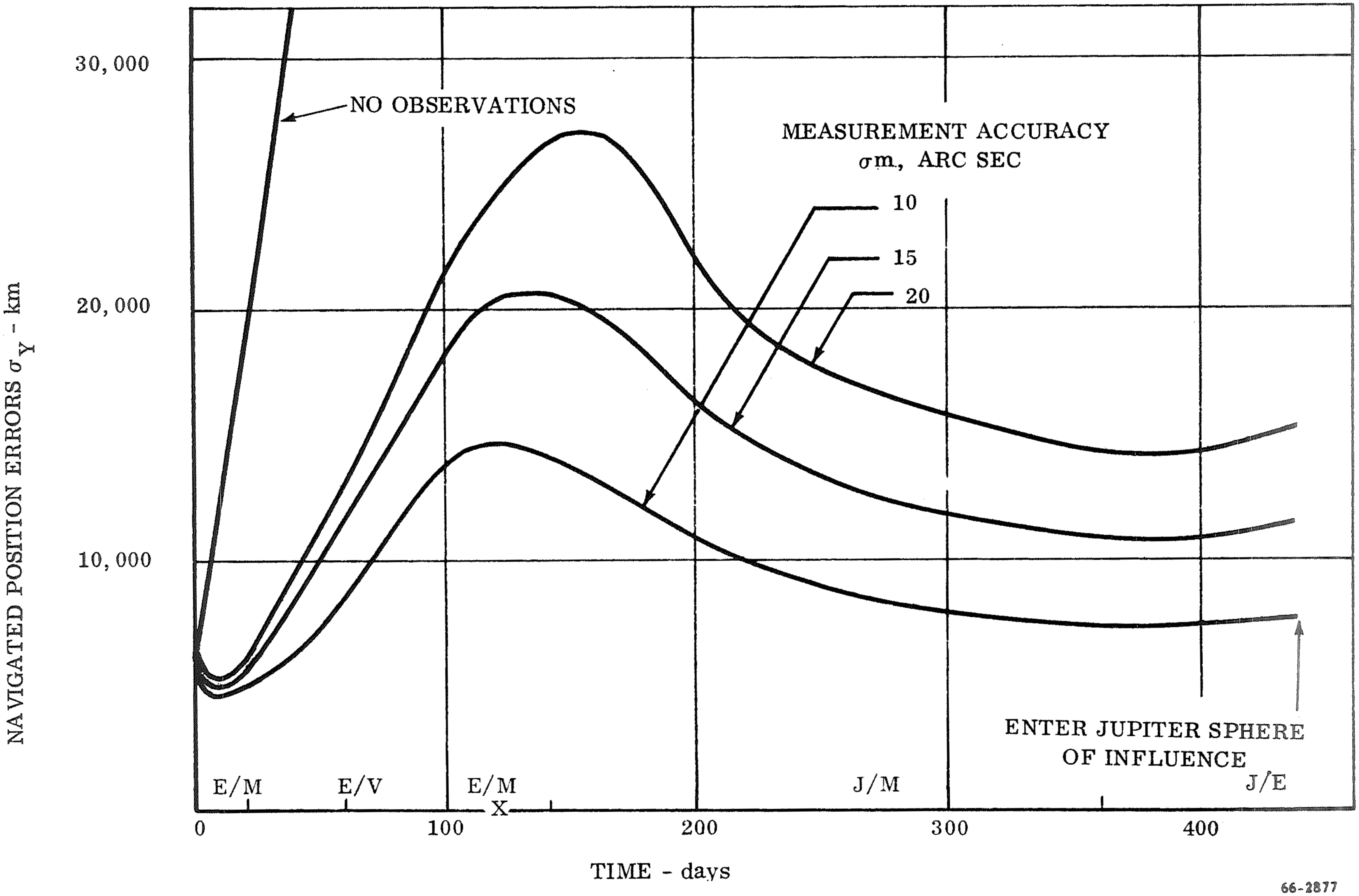

66-2877

Figure 13 LOF Navigation Scheme, σ_Y Position Accuracy as a Function of Time

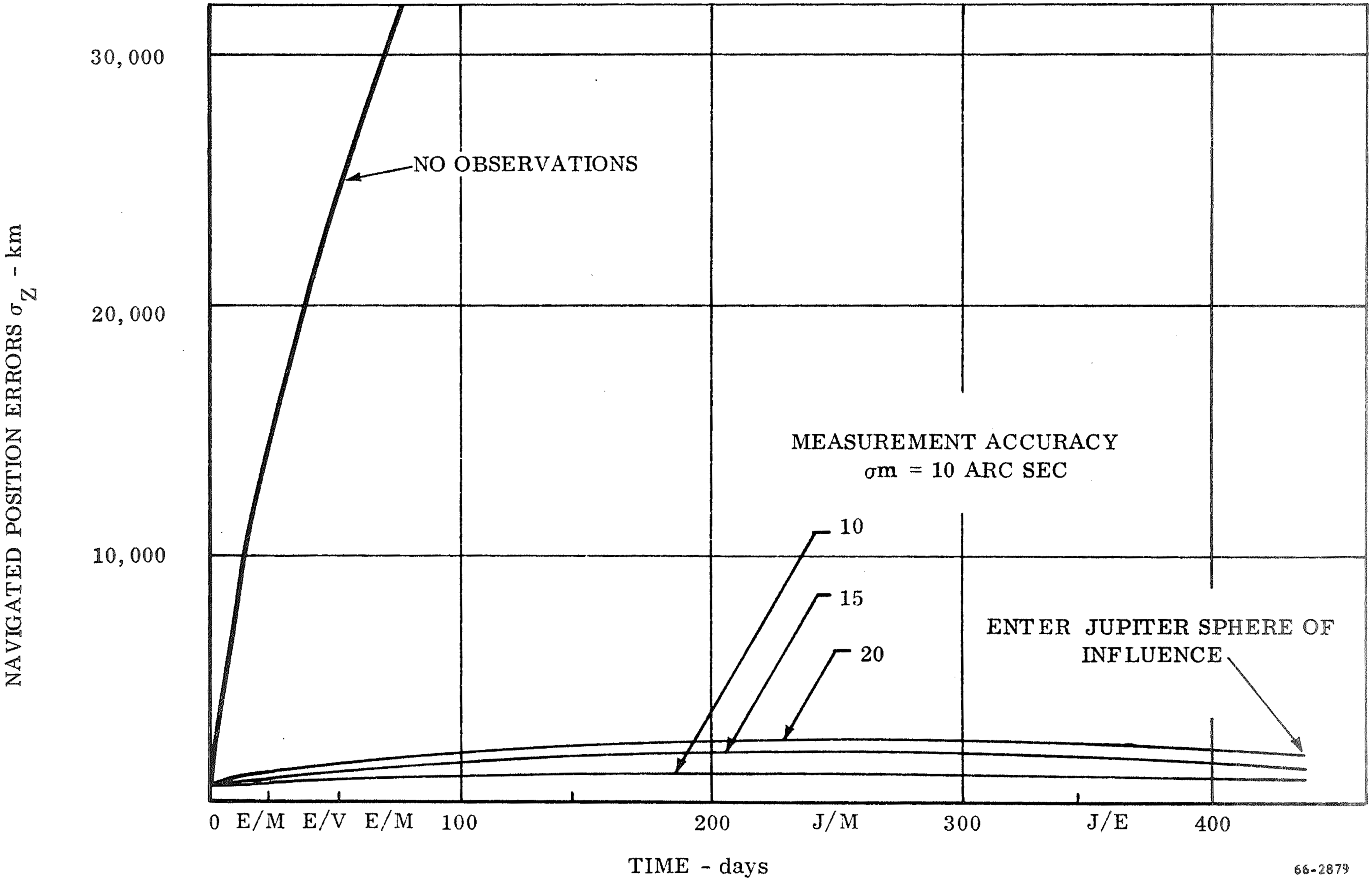

Figure 14 LOF Navigation Scheme, σ_Z Position Accuracy as a Function of Time

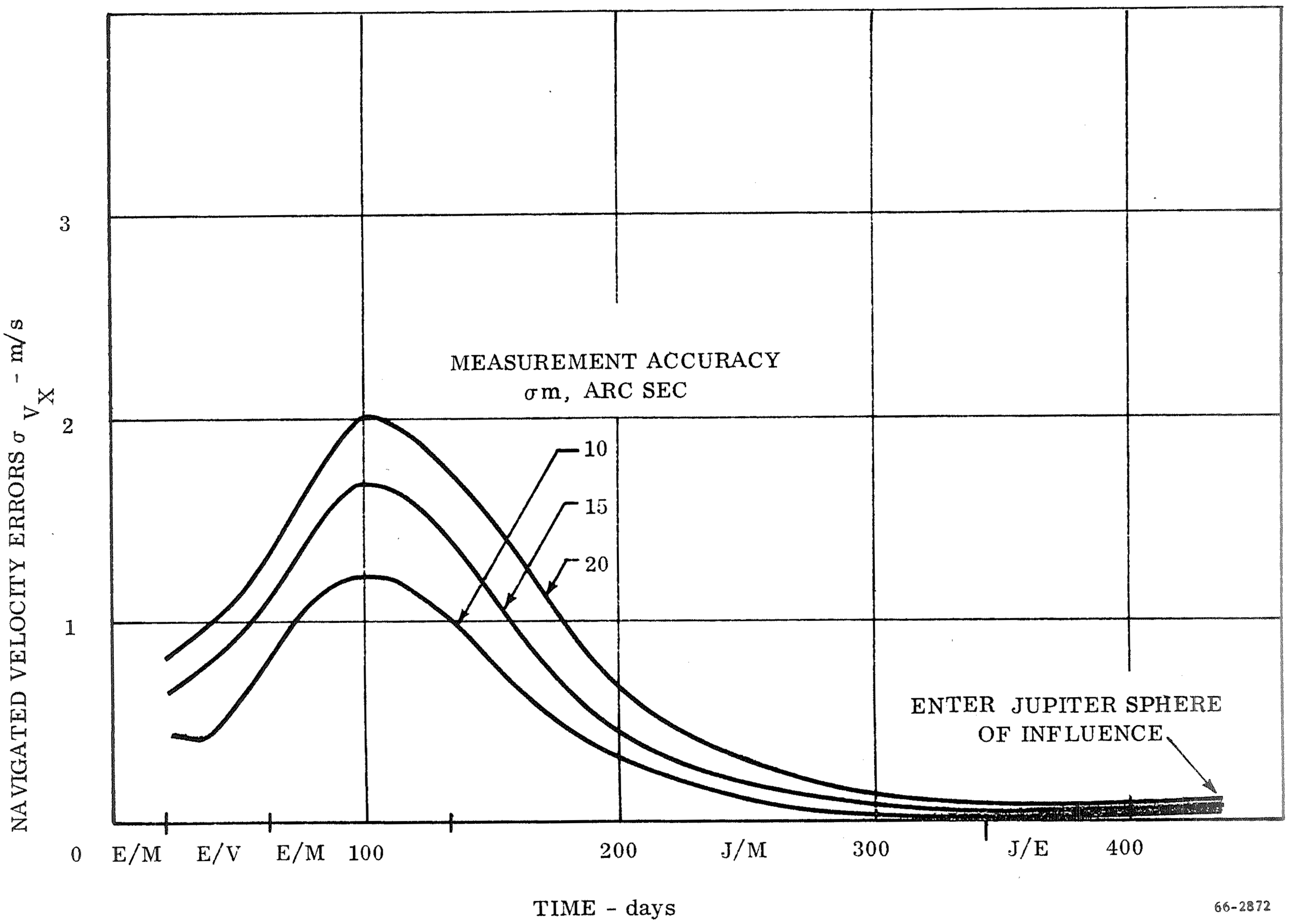

Figure 15 LOF Navigation Scheme, σ_{V_X} Velocity Accuracy as a Function of Time

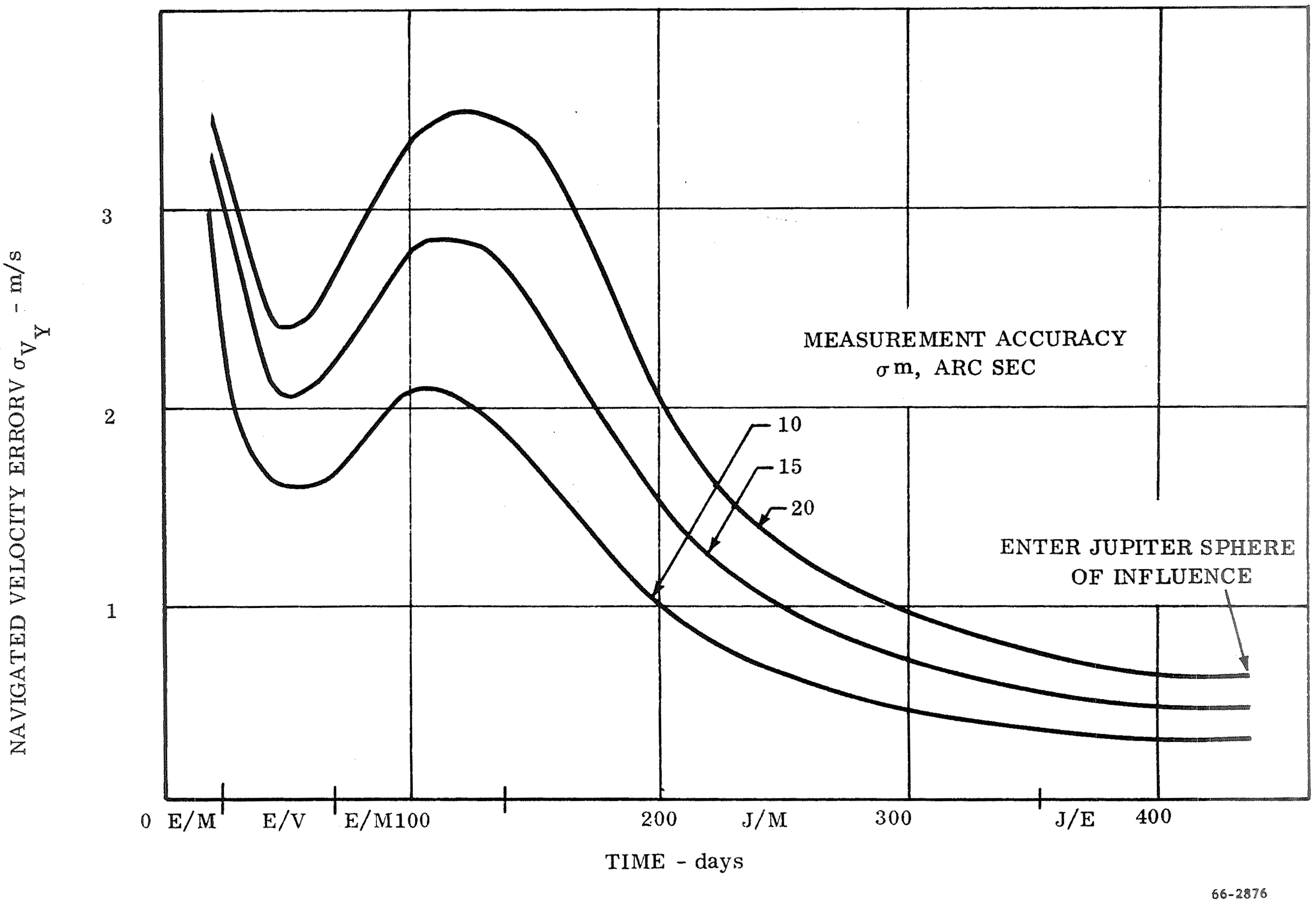

Figure 16 LOF Navigation Scheme, σ_{V_Y} Velocity Accuracy as a Function of Time

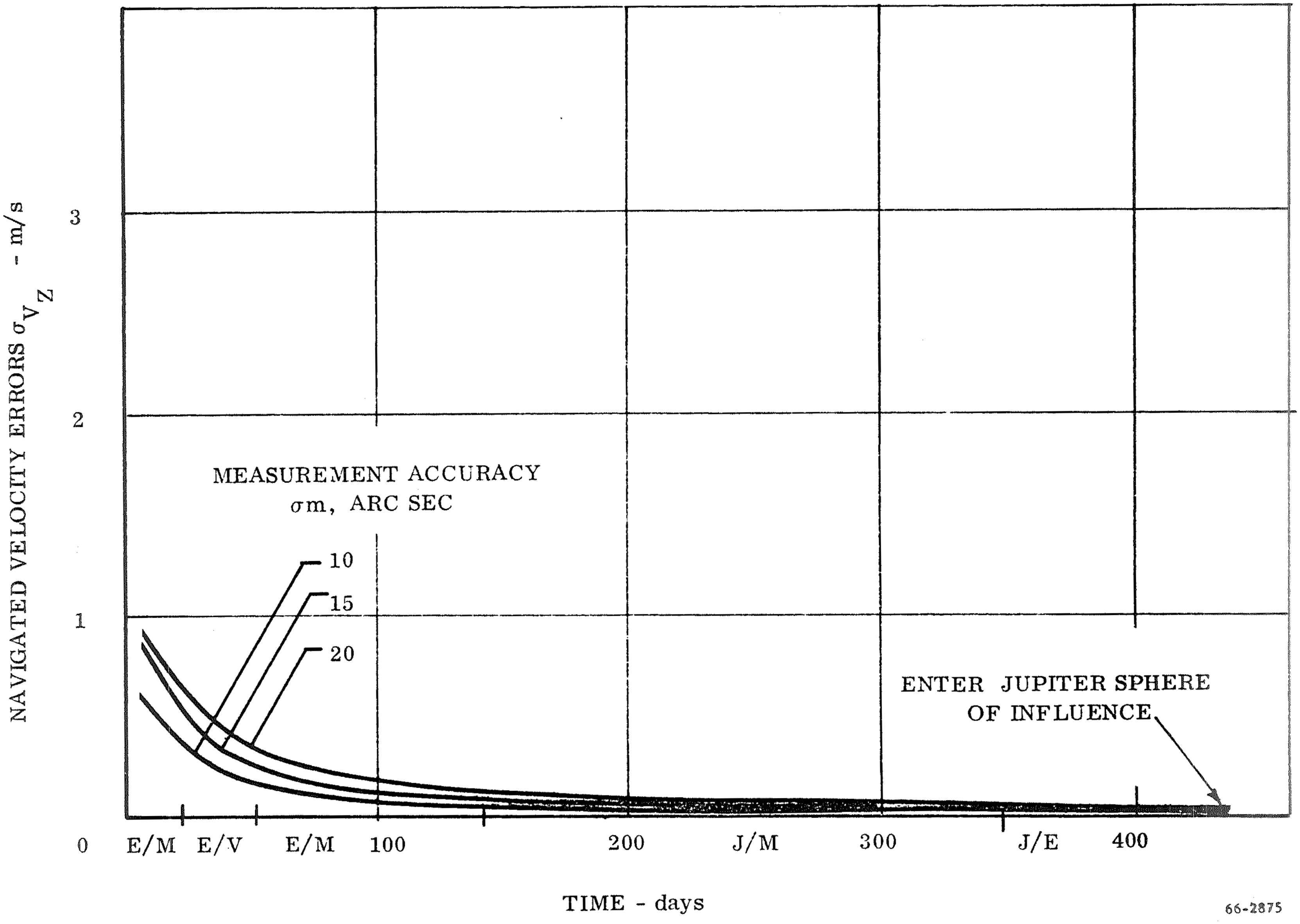

Figure 17 LOF Navigation Scheme, σ_{V_Z} Velocity Accuracy as a Function of Time

The large errors in the region of 150 days is due to the relatively long distance to the observables. In the region of 40 to 60 days the angles between the observables became relatively small and the rate of divergence is seen to increase rather rapidly. The effect of this, however, is seen most significantly in Figure 16, wherein the Y-velocity component starts to diverge again. By 120 days the angle relationships are much more favorable and the divergence rate is again decreased.

As Jupiter is approached and the observational range is decreased, the navigational error decreases to essentially a constant value, the magnitude of which is dependent on the observational accuracy. It is noted in Figure 13 that after switching from Jupiter/Mars to Jupiter/Earth observations at 350 days, the navigation error starts to diverge; this is probably caused by the greater distance to the Earth. The change in observation schedule at this point was necessary because Mars was passing in front of the Sun during this period.

It is thus seen that the navigation errors are strongly dependent on observational accuracy and the characteristics of the observable with regard to distance and their angular relationship to one another. It is postulated that the shape of the navigational curves could be controlled or shaped by varying the amount and distribution of observational data acquired. However, for a specific mission the characteristics of the observables are fixed. In this study no consideration was given to using the Sun as an observable. If a Sun sensor of equal accuracy to the planet sensor is available, the Sun should be considered in selection of the observation schedule to overcome the problem that exists in the region of Jupiter where the angle between the Sun and the nearer planets is relatively small, and much of the time these planets are obscured from view by the Sun.

The LOF simulation program was also designed to be run in a so-called Monte Carlo mode. This mode consists in running N runs with randomly selected injection and observation errors and computing the mean and standard deviation of the navigation errors. A comparison was made of the navigation error statistics generated by the LOF covariance matrix and those generated by a Monte Carlo run of the LOF program. The results of this study are shown in Figures 18 and 19 for a run in which N was ten. A sample of ten is very small, but using the theory of small samples a "chi squared" test shows that the sample statistics from the Monte Carlo run can be accepted as having come from the universe represented by the LOF covariance matrix statistics with a confidence limit of 90 percent. This study shows that it is not necessary to run the LOF simulation in the Monte Carlo mode and indicates that Monte Carlo runs of the ISN simulation for small N will give significant results.

ASSUMED AND APPLIED MEASUREMENT ERRORS { MEAN = 0.
STANDARD DEVIATION = 10 ARC SEC

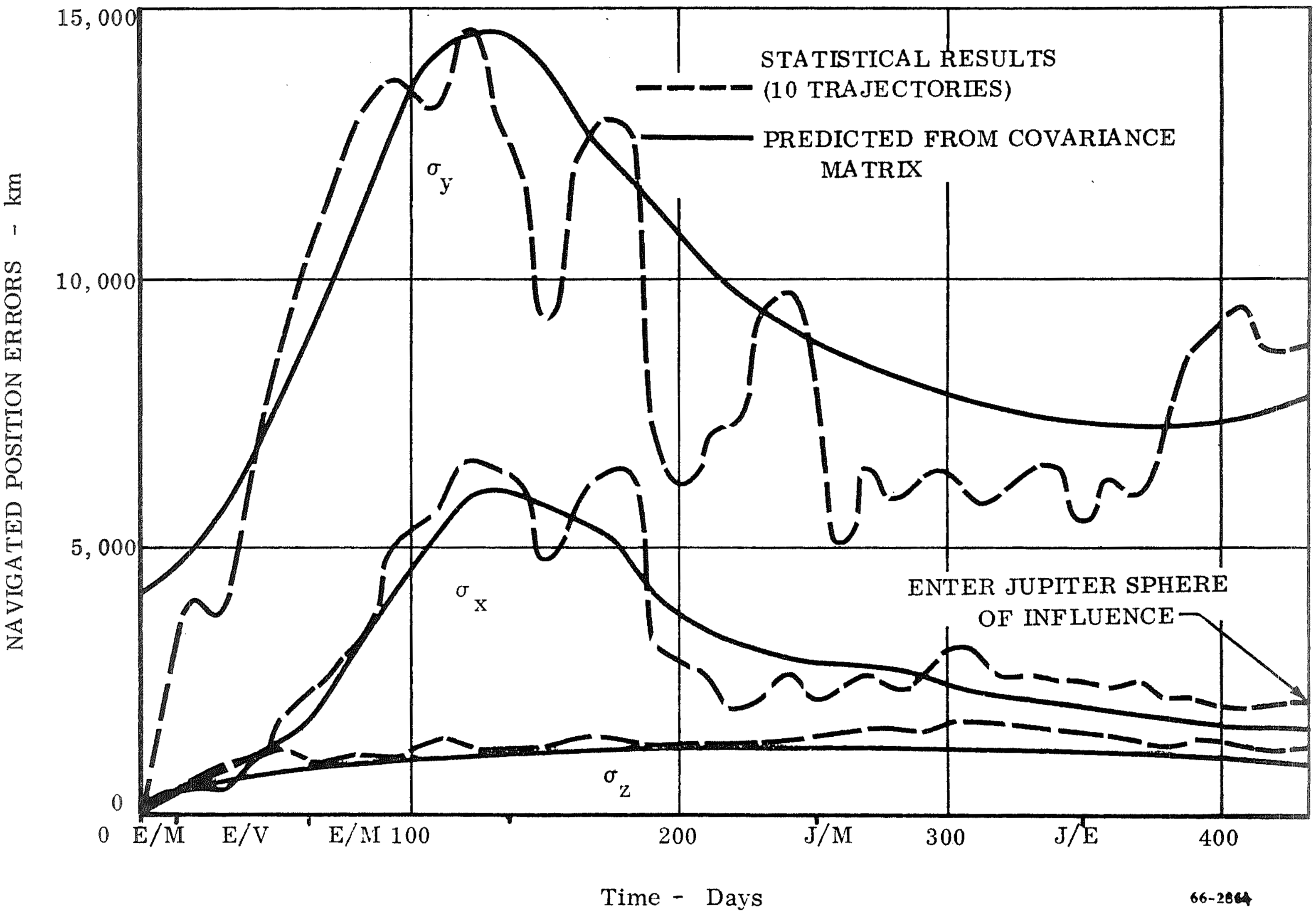

Figure 18 LOF Navigation Performance, N-Body, Position Accuracy as a Function of Time

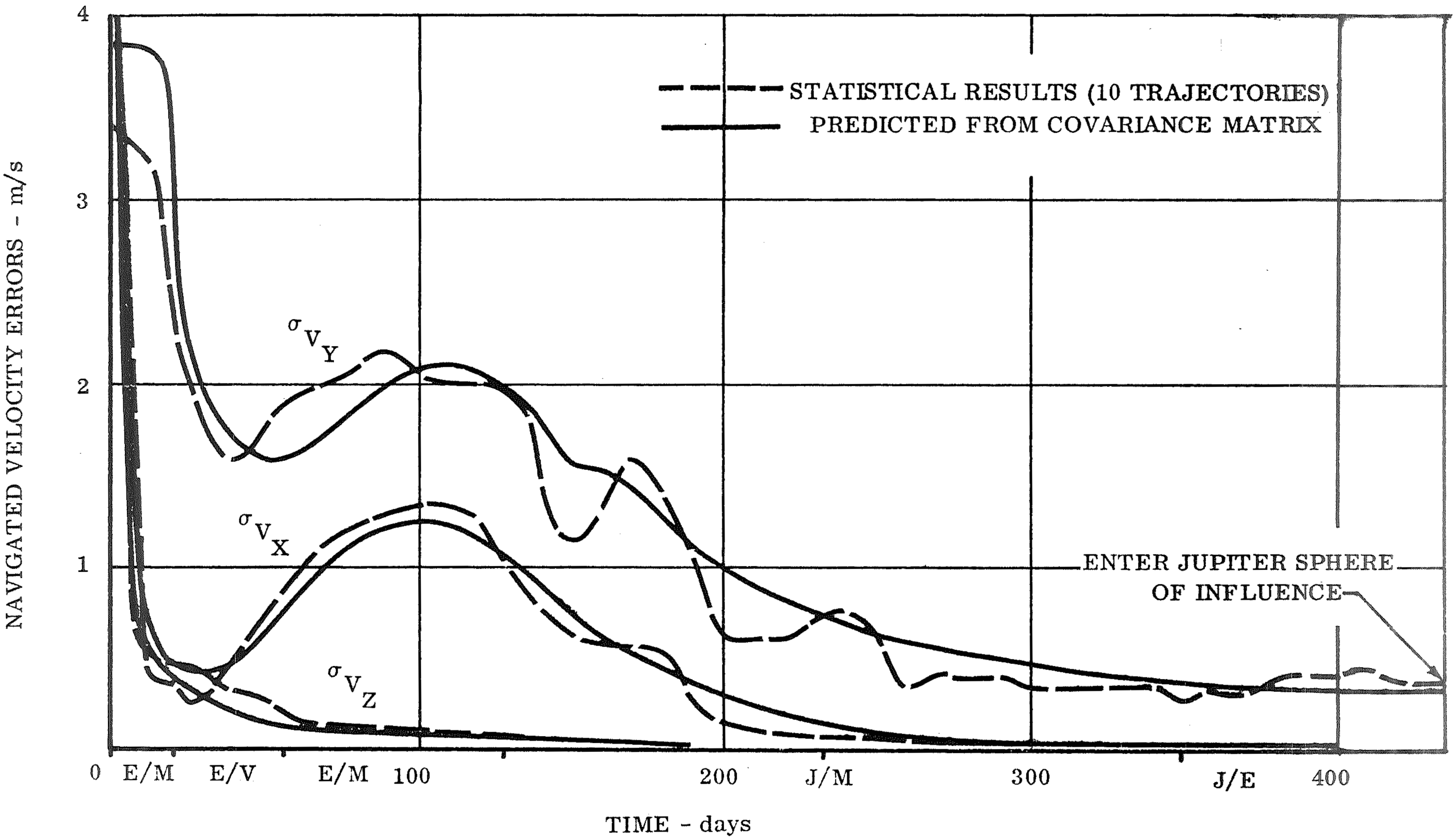

66-2870

Figure 19 LOF Navigation Performance, N-Body, Velocity Accuracy as a Function of Time

C. Navigation Requirements

The objective of the Jupiter Swing-by Mission is to place a vehicle into a post-encounter trajectory that is normal to the ecliptic plane and that has a semi-latus rectum of one astronomical unit. For purposes of determining navigational requirements for the system an evaluation of the effects of observational accuracy on the orbital parameter of the final heliocentric orbit was made. This evaluation assumed navigation to the point of entry into Jupiter's sphere of influence with perfect guidance and control. Thus, the only errors are those due to uncertainty of navigation.

The results of the runs of the LOF program reported in Section IV.B. were used with the sensitivity coefficients at entry to Jupiter's sphere of influence given in Table III to compute the standard deviation of the angle of inclination, i, and the semi-latus rectum, P, for 10-, 15-, and 20-arc second observation errors. The observational errors include the error associated with alignment and with calculation of the orientation of the vehicle as well as those of the optical sensor. Section VI contains a breakdown of the various error sources that indicate the total error with preset technology is 28 arc seconds.

The data of Figures 20 and 21 are presented such that the required observational accuracy may be defined for a given mission requirement with regard to the final heliocentric indication or semi-latus rectum, respectively. For the missions studied in this report, wherein the terminal points are in a plane normal to the ecliptic and 1 astronomical unit above the Sun, the inclination angle in radians is equivalent to a cross-range error measured in astronomical units. Thus, it is seen that the inclination error is about three times more sensitive than that of the semi-latus rectum. These figures indicate that the errors are linearly proportional to the observational accuracy, and the sensitivity is as follows:

Parameter	Error Sensitivity
Inclination	1.05×10^{-4} radians/arc second
Semi-latus rectum	0.36×10^{-4} AU/arc second

For an observation accuracy of 28 arc seconds the errors in the final orbital parameters are 0.00296 radians and 0.00102 astronomical units for the inclination and semi-latus rectum, respectively.

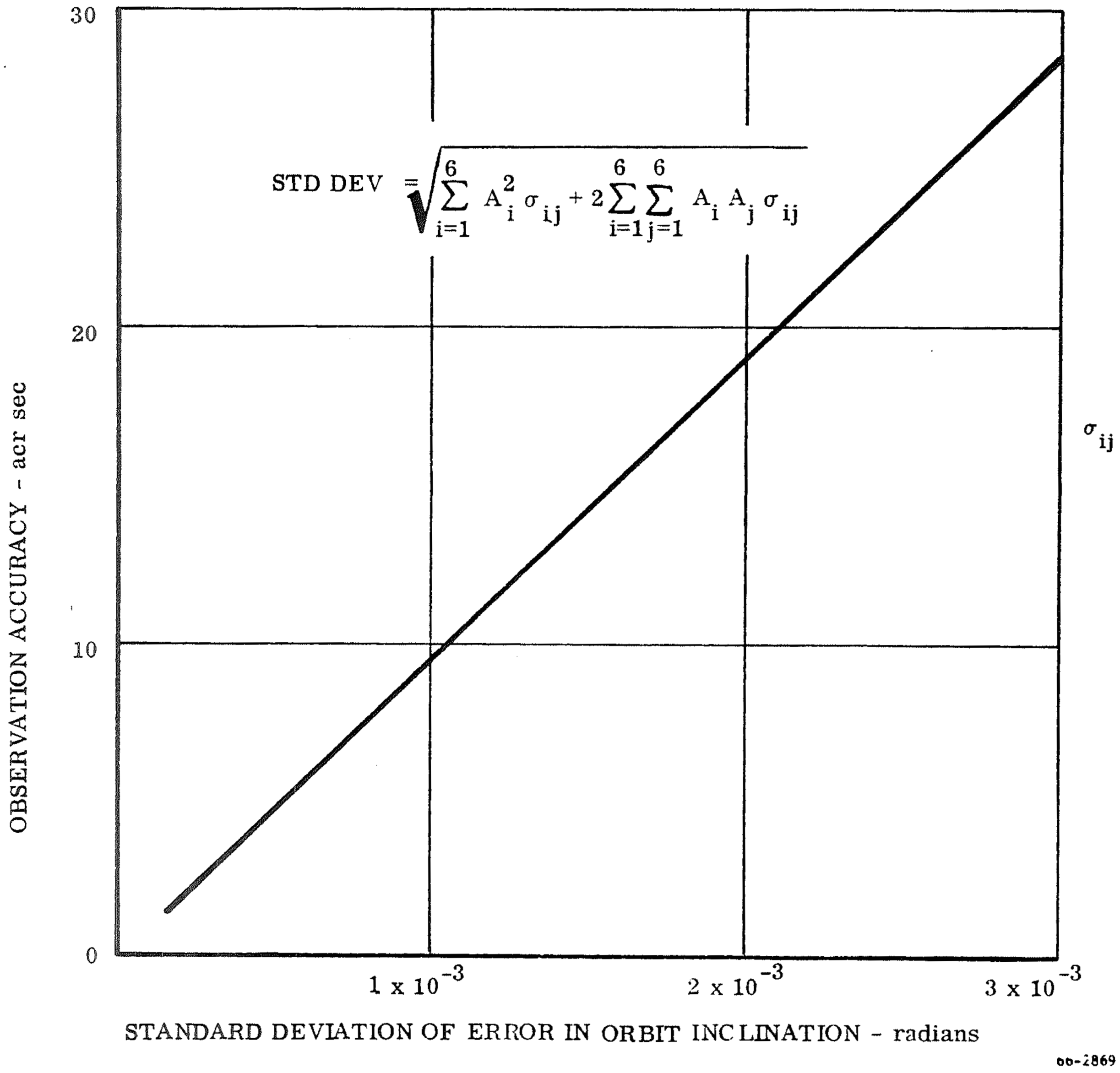

$$\text{STD DEV} = \sqrt{\sum_{i=1}^{6} A_i^2 \sigma_{ij} + 2\sum_{i=1}^{6}\sum_{j=1}^{6} A_i A_j \sigma_{ij}}$$

$$\sigma_{ij} = \begin{bmatrix} \sigma_X^2 & \sigma_{XY} & \sigma_{XZ} & \sigma_{XV_X} & \sigma_{XV_Y} & \sigma_{XV_Z} \\ \sigma_{YX} & \sigma_Y^2 & \sigma_{YZ} & \sigma_{YV_X} & \sigma_{YV_Y} & \sigma_{YV_Z} \\ \sigma_{ZX} & \sigma_{ZY} & \sigma_Z^2 & \sigma_{ZV_X} & \sigma_{ZV_Y} & \sigma_{ZV_Z} \\ \sigma_{V_X X} & \sigma_{V_X Y} & \sigma_{V_Y Z} & \sigma_{V_X}^2 & \sigma_{V_X V_Y} & \sigma_{V_X Y_Z} \\ \sigma_{V_Y X} & \sigma_{V_Y Y} & \sigma_{V_Y Z} & \sigma_{V_Y V_X} & \sigma_{V_Y}^2 & \sigma_{V_Y V_Z} \\ \sigma_{V_Z X} & \sigma_{V_Z Y} & \sigma_{V_Z Z} & \sigma_{V_Z V_X} & \sigma_{V_Z V_Y} & \sigma_{V_Z}^2 \end{bmatrix}$$

$A_1 = 0.4813 \times 10^{-6}$

$A_2 = 0.972 \times 10^{-7}$

$A_3 = 0.815 \times 10^{-6}$

$A_4 = 0.1636 \times 10^{-2}$

$A_5 = 0.165 \times 10^{-3}$

$A_6 = 0.2663 \times 10^{-2}$

Figure 20 Error in Inclination of Final Heliocentric Orbit as a Function of Observation Accuracy

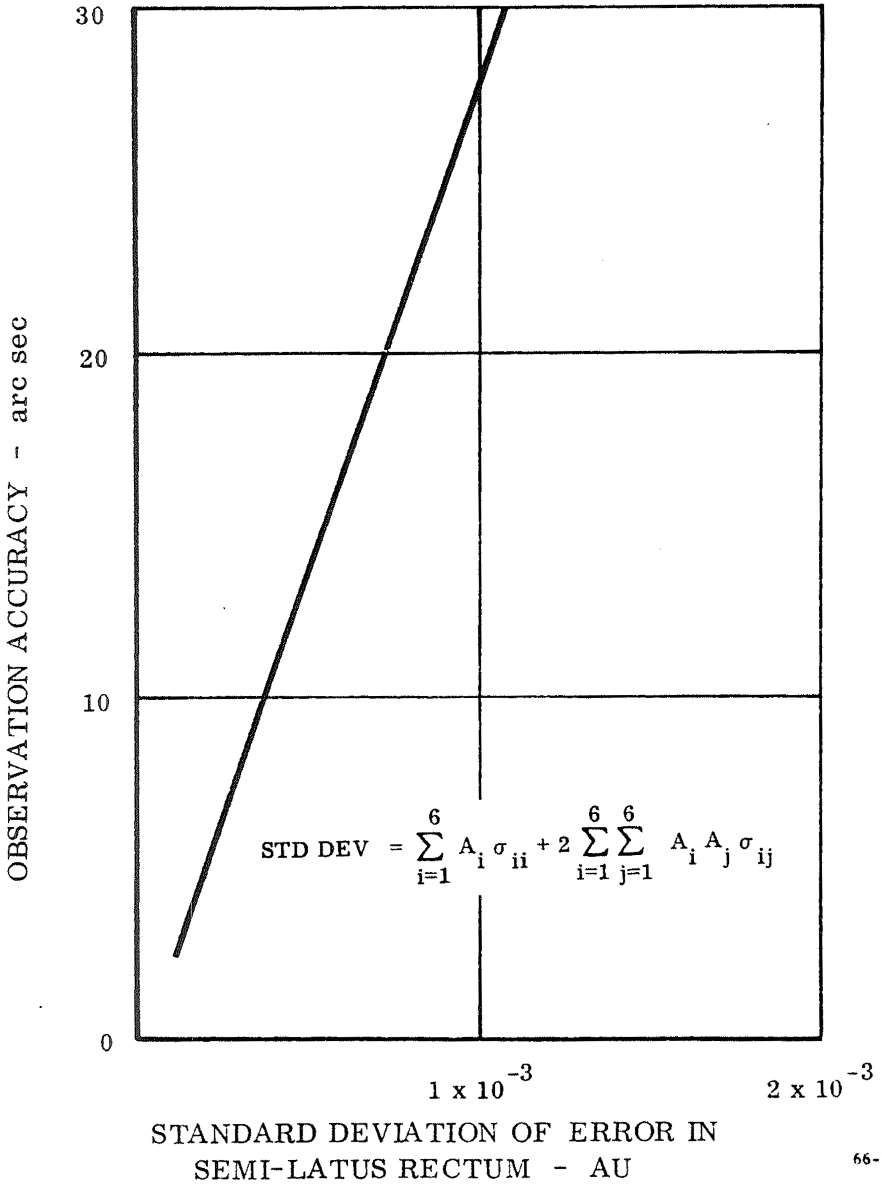

$$\text{STD DEV} = \sum_{i=1}^{6} A_i \sigma_{ii} + 2 \sum_{i=1}^{6} \sum_{j=1}^{6} A_i A_j \sigma_{ij}$$

66-2868

$$\sigma_{ij} = \begin{bmatrix} \sigma_X^2 & \sigma_{XY} & \sigma_{XZ} & \sigma_{XV_X} & \sigma_{XV_Y} & \sigma_{XV_Z} \\ \sigma_{YX} & \sigma_Y^2 & \sigma_{YZ} & \sigma_{YV_X} & \sigma_{YV_Y} & \sigma_{YV_Z} \\ \sigma_{ZX} & \sigma_{ZY} & \sigma_Z^2 & \sigma_{ZY_X} & \sigma_{ZV_Y} & \sigma_{ZV_Z} \\ \sigma_{V_X X} & \sigma_{V_X Y} & \sigma_{V_X Z} & \sigma_{V_X}^2 & \sigma_{V_Z V_Y} & \sigma_{V_X V_Z} \\ \sigma_{V_Y X} & \sigma_{V_Y Y} & \sigma_{V_Y Z} & \sigma_{V_Y V_X} & \sigma_{V_Y}^2 & \sigma_{V_Y V_Z} \\ \sigma_{V_Z X} & \sigma_{V_Z Y} & \sigma_{V_Z Z} & \sigma_{V_Z V_X} & \sigma_{V_Z V_Y} & \sigma_{V_Z}^2 \end{bmatrix}$$

$A_1 = -0.28693 \times 10^{-5}$

$A_2 = -0.30095 \times 10^{-5}$

$A_3 = +0.36485 \times 10^{-5}$

$A_4 = -0.95540 \times 10^{-2}$

$A_5 = -0.19548 \times 10^{-2}$

$A_6 = +0.12177 \times 10^{-1}$

Figure 21 Error in Semi-Latus Rectum of Final Heliocentric Orbit as a Function of Observation Accuracy

V. GUIDANCE

Explicit on-board guidance schemes were considered under the work of this contract to determine if further study of such concepts is warranted. In this area two guidance schemes were evaluated; one being a midcourse correction to control the point of entry into Jupiter's sphere of influence, the second being terminal correction scheme at entry into Jupiter's sphere of influence. These two schemes are described below and in Appendix C.

A. Guidance Schemes

1. Midcourse Guidance

Present guidance schemes are based on linearizations around a precomputed reference trajectory that passes through the desired end point. These techniques express end-point miss-distance as a linear function of the deviation of the present position and velocity from the reference trajectory using transition matrices evaluated along that particular reference trajectory. Because of several possible error sources during the launch phase, a number of such reference trajectories and associated sets of transition matrices must be precomputed and stored in the flight computer memory. This places a restriction on launch and abort procedures, since launch must be accomplished within a prescribed short period of time, and abort on trajectory alteration can only occur at specific "decision" points within the mission.

UACSC has developed an on-board midcourse guidance scheme that is completely self contained and requires no prelaunch computations. This guidance scheme, which is shown schematically in Figure 22, is a variation of the fixed time of arrival type of guidance. Prior to a scheduled guidance correction, the equations of motion are integrated ahead to the time, T, at which interception of a given point in space is desired. The initial condition used in the integration are the navigated position and velocity at the time the guidance correction is to be made, t_c. The transition matrix, $\phi(T, t_c)$, is generated simultaneously with the integration of the equations of motion. The calculated position at time T is compared with the desired position and the resulting deviation in position is operated on by the inverse of $\phi(T, t_c)$ to obtain the velocity correction needed at time t_c. A more detailed mathematical analysis of this procedure is given in Appendix C. This procedure of generating a new reference trajectory and a new transition matrix is repeated at each scheduled correction point.

The use of transition matrices is based on the assumption that the deviations from the reference trajectory are small. If the calculated deviation at time T does not satisfy this assumption then the calculated velocity correction is added to the computed velocity at t_c and with these revised initial conditions a new reference trajectory is

MIDCOURSE SCHEME - FIXED TIME OF ARRIVAL

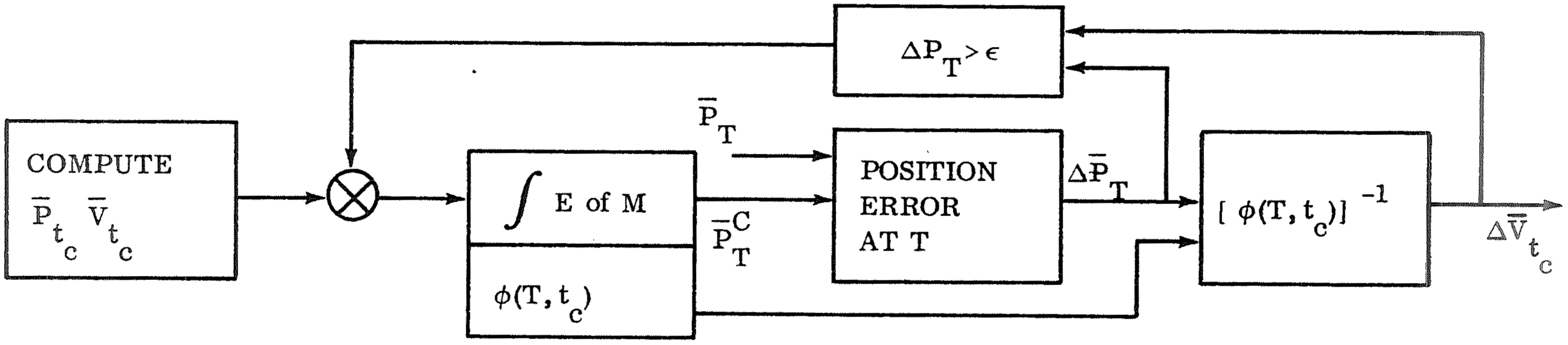

COMPUTE $\bar{P}_{t_c}$ $\bar{V}_{t_c}$
$\Delta P_T > \epsilon$
$\int$ E of M
$\phi(T, t_c)$
$\bar{P}_T$
$\bar{P}_T^C$
POSITION ERROR AT T
$\Delta\bar{P}_T$
$[\phi(T, t_c)]^{-1}$
$\Delta\bar{V}_{t_c}$

TERMINAL SCHEME - 2-BODY JUPITER TRANSFER

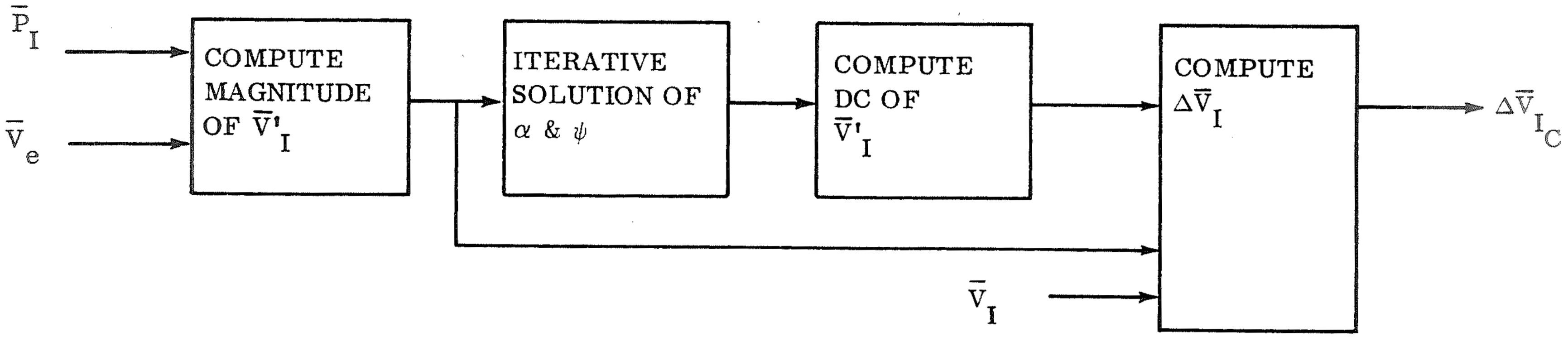

$\bar{P}_I$
$\bar{V}_e$
COMPUTE MAGNITUDE OF $\bar{V}'_I$
ITERATIVE SOLUTION OF α & ψ
COMPUTE DC OF $\bar{V}'_I$
COMPUTE $\Delta\bar{V}_I$
$\Delta\bar{V}_{I_C}$
$\bar{V}_I$

Figure 22 Guidance Schemes, Explicit and Self-Contained

generated. This procedure is repeated until the deviation in position does satisfy the assumption of linearity. The accumulated velocity correction is then applied.

The deviation from the desired position at time T contains errors due to the integration method, to the potential function used in the equations of motion, and to the navigation errors associated with the initial conditions at time t_c. The computer velocity corrections reflect these errors. This difficulty is offset by the fact that the effect of these errors is reduced at subsequent correction points.

The correction schedule used in the simulation of the guidance scheme outlined above was based on making a correction at a fixed percentage of the time to go after the previous correction. The percentage used was 33%. The first correction was made 190 days after injection. This point was selected because the simulation of the LOF navigation scheme indicates substantial improvement in the estimation of position and velocity at this point.

2. Simplified Guidance

The objective of the Jupiter Swing-by Mission is to place a vehicle into a heliocentric orbit that is normal to the ecliptic plane and has a semi-latus rectum of one astronomical unit. The other elements of the orbit are not specified; therefore, it is not necessary that the vehicle be guided to a predetermined point on Jupiter's sphere of influence. Thus a simplified guidance scheme, which uses a single velocity correction at entry into Jupiter's sphere of influence, was developed. The mathematical analysis of this guidance scheme is presented in Appendix C.

The single velocity correction is not aimed at causing the vehicle to exit from Jupiter's sphere of influence at a predetermined point but to exit from the sphere with a given velocity vector. The simplified guidance scheme is based on the assumption that two-body equations hold within Jupiter's sphere of influence. This assumption results in a simple mathematical relationship to determine the velocity correction, which is easily mechanized in an on-board computer. The basic logic of this scheme is also shown in Figure 22. On the basis of the velocity at exit from Jupiter's sphere of influence, $\bar{V}_e$, and the position vector at entry into Jupiter's sphere of influence, $\bar{P}_I$, the magnitude of the required velocity vector V_I is computed, an iterative solution is made of the turning angle, α, and the angle, ψ, between the vectors $\bar{P}_I$ and $\hat{\bar{V}}_I$. Then the direction cosines of the vector $\bar{V}_I$ can be computed and compared with the actual velocity vector, $\bar{V}_I$, at entry into the Jupiter's sphere of influence. This establishes the velocity correction, $\Delta\bar{V}_{I_c}$, to be applied.

B. Comparison

The on-board midcourse guidance and simplified terminal guidance schemes were evaluated to determine if further study of such concepts is warranted. The results of these studies are presented in Table VII. Data for three guidance runs are presented, one with four midcourse corrections as shown, the second with the same midcourse corrections plus a terminal correction, and the third with only a terminal correction. For reference, auxiliary data is also presented for the final heliocentric orbital elements of the midcourse reference trajectory and the nominal trajectory with no corrections. The N-body final heliocentric orbital elements as listed represent the terminal conditions. Those of the two-body computation are presented only for comparison. The terminal guidance scheme is dependent on the validity of the assumption that the motion through Jupiter's sphere of influence may be represented by two-body motion.

All the runs except the N-body midcourse reference trajectory were run with a common set of initial condition errors listed below and 10 arc sec observation errors for the basic observational schedule described previously. The assumed initial conditions at entry into the Sun's sphere of influence on the heliocentric transfer orbit were:

$\Delta X = 418,874 \text{ km}, \quad \Delta V_x = -6.388$

$\Delta Y = 315.652 \text{ km}, \quad \Delta V_y = -28.571$

$\Delta Z = 25.014 \text{ km}, \quad \Delta V_z = 7.661$

All the ΔV corrections assumed zero control error.

Without any correction, the final heliocentric orbit would have an inclination of 44.86 degrees and semi-latus rectum of 0.22 AU. Thus, it is seen that both schemes are effective in guiding the vehicle into the desired orbit. For the conditions assumed, the midcourse correction required a total ΔV of 122.5 m/s. For this case the resulting N-body orbital parameters should be compared with those of the midcourse reference trajectory. The midcourse plus terminal corrections are seen to require a total correction of 174.1 m/s; in this case, however, the terminal correction made the final conditions worse rather than better. The terminal correction only case required a total correction of 384.75 or about three times that of the correction for the midcourse scheme; however, the performance of this case was the best. In both of the terminal correction cases the final elements are independent of the midcourse reference trajectory since the terminal correction attempts to attain a 90-degree, 1.0 AU final heliocentric condition based on two-body computations. It is seen that both of the terminal correction runs attain the desired two-body conditions yet N-body or actual terminal conditions are quite different. This

TABLE VII

COMPARISON OF GUIDANCE CORRECTION SCHEMES

Guidance Runs		ΔV m/s	Deviation from Reference		Final Heliocentric Elements				Perijove in Jupiter Radii
					N-Body		Two-Body		
			i degrees	P AU	i	P	i	P	
Midcourse									
Correction	Days								
1	190	120.239							
2	280	1.575							
3	340	0.582							
4	380	0.122							
	Total	122.518	2.6269	-.27957	87.0433	1.32948	89.5895	1.03690	5.80
Midcourse and Terminal									
Midcourse		122.518							
Terminal		51.616							
	Total	174.134	4.1901	.36646	85.8099	1.36646	89.8656	1.00275	5.45
Terminal		384.752	1.6335	.10504	88.3665	1.10504	89.8782	1.00005	6.74
Auxiliary Data:									
N-Body Midcourse Reference Trajectory					89.6702	1.04990	89.3082	.89115	7.15
Nominal Trajectory with No Corrections					44.8610	.21772	31.0580	.37043	23.7

would suggest that the degree of validity of the two-body computations varies between the various runs. Further investigation showed that the degree of validity or correlation between N-body and two-body results was a function of the point of closest approach to Jupiter. There is a value of this distance at which the correlation is very good. However, if you are closer than this, Jupiter's oblateness has a very strong effect; if you are further out the Sun's gravitational attraction invalidates the two-body computation. Thus, the relative effectiveness of the various guidance schemes appears to be overshadowed by the effects of variations of the perijove of the various trajectories on the final heliocentric orbital elements. For all these runs, except the trajectory with no corrections, the nondimensional perijove was between 5.4 and 7.2 Jupiter radii. In the no correction case, the perijove was 23.7 Jupiter radii.

The results of these guidance studies indicate that further work is warranted to better define these effects and to develop techniques and logic to provide compensation and insure application of terminal corrections which would improve the final heliocentric orbital parameters.

VI. COST FACTOR STUDIES

As part of the contract studies, a preliminary assessment was made of the cost factors involved in providing a navigation, guidance and control system for the Jupiter Swing-by Mission. These cost factors are in terms of system weight, power, propellant requirements, system accuracy, and system reliability. To make this assessment, a navigation, guidance and control system, termed the Deep Space Navigation System (DSNS), was mechanized by using existing system hardware and technology, and its operation and performance capabilities for the Jupiter Swing-by Mission were defined. This system, which is intended as a preliminary design to assess feasibility of mechanization, represents a single case example of the capabilities of existing hardware when using the example planet measurement schedule developed under this contract. The capability of current equipment on this mission could be optimized with respect to mission objectives and optimum system characteristics could be defined; however, such an optimization is beyond the scope of the present contract. Therefore, the intent of the work described in this section is to:

1. Define performance capability and characteristics of a navigation, guidance and control system based on existing hardware by using the example trajectory and planet measurement schedule described in Section IV.
2. Quantitatively establish trade-offs of certain cost factors, such as propellant requirements, power requirements, and system accuracy.
3. Examine in-flight operational procedures and define a realistic sequence of events.
4. Define the major system design and operational problem areas.
5. Develop the basis for an approach to and the analysis techniques for performing system trade-off studies to allow selection of optimum total system designs for space missions.

In this study, the DSNS has been mechanized with a strapdown inertial system to provide a navigation reference for acquiring observational data and/or executing guidance corrections. Optical sensors and other equipment used are those under development by UACSC or familiar to UACSC through industry survey activities. Peripheral equipment, such as the environmental control subsystem and telemetry and command subsystem, are not included in the DSNS mechanization. Although these equipments are needed for proper functioning of the DSNS, an undefined interface with upper stage payload exists, the solution of which was outside the intent of the study contract. Instead, these supporting equipments have been given cursory examination and tentative solutions for their design as well as problem areas are discussed in this report.

In this section a DSNS mechanization is described functionally and physically and an analysis of its accuracy for the Jupiter Swing-by Mission is presented. The operational philosophy for using this system on this mission is explained and the significant areas for system trade-offs are discussed.

A. Summary of Example System

The basic DSNS as mechanized for this mission consists of optical sensors (star/planet sensor and Sun sensor), which are used to obtain the celestial body measurements necessary for navigation, alignment and calibration; a strapdown inertial measurement unit (SDIMU), which is used to provide a navigational reference frame and sense vehicle motions and specific forces; and a general purpose flight computer, which processes inertial sensor data to maintain an inertial reference, performs the navigation, guidance and control computations based on the external optical measurements, controls the sequential operation of various vehicle equipment, and performs all required input/output functions. In addition, an attitude and velocity control propulsion unit and a power supply are required. In all cases, equipment used is that based on UACSC's knowledge of the current state of the art. In particular, a Star Angle Sensor under development by UACSC is used to obtain both star and planet measurements. Test data is available to show that the unit, which performs a dual function with a single sensor, is within the instrument capability for the planet-vehicle geometries expected on the Jupiter mission.

The DSNS is operated intermittently during the mission to obtain the planet measurements and to orient the vehicle for execution of guidance corrections. For the boost phase, the DSNS is not operating but gyro wheels are running to reduce the probability of galling of the gyro bearings under the boost environment. To obtain planet measurements, the DSNS is activated from a dormant mode and brought to operating temperature. Upon activation, the vehicle orients to place its longitudinal axis along the Sun line by using a Sun sensor and simple logic. A series of vehicle orientations are then made based on knowledge of present position to provide star sightings for alignment of the inertial reference and for trimming of gyro bias and scale factor. Planet sightings are then performed, and the system shut down until the next measurement cycle. Updating of the navigational data is performed after each sighting by using the planet measurements in a linear optimal filter process in the computer. At prescribed times, guidance computations are performed and a velocity correction made if required.

The DSNS has been estimated to be capable of taking planet measurements with a total measurement error of about 28.2 arc seconds. With this measurement accuracy, a one sigma error of 0.00296 radians in the inclination of the orbit nominal to the ecliptic can be obtained, with an error in the semi-latus rectum of 0.00102 AU.

The basic DSNS weighs 483 kilograms including the propulsion system for orientation and velocity correction and the power source weight. Of this weight DSNS hardware accounts for 34.7 kg. As mentioned previously, the environmental control system and the telemetry and command system are not included in this weight. The basic system occupies a volume of 0.4525 cubic meters and consumes an average power of 163 watts when taking planet measurements. It has a probability of mission success of 0.976 for the required intermittent operation over a period of 437 days (entry into Jupiter's sphere of influence), including a 60 percent degradation factor in MTBF over the life of the mission to account for the space environment and for on-off operation.

B. Operational Description

The overall system operational philosophy provides for the functions of navigation, guidance, and control to be performed on-board. However, monitoring of the operation is performed on the ground and control of the mission can revert to the ground at any time.

Planet measurements are taken 50 times during the 437-day mission with two planet sightings per measurement. The two planet sightings are taken consecutively with stellar trimming occurring between the sightings to provide two independent readings per measurement cycle. In this fashion, 100 planet sightings are performed. Measurements are taken once every six days up to the 86th day, and once every ten days thereafter. For the purpose of sizing midcourse velocity additional propellant requirements, four midcourse corrections were assumed. The first is applied 190 days from launch, the second at 280 days, the third at 340 days, and the fourth and last at 380 days into the mission. The frequency and distribution schedule for applying velocity corrections depends on the navigation accuracy along the trajectory and the resultant error when propagated forward to mission termination at entrance to Jupiter's sphere of influence. The velocity correction schedule is properly a subject of trade-off studies. These trade-offs, however, are beyond the scope of the present work and the schedule assumed above should provide a worst case condition.

To take these measurements on this long term mission, the operational philosophy selected for the DSNS provides for periodically restarting the system from a dormant mode, re-erecting, and trimming the system in space from star measurements, after which planet measurements are made to perform navigation through on-board processing of the planet measurement data. Space erection of the system is initiated from a random vehicle orientation. This operation was selected in the interest of a general approach, which provides high reliability and worst case propellant requirements. The DSNS could be operated continuously throughout the mission. However, this adversely affects system reliability and power requirements.

In the mode of operation selected, the DSNS operates only during the measurement phase. In the dormant mode, a clock and a receiver are left on and power is supplied to the heaters to maintain the DSNS above 0 degrees in the space environment. For this study, the operation of the DSNS was assumed to terminate after 437 days when the vehicle enters the sphere of influence of Jupiter. A requirement for a vehicle attitude reference may exist beyond this time, but the additional system requirements in this event were not considered in this work.

A sequence of events has been established for the DSNS for this mission, covering the period from system activation following the dormant mode, through planet sightings and system shutdown. The sequence of operational events is presented in Table VIII and includes a crude alignment phase, stellar trimming of the gyros, a fine alignment, and, finally, planet measurements. The complete cycle is executed for the first planet sighting, while for the second planet, the cycle starts with the stellar trimming process. This procedure provides two planet sightings that are independent of each other.

Crude alignment begins after system warmup and activation. In this phase, the vehicle is initially controlled through a pitch and/or yaw maneuver to seek the Sun and align the longitudinal axis along the Sun line by means of a Sun sensor in the forward part of the vehicle and a solar cell array located around the periphery of the vehicle and at the aft end. Once roll axis alignment with the Sun line is accomplished, the vehicle is stabilized in pitch and yaw. The star/planet sensor carried on board is designed with a single degree of freedom, such that its line of sight can rotate in a plane parallel to the pitch-roll plane. This arrangement conserves orientation propellant in that the entire celestial sphere can be viewed with only roll motions of the vehicle. Thus, when the vehicle has been stabilized along the Sun line in pitch and yaw, star sights for crude alignment are obtained by proper positioning of the star/planet sensor head, and roll motion of the vehicle. Prior to star measurements, the strapdown inertial system senses roll rate, and based on this knowledge, roll rate is brought to approximately 1.0 deg/sec. The initial alignment obtained in this fashion is termed crude because it is based on the long term (10-day) errors of the strapdown system and does not provide the most accurate possible alignment.

In the interest of achieving the most accurate measurement available with current equipment, a trimming procedure is performed to update gyro bias and scale factor compensation terms and provide the most accurate short term performance of the system. The trimming procedure involves a series of vehicle maneuvers to obtain star measurement data and requires the expenditure of propellant to achieve the most accurate performance. Gyro bias is calibrated about at least two of the three vehicle axes by stabilizing the star/planet sensor (S/PS) on any star for a sufficiently long period of time (850 seconds) to note the motion of the star in the field. Bias on the third axis is calibrated by rotating the S/PS head through approximately 90 degrees, and stabilizing on a second star for the same period of time. The positions of the two stars are fixed in inertial space; therefore, the apparent angular "motion" of these stars recorded over a fixed time period is a direct measure of gyro bias. Gyro scale factor is calibrated by sighting on a star and executing a 360-degree vehicle rotation to return to the star in a short enough time (100 sec) such that gyro bias error is not significant. (In this study, the angular rate to accomplish this is assumed to be

TABLE VIII
SCHEDULE OF OPERATIONAL EVENTS

	Operation	Time Required (sec)	Cumulative Time From Activation (sec)
1.	Start warmup	6200	
2.	Bring gyro wheels to speed and stabilize	1000	1000
3.	Activate computer and sun sensor	Negligible	
4.	Sun search and lock-on (*stabilize pitch and yaw)	50	1050
5.	Crude alignment		
	Bring roll rate to 1.0 deg/sec	Negligible	1050
	Rotate S/PS head (along pitch axis)	8	1058
	Roll and take at least two star sights	360	1418
	Compute crude alignment	Negligible	1418
6.	Sun sensor shutoff and activation of all channels of SDIMU	Negligible	1418
7.	Gyro bias calibration		
	Star tracking (first star)	850	2268
	Rotate S/PS head	8	2276
	Star tracking (second star)	850	3126
	Compute and update bias compensation values	Negligible	3126
8.	Gyro scale factor calibration		
	Roll maneuver (360 deg)	100	3226
	Pitch maneuver (360 deg)	100	3326
	Yaw maneuver (360 deg)	100	3426
	Compute and update scale factor compensation values	Negligible	3426
9.	Fine alignment (two star sights)	60	3486
10.	Planet sightings		
	Roll to ecliptic plane	50	3536
	Rotate S/PS head	8	3544
11.	Repeat sequence starting with operation 7	2126	4962
12.	Shutdown equipment		

* Activate and warm up S/PS during this phase.

3.6 deg/sec.) The angle difference from 360 degrees as recorded by the strapdown system is a direct measure of scale factor. Scale factor updating for all channels has been provided for in the operational procedures, even though such updating is needed only when velocity additions and associated pitch and yaw maneuvers are planned, or if a body-mounted S/PS without any degrees of freedom is used. When planet measurements alone are made with the S/PS arrangement described previously, only calibration of the roll channel need be performed because only roll motions are needed for star and planet sightings. Three-channel scale factor calibration and 360-degree rotations have been assumed to provide a worst case analysis for orientation propellant and power requirements.

After trimming and updating the inertial instrument compensation terms in the computer, a precise inertial alignment is performed and the system is then ready to perform accurate planet measurements. Two such planet sightings are taken in succession, a navigation computation is performed, and, if no velocity correction is to be made, the system is shut down. The entire sequence takes 4,962 seconds (1.4 hours) exclusive of warmup each time the two planet measurements are taken, and forms the basis for the power, reliability, and orientation propellant requirements estimates that follow.

It is emphasized that the described operations do not constitute a fully optimized case, but establish the feasibility of application of the DSNS for the Jupiter Swing-by Mission.

C. Functional Description

The DSNS provides the following primary functions:

1. It computes inertial position and velocity periodically along the trajectory based on celestial body observations.
2. It provides guidance based on self-computed navigation and generates velocity change signals to correct the trajectory at various points in the flight.
3. It establishes a true inertial reference and provides vehicle and optical sensor orientation commands with respect to inertial space.

To accomplish these primary functions, the DSNS also performs the following secondary functions:

1. It provides the logic for an initial crude space erection from a dormant mode.
2. It controls a stellar trimming process and computes gyro bias and scale factor compensation terms based on star measurements.
3. It transmits selected data to the DSIF for ground monitoring of its operation.

A functional block diagram of the DSNS is presented in Figure 23. (The telemetry function is not shown). The system is activated for each measurement cycle by means of a clock and sequencer which is preset prior to the mission. However, the system can also be turned on from the ground and/or the preset measurement cycle can also be changed by ground commands to a receiver, which is on for the entire mission. Upon activation, power is applied to heaters to bring the equipment to operating temperature, and the operational sequence described previously in Section VI B is commenced under control of sequence logic in the flight computer.

The operational sequence of events is positively controlled. That is, the completion of a particular part of the sequence generates an unambiguous signal, which initiates the next operation. Some of these signals are shown on the diagram.

Initially, the vehicle orientation control system is commanded by Sun-seeking logic based on signals from a Sun sensor and silicon cell sensors. Only pitch and yaw are controlled, roll motions are not. When the vehicle roll axis is aligned with the Sun line and the vehicle has been stabilized in pitch and yaw, the roll channel of the inertial reference system is brought into play and roll rates are sensed and reduced (or brought up to) approximately 1.0 deg/sec.

Appropriate stars for viewing are then selected based on a stored star catalog and knowledge of present position. The S/PS head is oriented to the proper angle to view these stars as the vehicle proceeds to roll and is stabilized in pitch and yaw by the Sun mode logic. Once sufficient star measurements have been taken, initial alignment of the inertial reference is established and all channels of the strapdown inertial reference measurement unit are activated to maintain an inertial reference. When the stellar alignment is established, the Sun mode operation is turned off.

The inertial reference is maintained by integrating the angular increments from the strapdown gyros in the angular equations of motion. If required, velocity increments are then resolved into the inertial frame by means of a body-to-inertial reference transformation for use in the guidance function. Prior to integration, the inertial sensor data is compensated based on predetermined system calibration data. Once in space, these compensation terms are updated each time planet measurements are to be made. The updating takes place under control of space calibration logic, which initiates both vehicle and S/PS orientation to provide the required star measurements. This logic also uses the measurement data to compute updated compensation values.

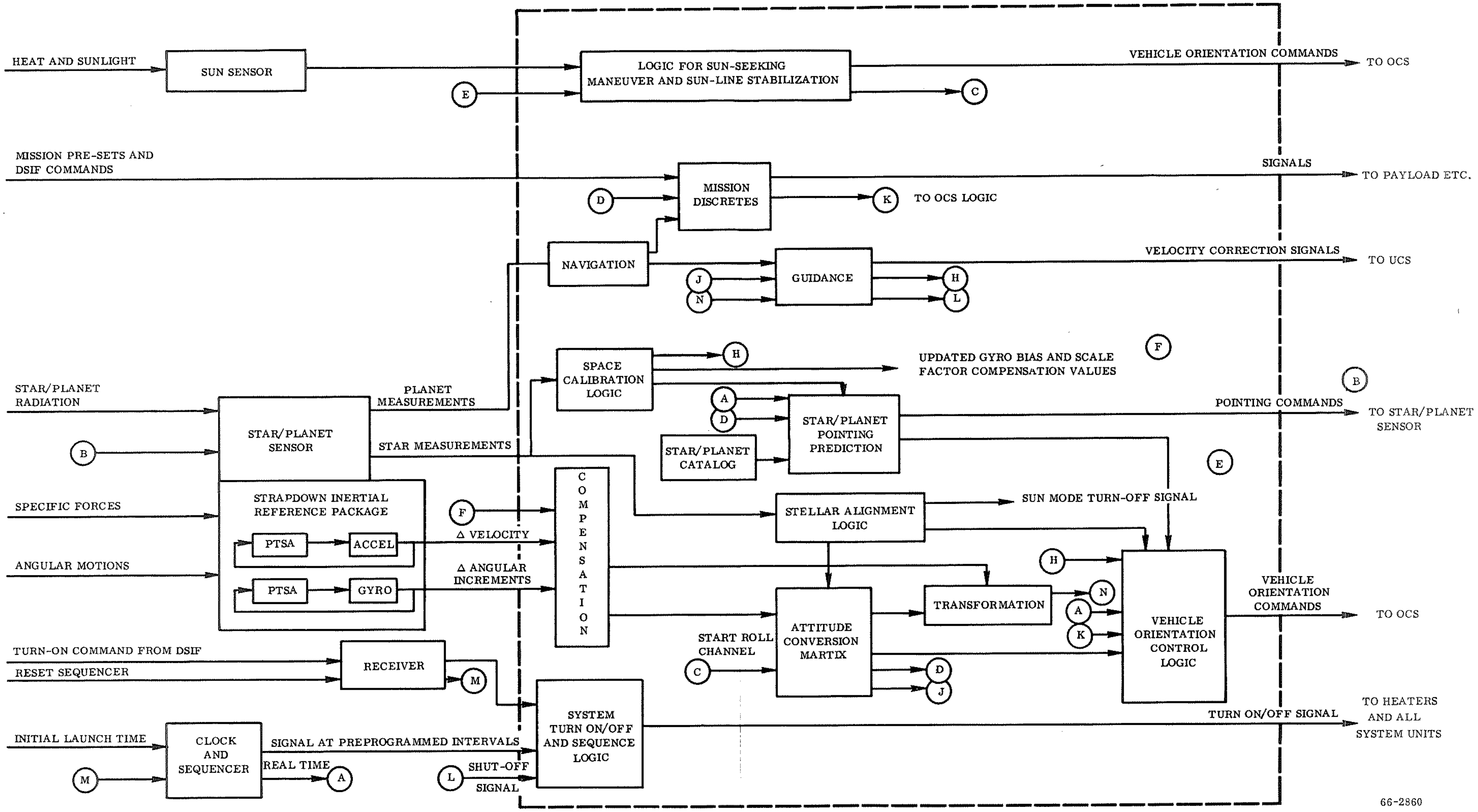
HEAT AND SUNLIGHT
SUN SENSOR
E
LOGIC FOR SUN-SEEKING MANEUVER AND SUN-LINE STABILIZATION
VEHICLE ORIENTATION COMMANDS
TO OCS
C
MISSION PRE-SETS AND DSIF COMMANDS
D
MISSION DISCRETES
SIGNALS
TO PAYLOAD ETC.
K
TO OCS LOGIC
NAVIGATION
J
N
GUIDANCE
VELOCITY CORRECTION SIGNALS
TO UCS
H
L
SPACE CALIBRATION LOGIC
H
UPDATED GYRO BIAS AND SCALE FACTOR COMPENSATION VALUES
F
B
STAR/PLANET RADIATION
PLANET MEASUREMENTS
A
D
STAR/PLANET POINTING PREDICTION
POINTING COMMANDS
TO STAR/PLANET SENSOR
B
STAR/PLANET SENSOR
STAR MEASUREMENTS
STAR/PLANET CATALOG
E
STRAPDOWN INERTIAL REFERENCE PACKAGE
SPECIFIC FORCES
F
COMPENSATION
STELLAR ALIGNMENT LOGIC
SUN MODE TURN-OFF SIGNAL
PTSA
ACCEL
Δ VELOCITY
ANGULAR MOTIONS
H
PTSA
GYRO
Δ ANGULAR INCREMENTS
TRANSFORMATION
N
A
K
VEHICLE ORIENTATION CONTROL LOGIC
VEHICLE ORIENTATION COMMANDS
TO OCS
START ROLL CHANNEL
C
ATTITUDE CONVERSION MARTIX
D
J
TURN-ON COMMAND FROM DSIF
RESET SEQUENCER
RECEIVER
M
SYSTEM TURN ON/OFF AND SEQUENCE LOGIC
TURN ON/OFF SIGNAL
TO HEATERS AND ALL SYSTEM UNITS
INITIAL LAUNCH TIME
M
CLOCK AND SEQUENCER
SIGNAL AT PREPROGRAMMED INTERVALS
REAL TIME
A
L
SHUT-OFF SIGNAL
66-2860

NOTE: OCS - Orientation Control System, VCS - Velocity Control System, PTSA - Pulse Torque Servo Amplifier

Figure 23 Deep Space Navigation Scheme, Functional Flow Diagram

Navigation is performed by using a Linear Optimal Filter that operates on planet measurement data. Guidance computations are performed at specific points along the trajectory on the basis of navigation data. The accelerometers are used to sense the velocity added and integration of these data provides a cut-off signal to the velocity control system as part of the control function.

Mission discretes are either preset into the computer prior to launch or can be input from the DSIF during the mission. As envisioned, guidance corrections generated on-board are transmitted to the DSIF for verification prior to execution. Velocity corrections, updated compensation terms, etc., fall into this category. Thus, the execution of the mission remains under control of the DSIF ground crew, even though the computations are performed on-board. In addition, other data on critical voltages and temperatures are also transmitted to the DSIF for system monitoring purposes.

D. System Accuracy

An error analysis that used existing hardware was performed to determine the measurement accuracy of the DSNS. As noted previously, the equipment is operated to provide the highest possible accuracy, wherein stellar trimming of the gyros is performed to obtain short term stability performance. The error analysis is based on these short term, high performance values.

The error analysis assumes a free space environment with no sensed accelerations except those due to vehicle thrusting. Table IX lists the system error sources, and their magnitude, and the resulting error present when a planet measurement is taken. Table IX includes errors in gyro stability and in the optical sensors used in making the sighting. The errors shown are those accumulated between the time of fine alignment and completion of the planet sighting. During this time period errors due to gyro drift occur. Also, the roll angular motion required to return the vehicle to the vicinity of the ecliptic plane after the last star sight used in the trimming process introduces a scale factor error in the roll channel. About 100 seconds elapse from alignment to completion of planet sightings. To cover all situations, a 180-degree roll rotation is assumed to return the S/PS line of sight to the ecliptic plane for planet sightings.

The total one-sigma measurement error of the system is estimated to be 28.2 arc sec based on a root sum square of the one-sigma errors of all error sources. This accuracy will provide placement of the vehicle into an orbit normal to the ecliptic with a one-sigma error of 0.00296 radians in inclination and 0.00102 AU in semi-latus rectum.

E. System Reliability

A reliability analysis based on existing hardware was performed to establish the probability of guidance system survival over the Jupiter Swing-by Mission. Table X

TABLE IX

DEEP SPACE NAVIGATION SCHEME (DSN) ERROR BUDGET

Error Source	Magnitude	Angular Errors	
		Pitch & Yaw (arc sec)	Roll (arc sec)
Alignment (Star Sightings)	10 arc sec	10	10
Gyros			
Input Axis Stability	5 arc sec	5	5
Bias	0.02 deg/hr	2	2
Scale Factor	15 ppm	0	9.7
Star and Planet Sensor	10 arc sec	10	10
	RSS	15.2	18.0

RSS (Total) = 28.2 arc sec

lists the equipment necessary to satisfy the guidance requirements of the mission along with the corresponding mean time between failures (MTBF) for existing nonredundant hardware.

TABLE X

DSNS INSTRUMENT RELIABILITY

ITEM	MTBF (Hours)
Strapdown Inertial Measurements Unit (SDIMU)	4006
Star/Planet Sensor (S/PS)	7700
Flight Computer	5250
Sun Sensor	100, 000
Power Supply	10, 000

The elements of the guidance system are related serially such that failure in any one item causes a complete system failure. Examination of Table X indicates that the inertial package has the lowest MTBF. The MTBF of this unit, assuming random failure, thus determines the probability of survival of the entire system according to the equation

$$Ps = e^{-\lambda\ t}$$

In equation (1)

Ps = probability of survival
λ = failure rate of SDIMU = $(MTBF)^{-1}$
t = time of SDIMU operation

Conceptually, the DSNS could be operated in one of two ways: (1) continuous operation of guidance equipment or (2) sequence of guidance system "start-up" and "shutdowns" occurring periodically as required throughout the mission duration.

The effect of continuous operation on reliability is shown in Figure 24. As shown in this figure, the probability of mission success for a 437-day mission is unacceptable for continuous operation. Redundancy could be introduced to increase the reliability of the system, with the associated penalty in weight and power. If a redundant system consisting of three gyros in a stand-by mode is used, the SDIMU reliability is improved to an MTBF of 16, 500 hours. However, because of the "serial connection" the system reliability is then limited by the MTBF of the flight computer. Reliability of the system is improved, but is still unacceptable, as shown in Figure 24.

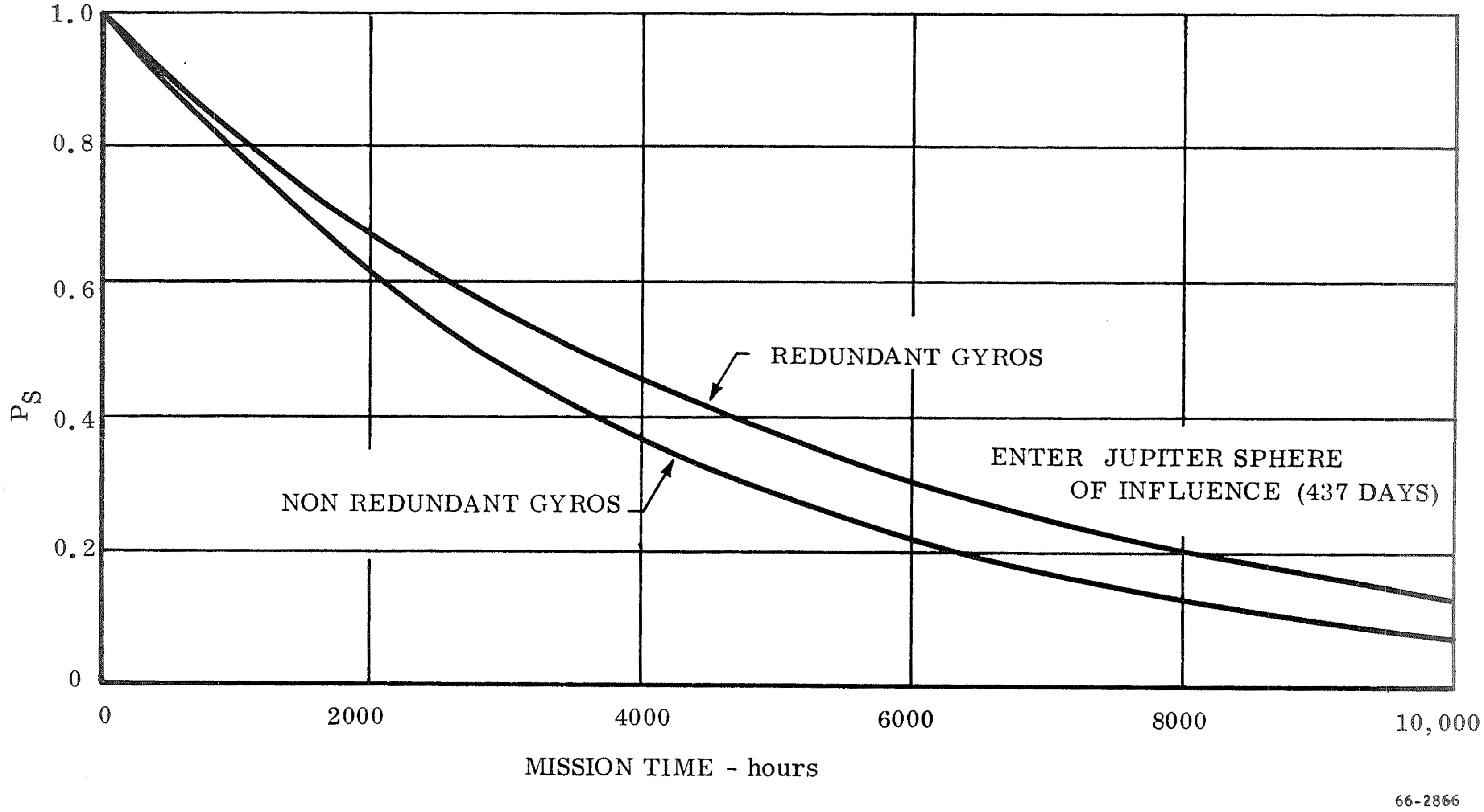

Figure 24 Deep Space Navigation Scheme, Probability of Survival, Continuous Operation

The alternative approach to continuous operation is a sequence of "start ups" and "shutdowns" occurring periodically throughout the mission. The effect of such a sequence on mission success is shown in Figure 25. The results of Figure 25 are based on two-hour operational time occurring once every 10 days, MTBF's of existing equipment, and a linear MTBF degradation of 60% over the total time of the mission to account for on-off operation and long term degradation in the space environment. The results presented indicate a probability of survival of 0.976, and are similar to reliability figures for four days of continuous operation in an Earth orbit. On the basis of this analysis, it is recommended, from a reliability standpoint, that the guidance system be activated and shut down at selected intervals during the mission to have a total operating time on the order of 100 hours over the full mission.

F. System Mechanization

This section presents a physical description of the guidance system for the Jupiter Swing-by Mission as configured by UACSC.

The basic Deep Space Navigation System consists of the following components:

1. Optical Sensors
    - a. Star/Planet Sensor
    - b. Sun Sensor
2. Strapdown Inertial Measurement Unit
3. Flight Computer

In addition the following supporting subsystems are required and sized herein:

1. Propulsion Systems
    - a. Orientation Control System (OCS)
    - b. Velocity Control System (VCS)
2. Power Supply

Additional equipment such as an environmental control system and a telemetry and command system are also required to support the overall operation of the DSNS. However, these items have a strong interface with the payload and the upper stage vehicle design, and no attempt was made to define their physical characteristics; instead, the general design problems of these equipments were examined.

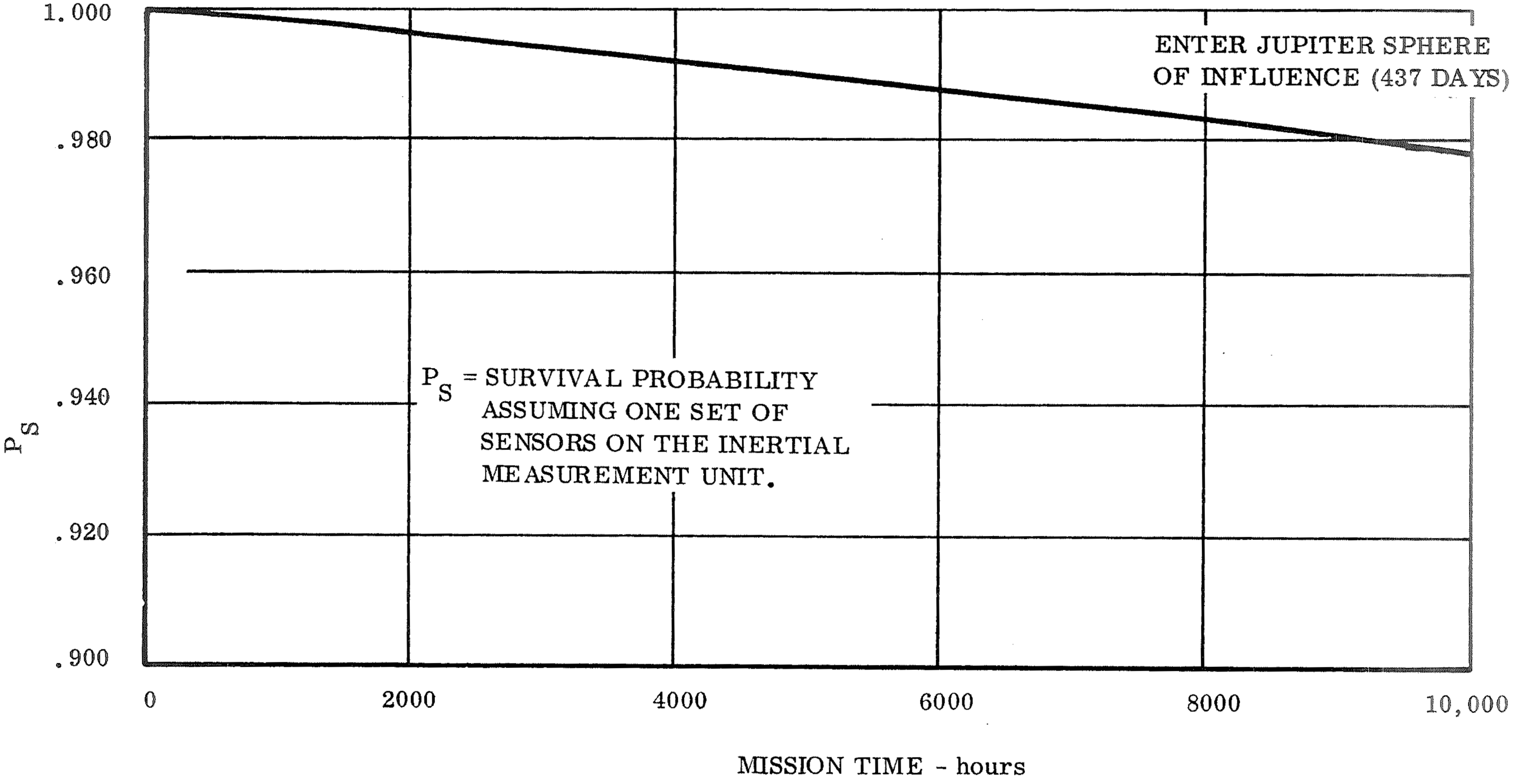

66-2865

Figure 25 Deep Space Navigation Scheme, Probability of Survival, Intermittent Operation

A breakdown of the weight, power, and volume of the components for the basic DSNS and associated subsystems are presented in Table XI. Each component includes its own power conditioning and signal processing electronics to provide compatibility with the computer interface. Total weight of the DSNS hardware is estimated to be 34.7 kg, which with a propulsion system and power supply weight of 448 kg, results in a total system weight estimate of 482.5 kg. Total average power required is 162.8 watts.

1. Optical Sensors

a. Star/Planet Sensor

The Star/Planet Sensor (S/PS) is a direct adaptation of the UACSC Star Angle Sensor (SAS) designed originally as a stellar navigation aide and developed expressly for compatible use with body-mounted inertial systems. The unit is body-mounted with the optic axis nominally aligned with the vehicle yaw axis. It has a deviating head with one degree of freedom, which diverts the boresight axis through 360 degrees to provide star/planet viewing anywhere in a plane normal to the vehicle yaw axis. The degree of freedom afforded by the deviating head coupled with a ± 180-degree rotation of the vehicle about the roll axis permits a view of any point on the entire celestial sphere.

The S/PS is designed to operate with +3 magnitude or brighter stars against both stellar and atmospheric backgrounds encountered in low Earth orbits. The instrument measures the angle between the target star and the deviated boresight axis within a two-degree total dynamic range and with a system accuracy of ±10 arc seconds rms or better. The ability of the SAS to operate as a planet sensor has been evaluated experimentally in UACSC laboratories by sighting the instrument on a series of illuminated discs of varying diameter and intensity rather than on a point light source associated with stellar observation. The results of these experiments indicated that the SAS could successfully operate as a planet sensor under the following restrictions:

1. The brightness of the light reflected from the planet be at least as bright as that of a +3 magnitude star.

2. The angle subtended by the planet is no greater than 1,000 arc seconds.

Analysis of the planet sighting schedule developed under this contract illustrates that a planet satisfying the above constraints is always available during the mission. The most stringent conditions occur 340 days out on the journey when Mars is sighted

TABLE XI
PHYSICAL CHARACTERISTICS

System Component	Weight (kg)	Avg. Power(1) (watts)	Volume (cu. cm.)
Star/Planet Sensor	6.2	20.8	12,850
Sun Sensor	0.8	1.0	352
Strapdown Inertial Package	11.8	81(4)	14,750
Flight Computer	15.9	60	13,100
Basic Hardware	(34.7)	(162.8)	
Power Supply (Nuclear Isotopes)(2)	103.2		65,500
Propulsion Systems(3)			
Orientation			
Hardware	41.8	NA	49,100
Propellant	207.0		199,000
Velocity Correction			
Hardware	27.9	NA	32,800
Propellant	68.0		65,500
TOTAL	482.6	162.8	

(1) During Measurement Cycle including conversion efficiency

(2) Does not include shielding

(3) Does not include boil-off or safety margins, assumes mass fraction (propellant/total) of 0.8

(4) Includes heater power of 32 watts

to establish a position fix; the brightness of Mars at this time is equivalent to a +2.7 magnitude star. These analyses have included partial illumination of the planets due to the Sun-vehicle geometry at the time of the sighting. Figure 26 presents the experimental variation of planet sensor accuracy as a function of the subtended planetary angle. As shown, optimum accuracy is obtained for planet subtended angles in the neighborhood of 5 arc seconds; no deviating head was used for these tests. However, due to the nature of the design, measurement accuracy is very sensitive to changes in planet angles of 500 arc seconds, beyond which measurement errors diverge as planet image size increases.

A sunshade permits the taking of sights on stars to within 20 degrees or more of the Sun. A Sun sensor-actuated shutter is provided to protect the S/PS from thermal damage by exposure to the Sun. The Sun sensor could be used for making observation of the Sun when the planets are less than 20 degrees from the Sun.

During the mission the S/PS is normally in a dormant or zero power mode and is activated just before the crude alignment of the computational reference frame during each navigational sighting sequence described in Section VI.B.

Conceptually the S/PS operates as follows: A rotating prism wedge converts the star/planet image angle with respect to the boresight into a time measurement. The processing electronics acquire and generate time interval measurements of the crossing of the image across a cross-hair slit arrangement from which the flight computer can determine the star angle within the dynamic range. Statistical averaging over 128 readings taken over a two-second period reduces random errors and permits accuracies of better than 10 arc seconds when stabilized to 1 mrad or better. The readout of the deviating head is also obtained as a time measurement. This is accomplished by a position reference on the telescope and deviating head synchronized with passage of a position reference on the constant speed rotating wedge. Further consideration of the S/PS design is necessary to evaluate its applicability to the long exposure of the space environment; however, the operational life presents no problems.

b. Sun Sensor

The Sun sensor used in the DSNS employs cadmium sulfide detectors as the photosensitive elements. The detectors are photoconductive and their impedance varies considerably with illumination. The detectors are arranged in a bridge-type network with the Sun sensor error signal as the bridge output. The detectors are placed in a housing that provides a method of changing the illumination incident on the detectors as the angle between the Sun and the vehicle changes. The detectors are positioned in the housing in such a manner that the housing casts a shadow on the detector. This shadow changes as a function of vehicle attitude.

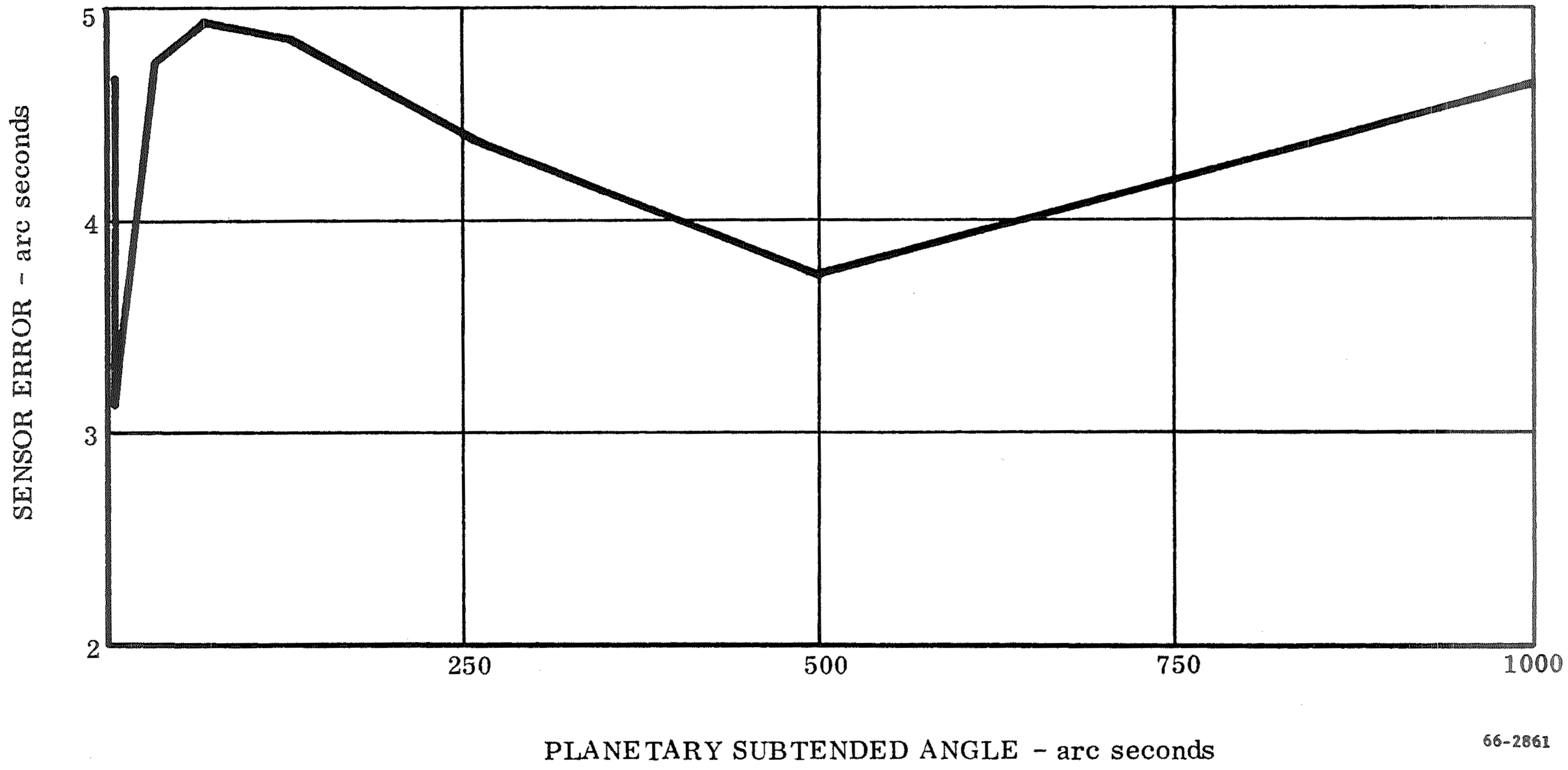

Figure 26 Star/Planet Sensor Measurement Accuracy vs Subtended Angle of Planet

When pointing directly at the Sun, the shadows cast on the detectors of the bridge network are equal. This creates a null point at which the electrical voltage output is zero. If the Sun sensor is not pointed directly at the Sun, the shadows cast on the detectors are not equal. This inequality produces a bridge unbalance and consequently a net output voltage which signals an orientation change.

2. Strapdown Inertial Measurement Unit

The strapdown package is similar to the Lunar Excursion Module (LEM) Abort Sensor Assembly (ASA) currently being manufactured by UACSC for the NASA Apollo program. The ASA is designed to sense the inertial angular and linear motion of a vehicle to which it is rigidly attached and to translate this motion into a series of digital signals. This signal output is used by an on-board computer to maintain an inertial computational reference coordinate system.

Briefly, the SDIMU is mechanized as follows: Inertial sensors in the SDIMU respond to all vehicle linear and angular motions above instrument threshold to produce an error signal. Pulse torque servo amplifiers (PTSA's) provide digitized torquing signals of high resolution and precision to rebalance each of the sensors. This torquing signal is a measure of the incremental values of angular displacement and linear velocity along each of the body axes. The digital signal from the PTSA's is accepted by the on-board computer, which sums these pulses, compensates for deterministic errors, and uses the data in a numerical integration of the angular equations of motion. The angular information from the three strapdown gyros is integrated in a Base Motion Isolation calculation to provide a precise inertial reference; sensed acceleration data from the three accelerometers are then transformed from body coordinates to inertial coordinates to produce a complete inertial measuring system.

The six inertial sensors are oriented in the optimum configuration for system performance and accuracy. Thus input axes of the gyros are arranged in an orthogonal triad. The input axes of the accelerometers are mutually aligned with those of the gyros. To cope with the severe temperature conditions of deep space, thermal control is provided by enclosing the SDIMU in foam insulation. In normal operation, the SDIMU is operated at a constant temperature between 120 and 160°F. The selection of the operating temperature is a design variable. During long periods of equipment "shutdown" the SDIMU is maintained at 0°F by addition of power to heaters within the SDIMU.

3. Flight Computer

Several advanced flight computer design philosophies to provide the reliability and operational flexibility needed for future extended deep space scientific missions are currently being studied. UACSC is presently under contract to NASA-ERC to develop the logic for and to breadboard a modularized computer for the Advanced Kick Stage Mission. The modularity within the UACSC configuration provides functional redundancy among the various elements within the computer.

While such a computer is desirable, it is of an advanced design. Accordingly, to remain within the framework of the present state of the art, a flight computer that uses current technology considerations was configured to perform with the DSNS. The flight computer is based on the estimated computational requirements for the Jupiter Swing-by Mission operations. The flight computer for the Jupiter Swing-by Mission is a high speed parallel, lightweight, general purpose computer. It is capable of accepting inputs from many different sources through a single input switching matrix. These inputs include inertial sensor information such as gyro, Sun sensor, and star/planet sensor data.

The machine has the capability for storing the required program and memory data in 30-bit words. The computer contains three index registers to facilitate subroutine operation. The add time is 8 μsec and the multiply time is 80 μsec.

The flight computer consists of the following functional units plus a self-contained power supply.

1. Memory Unit
2. Control Section
3. Arithmetic Section
4. Central Timing
5. Input Section
6. Output Section

The memory system recommended contains a linear core rope for the program memory plus a coincident current torroidal core matrix for data memory. The two-memory system, with the program memory a linear core rope and the data memory in a coincident current configuration, has advantages of lower weight, lower power, smaller size, and nondestructive readout of program relative to a configuration with two coincident current memories. Using two memories is an efficient mechanization based on the memory word length requirements. The program memory contains 18-bit words whereas the data memory contains 30-bit words.

The core rope program memory utilizes torroidal cores, which have a linear B-H curve. These cores permit low power operation because the cores are not switched and they do not have to be primed. The entire memory system logic circuitry consists of integrated circuits, which include the core drivers and sensing circuits. The coincident current memory uses integrated circuits for matrixing and sensing and discrete components for the core drivers. The computer is a single address sequential machine. Multiplication is performed in an iterative manner by examining each bit of the multiplier in sequence. Division and square root are performed using nonrestoring algorithms to obtain higher speed operations. The input-output instructions transfer data into or out of the accumulator. The input-output channels have indicators to show whether data is available or is being requested. The general purpose input channels permit a flexible input capability that is compatible with the speed requirements in this application.

4. Propulsion Systems

The weight of the orientation and velocity control propulsion system has been estimated because it is a significant contributor to total upper stage weight and because its design is strongly interrelated with the events and mission operations required to perform the navigation function. No attempt has been made to optimize or detail the propulsion system design, but rather to illustrate sensitive preliminary design parameters. The design philosophy is based on the use of storable hypergolic propellants and a conventional six-nozzle thruster configuration to provide attitude control. Higher thrust levels are provided by a separate nozzle which is used to execute the velocity corrections; the two control systems, however, share the same tankage and pressurization systems.

Economical attitude control system (ACS) propellant usage is an important factor in the design of the Jupiter Swing-by space vehicle system because the weight of propellant expended during the mission, although not large during any one period of activation, when summed over the 100 planetary sightings scheduled during the flight constitutes a significant fraction of the total space vehicle weight. A space craft physically similar to the Agena vehicle was assumed for the purposes of this analysis. The characteristics of this vehicle are shown in Table XII. These may be very conservative estimates but are used primarily for illustration of the relationship of propulsion weight to the guidance system weight.

TABLE XII
JUPITER SWING-BY SPACECRAFT CHARACTERISTICS

Weight	1635 kg
Moment of Inertia	
Pitch, Yaw	17,350.0 kg m^2
Roll	418 kg m^2
ACS Thruster Moment Arm	
Pitch, Yaw	4.27 m
Roll	0.56 m

Propellant requirements are sized to perform the velocity correction and attitude control functions to carry out the mission operations described in Section VI. B.

A conservative 250-second specific impulse estimate for storable hypergolic propellant indicates that approximately 1.3 kilograms of ACS propellant are used to execute the attitude maneuvers required for the erection, gyro trimming, and planet measurement phases of each planet sighting sequence. An additional 0.68 kilograms of propellant are needed to maneuver the vehicle to the proper attitude to apply a velocity correction. The total ACS propellant required for the mission based on making 100 planet sightings and 4 velocity corrections during guided flight is therefore 207 kilograms. A weight breakdown of this propellant according to usage is presented in Table XIII. This is a definite area for trade-off studies to evaluate the effects of the angular rate on propellant and measurement accuracy.

A propellant allotment of 68 kilograms sufficient to make a total ΔV correction of 100 m/sec is also included in this Table, which brings the total attitude and velocity control system propellant requirement to 275 kilograms. The total attitude and velocity control system weight including tankage, propellant, nozzles, etc., is then estimated to be 345 kilograms based on a mass fraction of 0.8. The relatively large propellant associated with the planet sightings suggests re-examination of this procedure to establish whether more efficient operational techniques are possible.

5. Power Source

The average power required by the DSNS to obtain a planet sighting is 162.8 watts. Fifty such planet sightings are performed which produces an average watt-hour requirement of 16,280 watt-hours (based on roughly two hours/sighting) In addition, a power requirement exists to provide warmup of the system from zero degrees. Warmup time is not critical; therefore, the power level for warmup has been made equal to the average operating power level of the system. Additional power is consumed by the environmental control system, which maintains the system at about zero degrees, and by a receiver, which is kept on over the span of the mission. These latter requirements while of long duration are of low power level (less than 10 watts). Hence the selection of a power source for the DSNS is based on the average operational power requirements of the system. The total power consumption of the system including all power usage is about 150,000 watt-hours.

For the power requirements and mission duration, a nuclear isotope energy source appears to provide the lightest system with a high reliability. Figure 27 presents the weight trade-off of several types of energy source power systems as a function of mission duration for a 100 to 500 watt power requirement level. As shown, the specific weight of battery and fuel cell energy source systems diverge rapidly beyond mission durations of several days and one month, respectively, yielding unrealistically high power system weights for an extended mission. The weight

TABLE XIII
TOTAL ON-BOARD PROPELLANT REQUIREMENTS*

Function	Propellant Weight (kg)
Attitude Control	
Planet Sighting	136.0
Velocity Correction	2.8
Stabilization	68.0
Velocity Control (ΔV Correction)	68.0
TOTAL	274.8

*Excluding allotment for reserve and leakage propellant

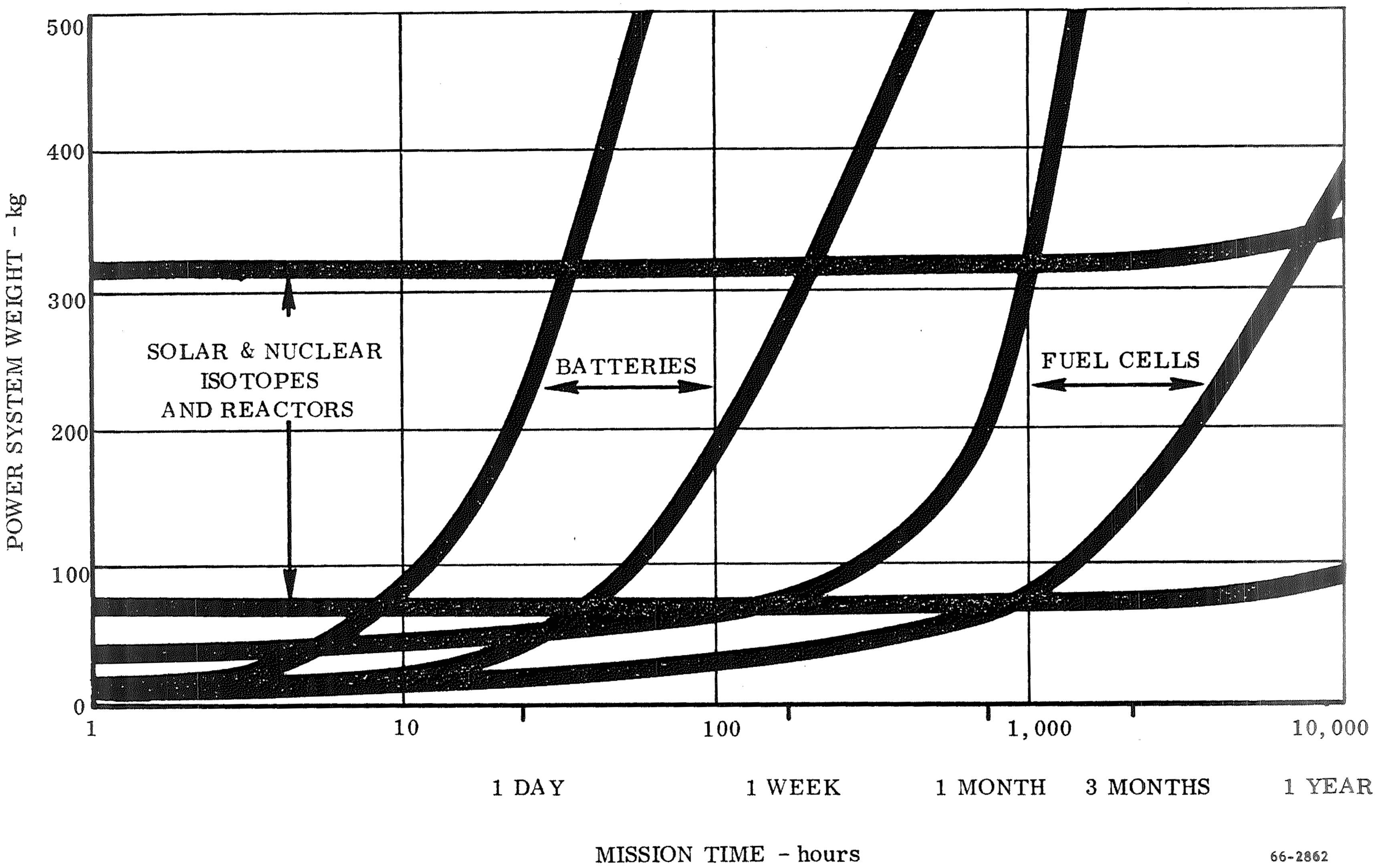

Figure 27 100 - 500-Watt Electric Power System, Weight vs Mission Time of both solar cell and isotope based systems is less dependent on mission life than the other two energy sources considered, and are competitive on a weight basis for near Earth operations. Solar cells lose their competitive position for deep space operation since the effectiveness of the cells is lowered when operating in the reduced solar radiation levels encountered as the vehicle moves toward Jupiter. Also, solar cells for the Jupiter Swing-by Mission would be directly exposed to space for an extended period making them susceptible to damage from space particles.

On the basis of these considerations, a nuclear isotope power source was assumed for this application. This power source has an estimated specific weight of 0.63 kilograms/watt. Hence for the total power requirement of DSNS, a power source weight of 131 kilograms is estimated.

6. Supporting Equipment Design Analysis

a. Environmental Control System

All components in the inertial sensor package from inertial sensors and PTSA's (which are mounted in the IMU sensor housing) to the power supply require a certain degree of temperature control. When operating, all of these components dissipate heat from internal power and must, therefore, be provided a thermal path to a heat sink for temperature control during operation. Generally, the design approach is to provide an adequate heat flow that is sized to maintain operating temperature under conditions of highest ambient temperature. As ambient temperature drops, heaters are provided to supply heat to satisfy the heat flow design while maintaining system temperature control. The present ambient isolation technique of providing an adequate insulating cover around the inertial sensor package minimizes the heat interchange between package and ambient under all environmental conditions. This technique is valid for small excursions of ambient temperature. However, for the Jupiter Swing-by Mission the ambient excursions are extreme, from +125°F near Earth to -313°F near Jupiter, as shown in Figure 28. These extreme environments require a new approach to temperature control of the system.

To achieve an optimum design implementation in terms of performance, reliability, power, and configuration parameters, the following design concept is postulated. The Jupiter Swing-by inertial package will operate at +125°F with heaters providing temperature compensation for ambient and heat sink shifts. Temperature compensation and isolation from ambient environment will be utilized. The heat sink will have integrated sublimator-radiator functions, with variable conductance devices included to interface with the inertial package.

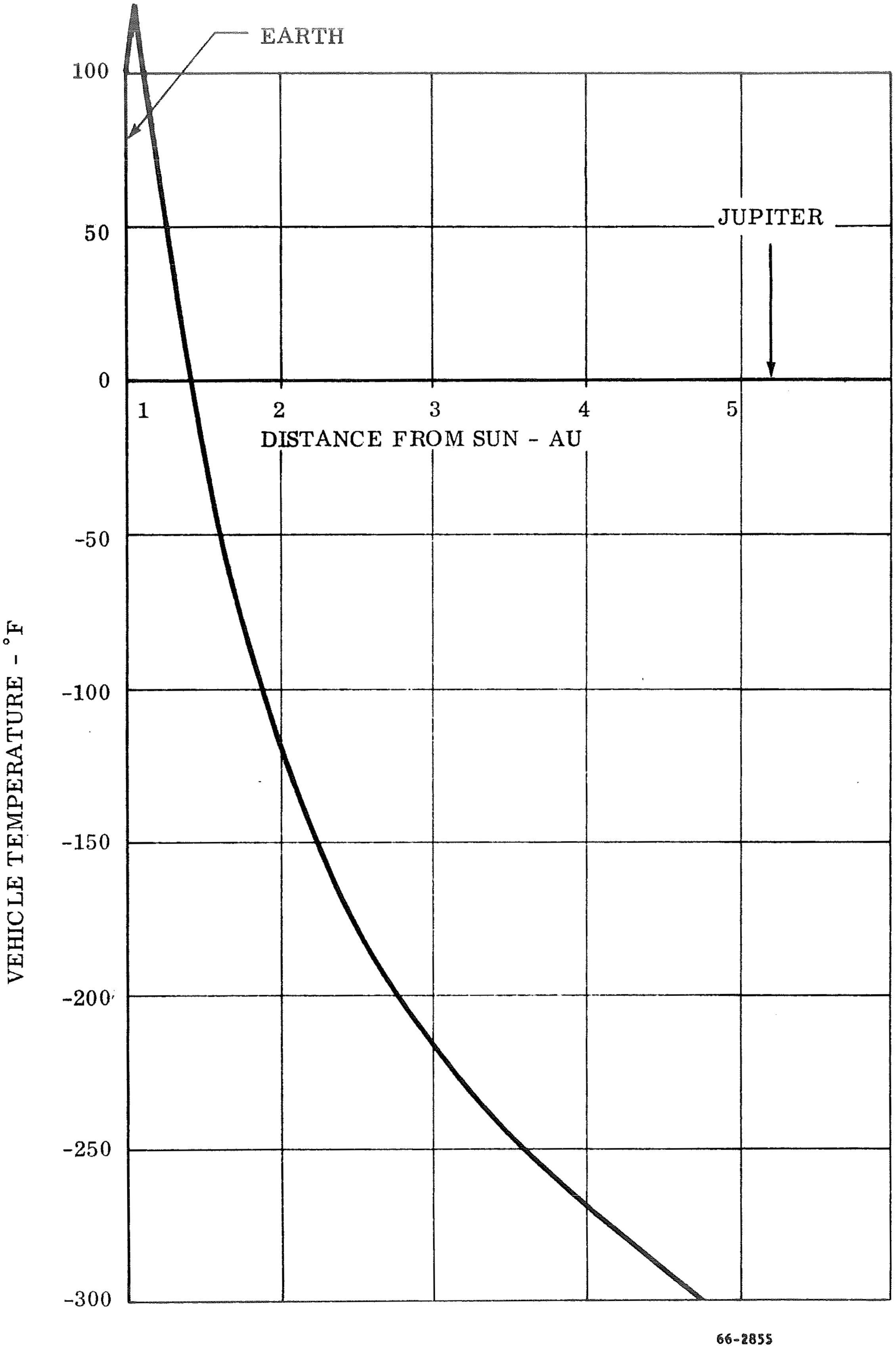

Figure 28 Jupiter Swing-by Vehicle Temperature

The design concept would be to isolate the system as much as possible from the extreme environment. This would reduce the heat loss during the inoperative mode to a minimum. Variable conductance paths would be used to provide the required heat path during operation and a zero heat path when inoperative. An estimate of heat loss through radiation has been made for the DSNS, and a make-up heat requirement of 8.5 watts has been computed to maintain the system above zero degrees when inoperative.

b. Telemetry and Command Systems

Selection of a telemetry and command system for the Jupiter Swing-by Mission is governed by the type and quantity of data to be transmitted by both the DSNS and the payload. In addition to the transmission of scientific data, the degree and accuracy of two-way communication between the ground and the vehicle must be established. From a guidance standpoint, it is desirable to provide such communication to monitor system performance and override preplanned maneuvers if unexpected difficulties arise. However two-way communication imposes a weight and power penalty which depends on the type and amount of data to be transmitted. In addition, specific results and data expected from the mission must be defined and considered in the selection of a deep space communication system.

G. System Trade-off and Areas for Further Investigation

The system mechanized for the Jupiter Swing-by Mission is only an example case of the many possibilities which present themselves both in mission operational procedures and system mechanization. The study to mechanize a navigation, guidance, and control system has demonstrated the wide latitude of operational and system design choices available, and has pointed up the major trade-off and problem areas.

Trade-offs occur independently in three areas:

1. Concept and Operation
2. System Mechanization
3. Sensor and Subsystem Design

Operational trade-offs fall into two categories: (1) those associated with the concept of performing navigation and guidance and (2) those connected with mission and vehicle operations to carry out the concept. Category 1 is concerned with the method used to navigate and guide, and the consequent effect on navigation accuracy.

Category 2 deals with the operational techniques required to implement the concept, and influences propellant weight (for orientation control and velocity addition), system power requirements, and system measurement accuracy.

System mechanization trade-offs involve the general selection of equipment to perform the required mission operations, and consideration of the design of supporting subsystems, such as the environmental control system, the power source, telemetry and command subsystems, and propulsion system configurations. These trade-offs influence system weight, power consumption, and propellant requirements. The choice of a system mechanization can also influence the system operational procedures as well as measurement accuracy.

The last area of sensor and subsystem design trade-offs covers a lower level of decision involving design choices within the sensors and equipment themselves. For example, various design concepts for the optical sensors affect the sensor accuracy, weight, and power. Similarly, a trade-off study of the environmental control system will influence overall system weight and power consumption.

1. Concepts and Mission Operations

Navigation accuracy affects all the total system characteristics. Improved navigation accuracy will reduce the amount of velocity correction propellant required. In addition, accurate navigation early in the mission will allow corrections to be made early in the mission, which provides for early termination of the guidance functions with a resultant reduction in overall power and orientation propellant requirements. Achievement of better navigation accuracy also entails other trade-offs that influence the design and operation of the system. More planet measurements can be made or their distribution can be changed. The measurement schedule used in this study is one of an infinite family and is by no means optimized. Therefore, studies are indicated to obtain optimum shaping of the navigation performance throughout the mission by judicious selection of the measurement schedule to provide the best overall system trade-off.

The use of information obtained external to the vehicle, such as radio tracking by the Deep Space Information Facility during the initial phases of the flight, should be investigated. An improvement in guidance accuracy during this portion of flight could substantially reduce the fuel requirements for velocity corrections at later times. Such an investigation would also determine the range from Earth at which the ground tracking should be terminated in favor of the use of on-board measurements. Guidance concepts and their mechanization for the on-board system must be evaluated with respect to mission success criteria. The system example described in the preceding sections is not claimed to represent an optimum system and should be reevaluated with respect to both the particular types of measurements to be made (e.g., the inclusion of a horizon sensor may prove to be valuable for terminal guidance) and their frequency distribution over the flight. The frequency distribution of velocity corrections to be applied must also be optimized with respect to the total propellant weight required for the mission.

Various operations to accomplish the mission are possible. The accuracy obtained by the stellar trimming operation can be traded with the orientation propellant and with added power consumed to conduct the trimming process. Maintaining the vehicle in a preferred orientation between planet measurements will eliminate space erection procedures and reduce orientation propellant, but power and reliability are adversely affected. These and other mission operations to implement the navigation and guidance concepts should be further examined.

2. System Mechanization

System mechanization has trade-offs primarily in weight, power, cost, and accuracy. Attitude control propellant expended for the periodic calibration of the gyro scale factors in space could be eliminated by the use of a gimbal on the star/planet sensor to provide an added degree of freedom. However, sensors with several degrees of freedom will impose viewing problems and compromise the overall packaging of the upper stage.

The problem of providing a proper operating environment must be studied to include overall system requirements. A system could be designed to operate in the low temperatures of space but the design would be costly and heavy or else inaccurate. The other alternative of providing an environmental control system requires additional expenditure of power and increases weight.

Another area for extensive trade-off studies is in the selection of the inertial instruments themselves. Here calibration and trim requirements, which are reflected in fuel and power, can be traded against the basic instrument design performance as reflected by weight and cost. Also, the effects of redundancy of inertial instruments on the probability of mission success should be evaluated with respect to the increased weight and power requirements imposed.

3. Sensor and Subsystem Design

Trade-offs in this area are related to the internal details of the design of a particular sensor. Generally these should be performed in a nominal way to establish design requirements for the sensor and effect a design that is not highly sensitive to the design parameters. These trade-offs are generally reserved for the design phase of the equipment.

The trade-off studies described briefly above should be considered as part of the next step in a continuation of the analysis of a Jupiter Swing-by Mission. The cost of these studies may be minimized by using two-body simulation programs throughout, and then verifying the results obtained for the selected system through the use of the N-Body navigation programs developed under this contract . The performance of these studies for the Jupiter Swing-by Mission will define the operational procedures and guidance and control requirement for the Kick Stage vehicle. It will also provide trade-off data to substantiate these requirements. This data will be essential to the overall design trade-offs for the selection of the Kick Stage vehicle configuration.

APPENDIX A

TRAJECTORY ANALYSIS AND SELECTION FOR JUPITER SWING-BY MISSION; SCIENTIFIC REPORT NO. 1

The study herein presented was performed in partial fulfillment of Contract No. NAS 12-40 and was reported to NASA/ERC on November 9, 1965 as Scientific Report No. 1. This appendix is also identified as United Aircraft Corporate Systems Center Report SCR-247 and is included in the final report for the convenience of the reader who did not receive a copy of the original issue.

TABLE OF CONTENTS

Section Page

I. SUMMARY 1

II. INTRODUCTION 2

III. TRAJECTORY ANALYSIS 4
   A. Trajectory Requirement 4
   B. Trajectory Parameters 4
   C. Trajectory Limitations 10

IV. SELECTION OF TYPICAL TRAJECTORY 17
   A. Parameter Sensitivity 17
   B. Selected Trajectory 17

V. REFERENCES 21

APPENDIX MATHEMATICAL FORMULATION OF PROBLEM 22

GLOSSARY OF SYMBOLS 25

LIST OF ILLUSTRATIONS

Figure Page

1. Typical Heliocentric Trajectories 5
2. Orbital Elements of Final Heliocentric Trajectories 5
3. Transfer Plane Through Jupiter's Sphere of Influence 8
4. Transfer Plane Geometry 9
5. Earth-Jupiter Transfer (1972) 11
6. Aphelion Velocity of the Final Heliocentric Trajectory Vs Hyperbolic Excess Velocity at Jupiter 12
7. Velocity Impulse Required to Boost Into Hyperbolic Trajectory 13
8. Normalized Miss Distance Vs Turning Angle 15
9. Time of Flight Vs Eccentricity of Final Heliocentric Trajectories 16
10. Heliocentric Orbit Inclination Sensitivity to Injection Velocity Errors 18
11. Heliocentric Orbit Perhelion Sensitivity to Injection Velocity Errors 19
12. Heliocentric Orbit Eccentricity Sensitivity to Injection Velocity Errors 20

I. SUMMARY

The United Aircraft Corporate Systems Center is conducting an analytical study of simplified navigation and guidance schemes for a Jupiter swingby mission for NASA/ERC. The results of this study will also have general application to interplanetary missions that have similar requirements. As part of this study an analysis was made to determine the parameter that affects deflection out of the ecliptic plane by a Jupiter swingby and to select a representative trajectory for use in the navigation and guidance study. The results of this analysis, which are presented in this report, show that heliocentric trajectories normal to the ecliptic plane with eccentricities ranging from 0 to 1 can be obtained with substantial reductions in the velocity increments required over those needed for direct injection from the earth. The representative trajectory recommended is one with an eccentricity of approximately 0.8 and one which passes over the sun at a distance of 1 astronomical unit.

II. INTRODUCTION

The United Aircraft Corporate Systems Center is conducting an analytical study of simplified navigation and guidance schemes for a Jupiter swingby mission for NASA/ERC. The results of this study will also have general application to interplanetary missions that have similar requirements. The objective of this study is to define the navigation and guidance requirements for a small energetic kick stage for a typical mission in which the gravitational field of Jupiter is used to deflect the vehicle into a heliocentric orbit about the sun in a plane normal to the ecliptic. These objectives will be met by extending the navigation concept and hardware technology developed over the past six years by UACSC in its strapped-down optical-inertial navigation systems program. As part of UACSC's program, a strapped-down inertial measurement unit is currently being developed for the LEM Abort Guidance System of the NASA Apollo program. The subject study, which is being conducted under NASA Contract 12-40, will consider the applicability of this hardware to these much longer missions and devise means of extending the life and reliability on the basis of current and future technology.

This study is primarily for the evaluation of navigation and guidance techniques; however, the first task under the contract is to conduct a preliminary mission analysis. The objective of this initial task is to define the mission spectrum and to select a typical trajectory for the navigation study on the basis of nominal propulsion limitations and navigation sensitivity. A review was made of the work of previous investigators (References 1 and 2), which defines in general the types of missions and energy requirements that demonstrate the advantages of energy management for Jupiter swingby missions.

One of the scientific missions being considered by NASA is exploration of the environmental conditions out of the ecliptic plane in the vicinity of the sun. To place a vehicle into a trajectory in a plane that has a large inclination to the ecliptic directly from the earth requires a large expenditure of energy; therefore, the use of the gravitational fields of certain planets to shape the trajectory was considered. Hunter (Reference 1) has shown that the required impulsive velocity can be reduced by as much as a factor of three from a direct injection from earth if a swingby of Jupiter is used. Another study was recently made for NASA (Reference 2) of the advantages of using Jupiter's gravitational field in solar and deep space missions limited to the ecliptic plane. For this study a two-dimensional coplanar model was assumed.

The study reported herein uses a three-dimensional model of the solar system with the planets in elliptic non-coplanar orbits. It is felt that this approximation of the solar system is sufficient to determine the critical parameters that affect deflection of space vehicle out of the ecliptic plane. The analysis is restricted to missions in which the final heliocentric portion of the trajectory lies in a plane normal to the ecliptic and which have their aphelions in the vicinity of Jupiter. Although the deflecting body used was Jupiter, which has the largest planetary mass, the method of analysis is general and can be applied to any other body in the solar system.

This report presents the results of preliminary mission studies and the characteristics of the selected mission trajectory to be used for the next task of evaluating the navigation and guidance requirements. An n-body program is being adapted for the navigation and guidance task which will permit further definition and refinement to the selected trajectory and sensitivity coefficients established by this preliminary mission study.

III. TRAJECTORY ANALYSIS

A. Trajectory Requirement

The objective of the mission to be studied is to place a vehicle into a trajectory about the sun in a plane which is normal to the ecliptic. Hunter (Reference 2) has shown that the velocity required for such missions when made directly from the earth range from 32.0 Km/s for the closest possible approach to the sun to 42.7 Km/s for an orbit with the distance of closest approach of 1 astronominal unit. The corresponding trajectories obtained by using Jupiter's gravitational field require 15.2 Km/s and 15.8 Km/s, respectively. The trajectories are equivalent only in the sense that they have the same perihelion distances. Trajectories having a perihelion of one astronomial unit are illustrated by trajectories 2 and 4 in Figure 1. The characteristics of trajectories that can be obtained with aphelion at Jupiter are illustrated in Figure 2a as a function of the total characteristic velocity increment of the space vehicle, ΔV. They range from direct impact on the sun ($e = 1.0$) to circular ($e = 0$). The circular trajectory requires a ΔV of 16.9 Km/s. All of the velocities discussed are for a near optimum launch date and do not include any allowance for drag and gravity losses in the boost phase of flight. However, the relationship between the hyperbolic excess velocity at Jupiter and ΔV shown in Figure 2b includes an assumed gravity and drag loss of 1.52 Km/s.

B. Trajectory Parameters

The motion of a vehicle in interplanetary space is an n-body problem and as such has no known analytical solution. It was decided that the degree of approximation obtained by using patched conics would be sufficient for determining the parameters that affect deflection out of the ecliptic plane. In a patched conic program, it is assumed that the two body formulas hold within each sphere of influence. The radius of the sphere of influence is defined from the following considerations. When a body is influenced by two other bodies, the equations of motion may be written with the coordinate system centered at either of the bodies. Which formulation is most advantageous depends on which body dominates the motion. One measure of this is the ratio of the disturbing force (the force due to the presents of the body not being used as the center of the coordinate system) to the central force. The radius of the sphere of influence is defined by equating this ratio from the two formulations. The radius of the Earth's sphere of influence is 924,000 kilometers while that of Jupiter is 48,200,000 kilometers. The patched conic program that was used consists of a heliocentric trajectory from the Earth's sphere of influence to Jupiter's sphere of influence, a hyperbolic Jupiter centered trajectory through Jupiter's sphere of influence followed by a heliocentric trajectory beyond Jupiter. The standard two body formulas were used in each region with the positions of the Earth and Jupiter being computed from the standard formulas by using the orbital elements for a given epoch.

TRAJECTORY NO.	ECCENTRICITY e	PERIHELION DISTANCE	SEMI-LATUS RECTUM
1	0	5.2 A.U.	5.2 A.U.
2	.68	1 A.U.	1.7 A.U.
3	.81	.55 A.U.	1 A.U.
4	0	1 A.U.	1 A.U.

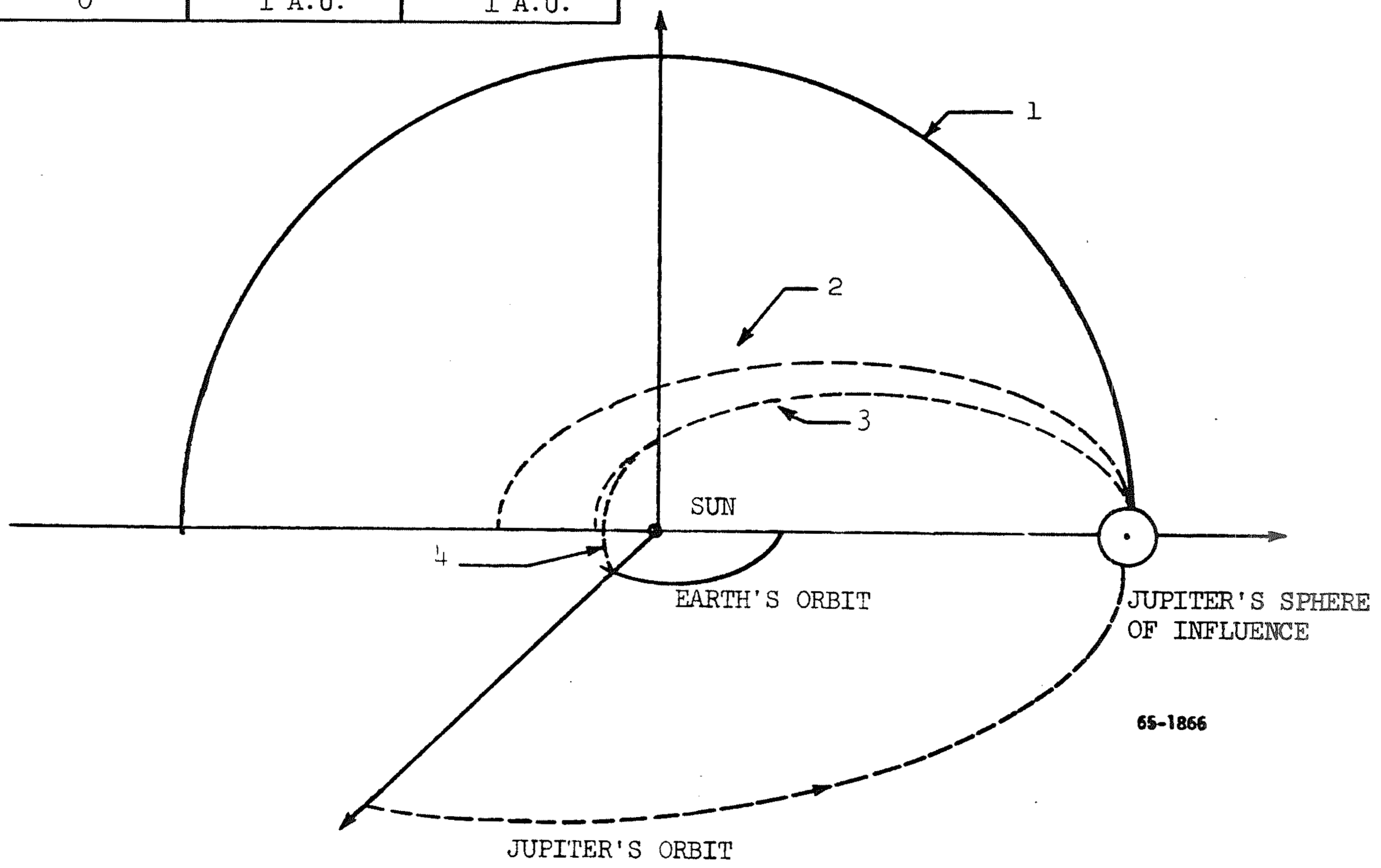
1
2
3
SUN
4
EARTH'S ORBIT
JUPITER'S SPHERE OF INFLUENCE
65-1866
JUPITER'S ORBIT

Figure 1 Typical Heliocentric Trajectories

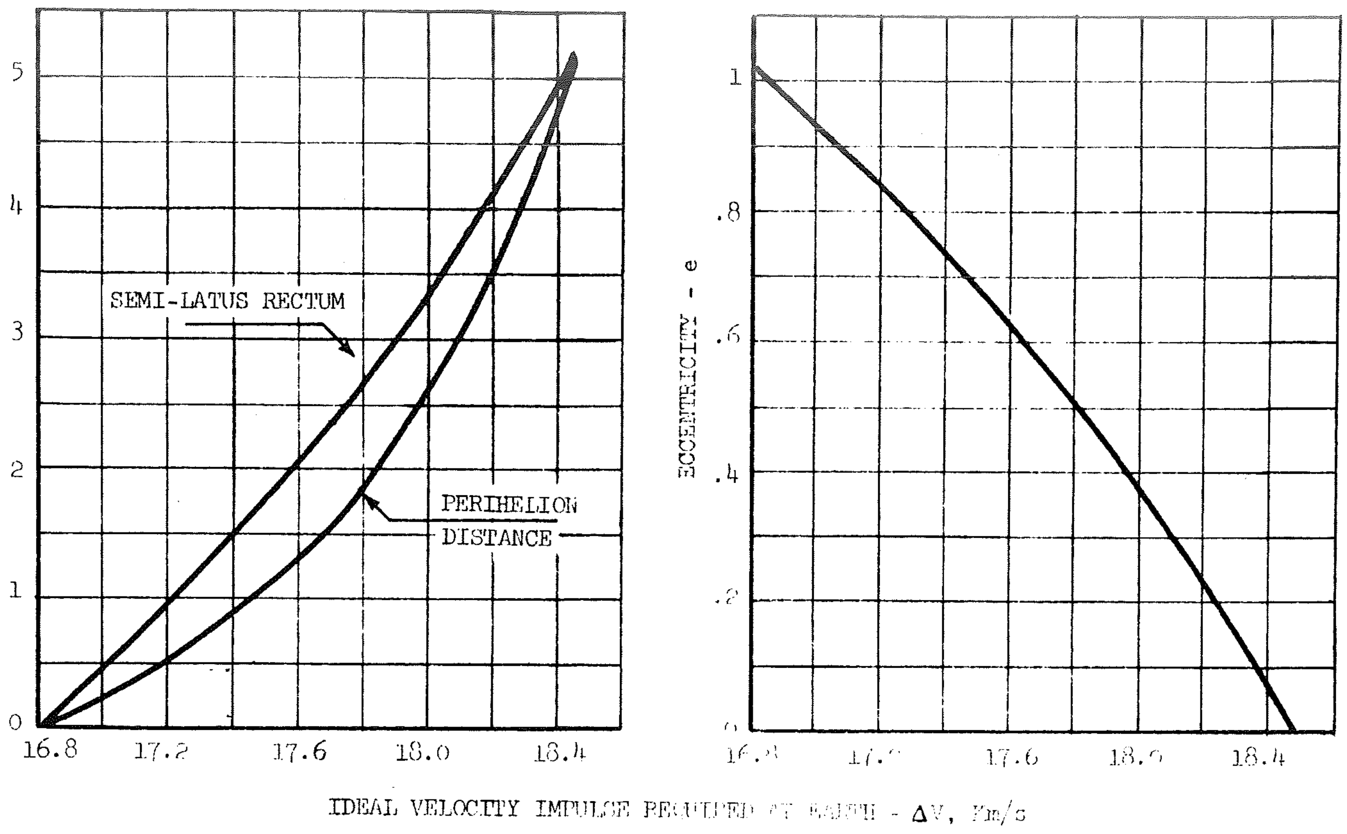

a) Ideal Velocity Impulse Required at Earth vs Orbital Elements

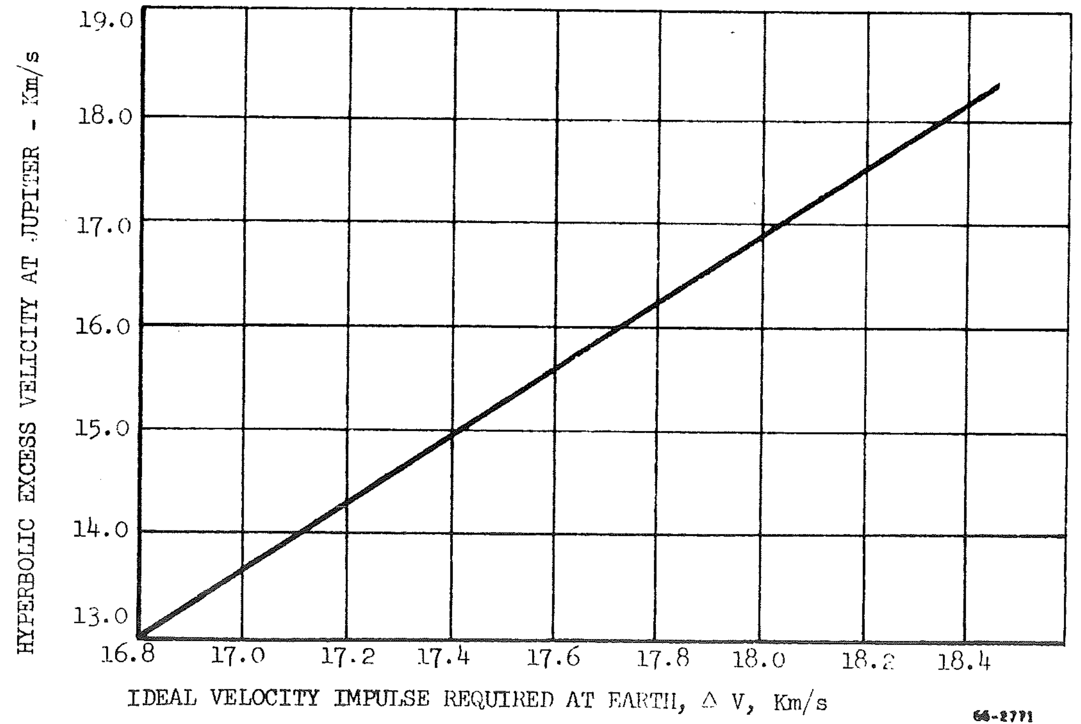

b) Ideal Velocity Impulse Required at Earth vs Hyperbolic Velocity at Jupiter for Launch Date J.D. 2441380

Figure 2 Orbital Elements of Final Heliocentric Trajectories

The objective of the mission, which is to place a vehicle in a heliocentric trajectory that is normal to the ecliptic with a given perihelion, governs the conditions that must exist at the exit from Jupiter's sphere of influence. The velocity vector must lie in a plane that is defined by the normal to the ecliptic plane and the vector from the sun to the position of the vehicle at the point of exit. It was decided to restrict the study by making the velocity vector normal to the ecliptic at the exit point. Thus, the aphelion of the final trajectory will lie close to the exit point or essentially be equal to 5.2 astronomial units. The magnitude of the velocity vector is governed by the perihelion distance desired. Once the velocity vector at exit is fixed, the velocity vector relative to Jupiter is easily computed.

Within the limitations of the patched conic program the magnitude of the velocity vector relative to Jupiter (V_i) at entry into Jupiter's sphere of influence must be equal to that at exit (V_o). By adding the velocity of Jupiter, V_j, with respect to the sun, the vehicle velocities (V and V_a) relative to the sun at entry and exit, respectively, are then known (see Figure 3.) The direction cosines of the entry velocity vector (V_i) are determined by the launch date, the desired hyperbolic excess velocity at Jupiter and the point of entry into Jupiter's sphere of influence. The excess hyperbolic velocity is defined as the velocity at infinity (V_∞) of a vehicle in a hyperbolic orbit about a central body. In this report it is taken to be the velocity of the vehicle relative to the sun minus the velocity of the planet relative to the sun at the sphere of influence of the planet. The difference in the case of the earth is less than 60 m/s.

The entry and exit velocity vectors relative to Jupiter completely determine the transfer plane through Jupiter's sphere of influence. The cross product of these vectors is the normal to the transfer plane. The in-plane geometry is shown in Figure 4. To completely define the transfer trajectory, it is necessary to determine the point of entry into Jupiter's sphere of influence. It is shown in the appendix that the direction cosines of the position vector in a Jupiter centered coordinate system can be derived from the following three conditions:

1. The position vector must lie in the transfer plane
2. The position vector must make a fixed angle with the entry velocity vector
3. The sum of the squares of the position vector's direction cosines must equal one.

The first condition follows from the fact that within Jupiter's sphere of influence two body conditions are assumed to exist, therefore, the motion is planar. The second condition follows from the fact that once the entry and exit velocity vectors are fixed, the turning angle α (Figure 4) is known. For a given velocity magnitude, the amount of turning desired and the gravity potential of Jupiter then determines the miss distance d which in turn fixes the angle that the entry position vector and velocity vector relative to Jupiter's coordinate system make with each other. The third

$\vec{V}$	THE VELOCITY RELATIVE TO THE SUN AT ENTRY TO JUPITER'S SPHERE OF INFLUENCE
$\vec{V}_j$	JUPITER'S VELOCITY RELATIVE TO THE SUN
$\vec{V}_i$	THE VELOCITY RELATIVE TO JUPITER AT ENTRY TO JUPITER'S SPHERE OF INFLUENCE
$\vec{V}_o$	THE VELOCITY RELATIVE TO JUPITER AT EXIT FROM JUPITER'S SPHERE OF INFLUENCE
$\vec{V}_a$	THE VELOCITY RELATIVE TO THE SUN AT EXIT

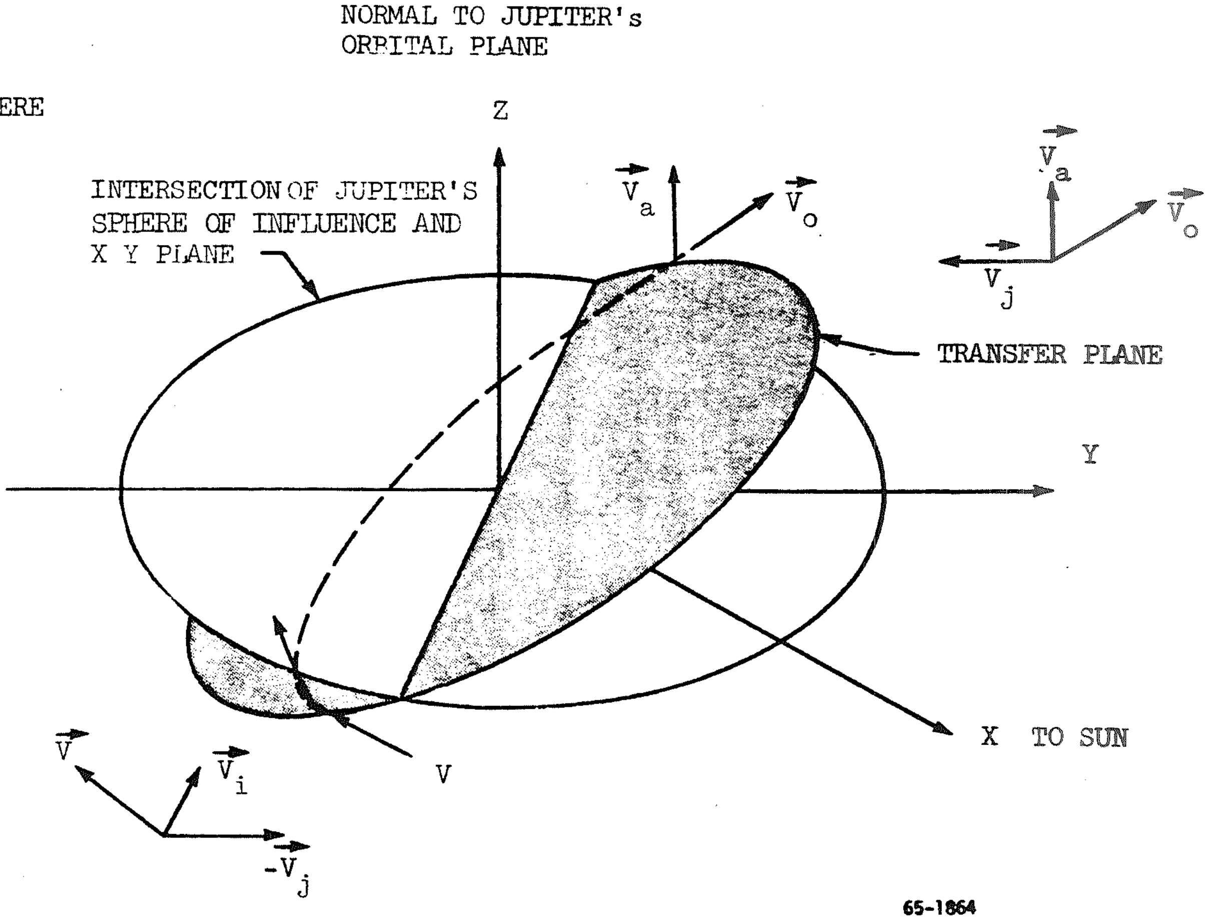
NORMAL TO JUPITER's ORBITAL PLANE
Z
INTERSECTION OF JUPITER'S SPHERE OF INFLUENCE AND X Y PLANE
$\vec{V}_a$
$\vec{V}_o$
$\vec{V}_a$
$\vec{V}_o$
$\vec{V}_j$
TRANSFER PLANE
Y
X TO SUN
$\vec{V}$
$\vec{V}_i$
V
$-\vec{V}_j$
65-1864

Figure 3 Transfer Plane Through Jupiter's Sphere of Influence

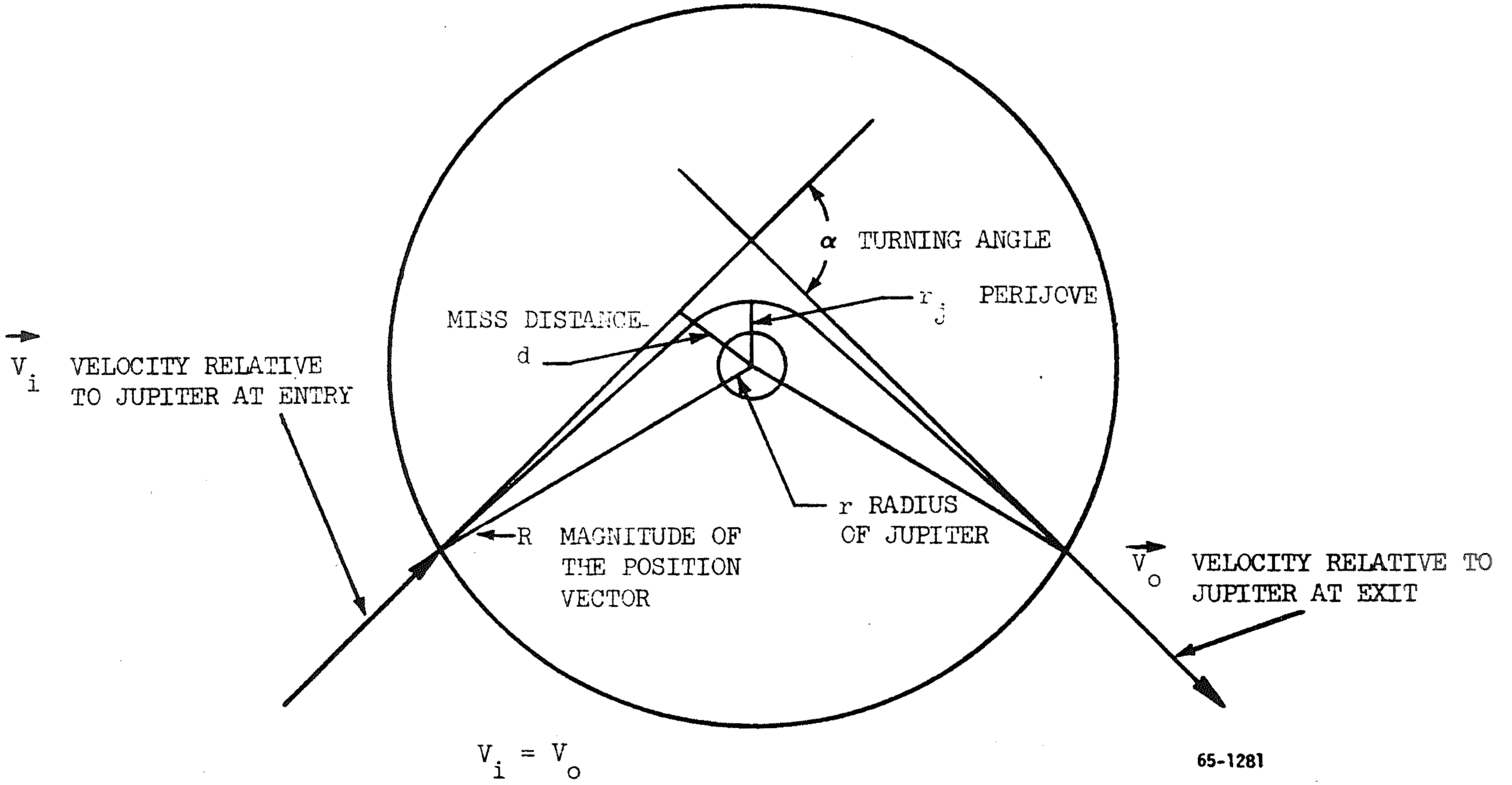
$\vec{V}_i$ VELOCITY RELATIVE TO JUPITER AT ENTRY
MISS DISTANCE d
α TURNING ANGLE
r_j PERIJOVE
R MAGNITUDE OF THE POSITION VECTOR
r RADIUS OF JUPITER
$\vec{V}_o$ VELOCITY RELATIVE TO JUPITER AT EXIT
$V_i = V_o$
65-1281

Figure 4 Transfer Plane Geometry

condition follows from the definition of a unit vector. Thus, the specification of the exit velocity vector and the orientation of the entry velocity vector define the magnitude of the entry velocity vector and its point of entry into the sphere of influence. Therefore, the desired heliocentric orbit can be obtained if the conditions of velocity magnitude and position of entry can be achieved. Given a launch date there is some hyperbolic excess velocity at earth which will put the vehicle at Jupiter's sphere of influence with the desired hyperbolic excess velocity. The velocity vector at Jupiter's sphere of influence is relatively insensitive to the point of entry but an iteration is necessary to obtain the precise launch condition. For this study, the velocity increment needed to achieve a given hyperbolic excess velocity at the Earth's sphere of influence was computed by taking the ΔV needed to achieve a 200 kilometer circular orbit (9.30 Km/s ideal velocity assuming a gravity and drag loss during boost of 1.52 Km/s) and adding the ΔV needed to arrive with a given hyperbolic excess velocity at the Earth's sphere of influence from the circular orbit.

C. Trajectory Limitations

There are two limitations on the ability to obtain a given heliocentric trajectory from a Jupiter swingby. They are the propulsion characteristics of the space vehicle and booster and the physical dimensions of Jupiter. The first is a variable limitation created by the size of the available propulsion systems whereas the second is a fixed limit which cannot be removed.

The hyperbolic excess velocity at earth needed to achieve a given hyperbolic excess velocity at Jupiter is a function of the relative position of the two planets and the flight time or the launch date and the flight time. The hyperbolic excess velocity for a fixed flight time is periodic with a period of approximately four-hundred days equal to the synodic period of Jupiter superimposed on a longer period of approximately twelve years equal to the siderial period of Jupiter. A typical launch window is shown in Figure 5. (The data shown in this figure was taken from Volume V of NASA Space Handbook.) Figure 6 shows that the hyperbolic excess velocity at Jupiter ranges from 13.1 Km/s for the closest possible approach ($V_a = 0$) to the sun to 18.5 Km/s for a near circular orbit ($V_a = 13.1$ Km/s). Figure 5 shows a near optimum launch period, which gives hyperbolic excess velocities at earth that range from 10.7 Km/s to 12.8 Km/s, respectively, for these two trajectories, shown as points A and B in the figure.

The hyperbolic velocity at Earth is converted to the total ideal velocity required by the use of Figure 7. The ideal velocity contains an allowance of 1.52 Km/s for drag and gravity loss during boost. The required ideal velocity is seen to vary from 16.8 Km/s to 18.4 Km/s for the mission spectrum. Thus, if the propulsion system used is not capable of supplying a ΔV of 18.4 Km/s, the full range of trajectories cannot be obtained.

The orientation of the velocity vector at entry into Jupiter's sphere of influence determines the amount the vector must be turned in the transfer trajectory. The amount of turning that can be obtained is a function of the magnitude of the entry velocity vector and the miss distance d. It is shown

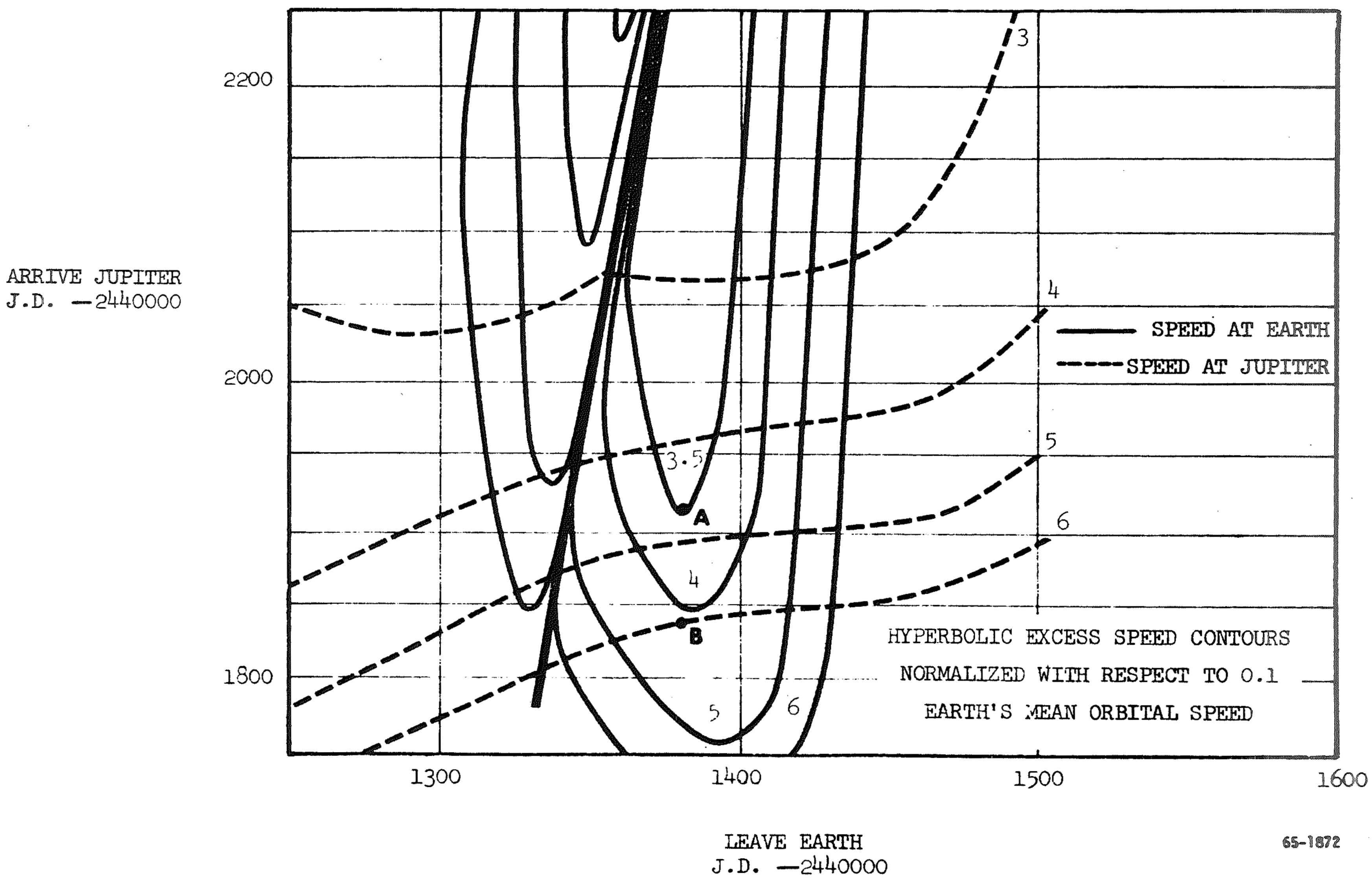

Figure 5 Earth-Jupiter Transfer (1972)

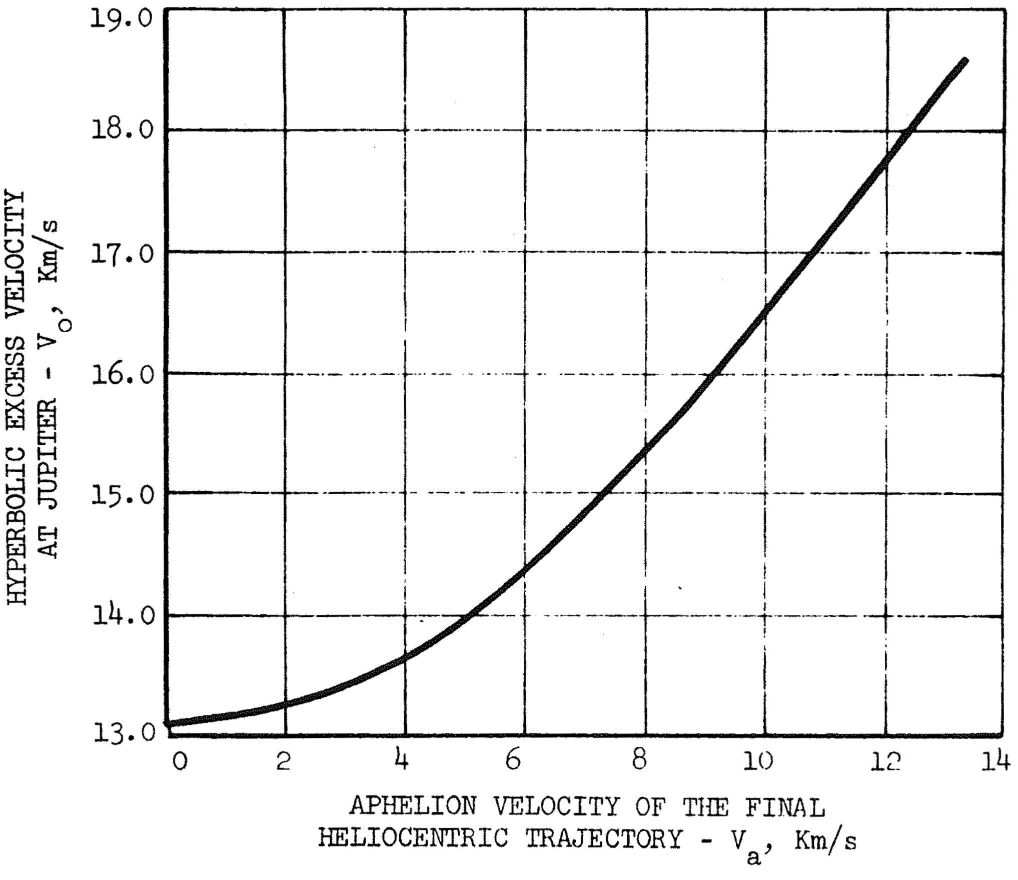

65-1865

Figure 6 Aphelion Velocity of the Final Heliocentric Trajectory Vs Hyperbolic Excess Velocity at Jupiter

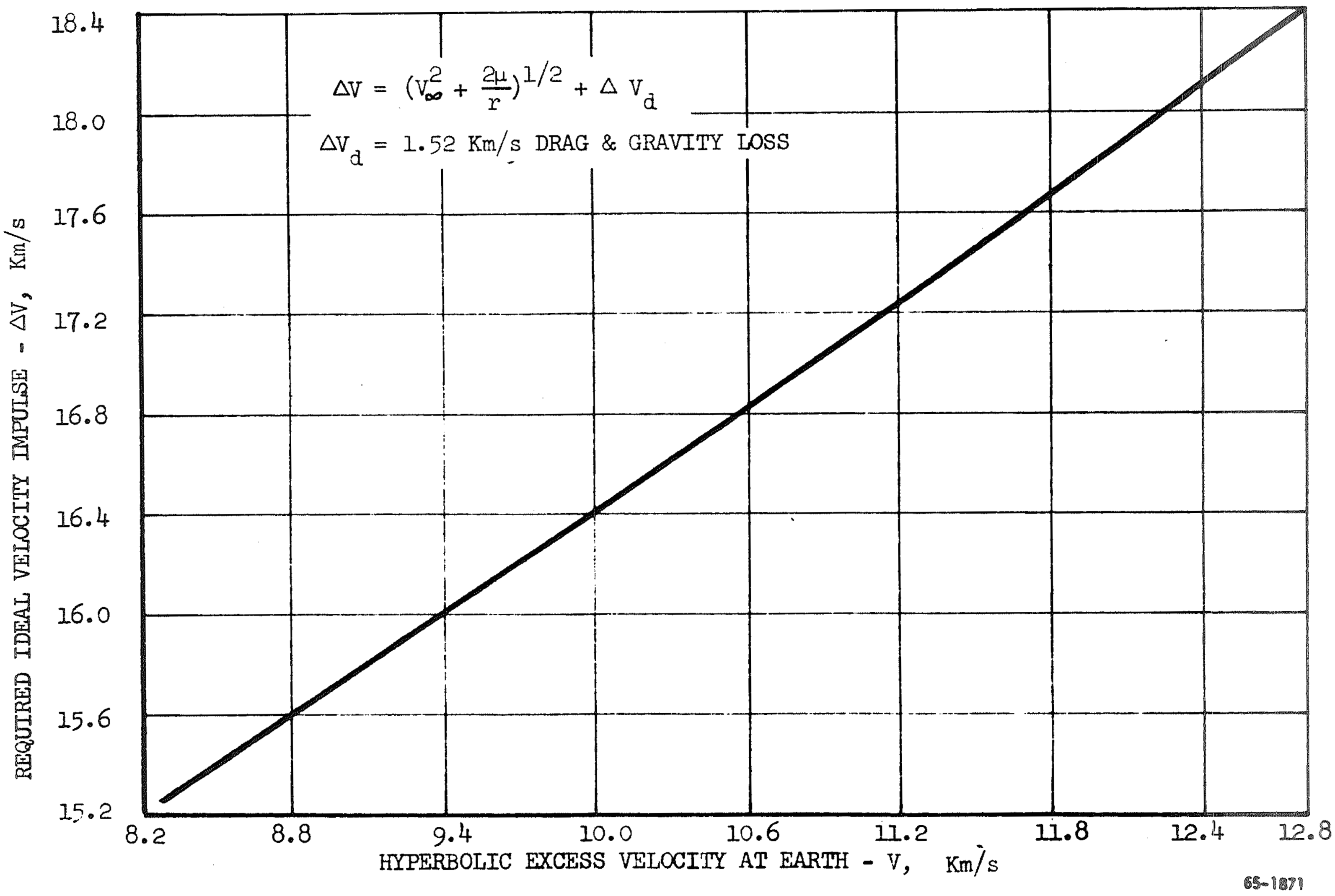

Figure 7 Velocity Impulse Required to Boost Into Hyperbolic Trajectory

in Figure 8 that for certain velocities, orientations and turning angles the vehicle would impact on Jupiter ($\frac{r_s}{r} \leq 1$). Figure 8 also shows that for the launch date used in the study, J.D. 2441380 (March 3, 1972), these extreme cases do not occur and the distance of closet approach is 3.0, Jupiter radii for a near circular helicoentric trajectory. The extreme cases occur when the vehicle arrives at Jupiter's sphere of influence with high hyperbolic excess velocity nearly parallel with Jupiter's velocity vector relative to the sun. Such conditions cannot be obtained from an Earth launch, thus, the physical size of Jupiter does not restrict the heliocentric trajectories that can be obtained.

The total time of flight from launch to perihelion passage is one of the factors governing trajectory selection. Representative flight times are shown in Figure 9. It is seen that the major portion of the time is spent in the Jupiter to perihelion phase of the flight and for near circular trajectories the total time is 2600 days (about 7 years). If the flight is assumed to end at the semi-latus rectum (the point directly over the sun), the flight time for low eccentricity is reduced to 1500 days (about 4 years).

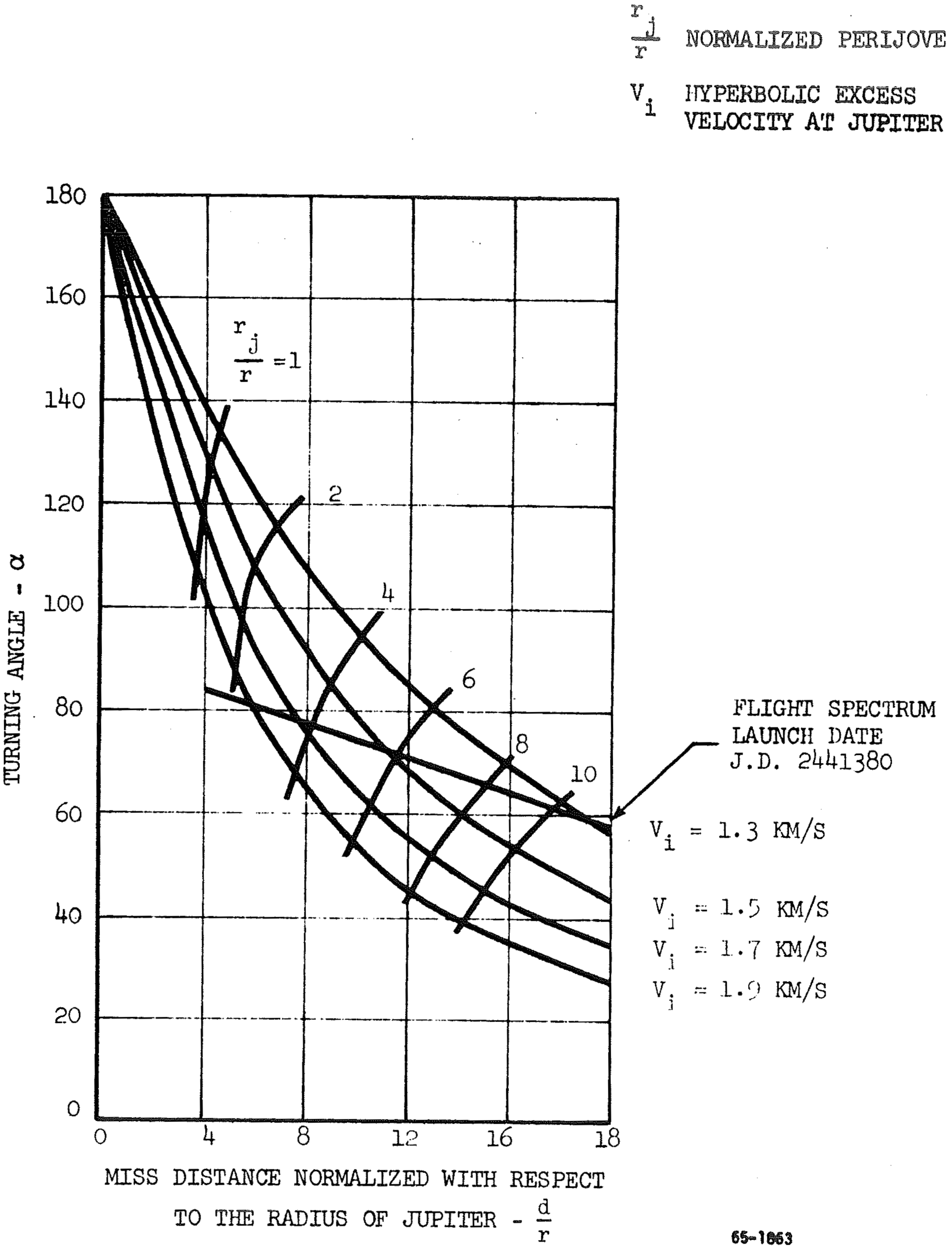

Figure 8 Normalized Miss Distance Vs Turning Angle

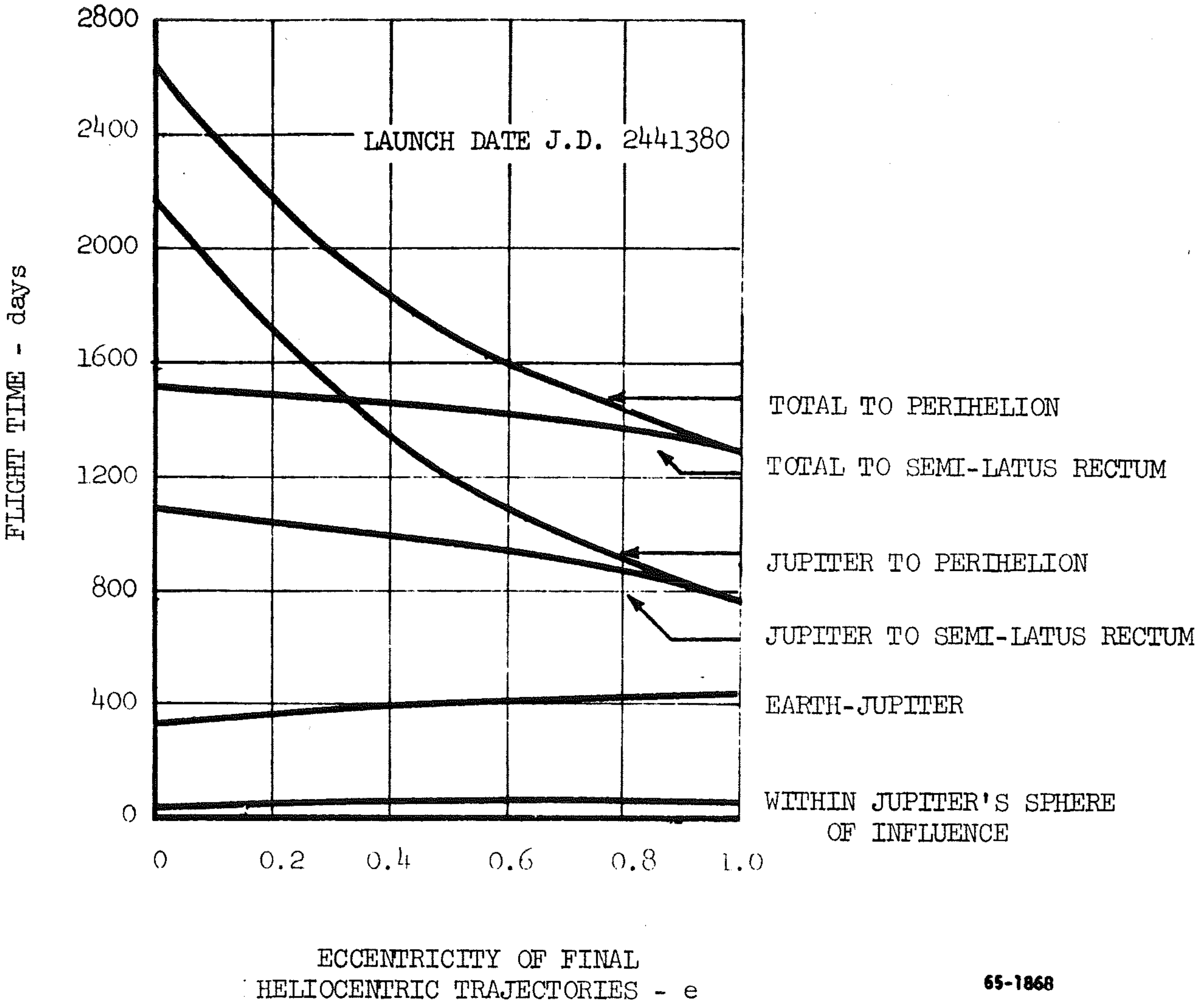

65-1868

Figure 9 Time of Flight Vs Eccentricity of Final Heliocentric Trajectories

IV. SELECTION OF TYPICAL TRAJECTORY

A. Parameter Sensitivity

Using a set of reference trajectories computed with the patched conic program, a study was made of the sensitivity of the elements of the final heliocentric orbits to changes in the injection velocity. The reference heliocentric trajectories were normal to the ecliptic with eccentricities ranging from 0.03 to 0.91. The results of the calculations for the variation in inclination, perihelion and eccentricity for perturbation of the velocity components are presented in Figures 10, 11 and 12, respectively. It can be seen from these results that the variations are similar for the three elements studied and that the low eccentricity (almost circular) orbits are the most sensitive. The sensitivity of the high eccentricity orbits are relatively low and uniform. The sensitivity parameters for the z components of velocity has a reversal of sign.

B. Selected Trajectory

The selection of a reference trajectory for use in the navigation and guidance phase of this study is governed by the limitations on propulsion and flight time and by the desire to select one with average guidance requirements. The propulsion limit of 16.8 Km/s suggested by NASA is marginal for all of the missions while the recommended time limit of six years is marginal for the near circular missions. The variations in the elements of the final heliocentric orbits as shown by the limited sensitivity study are small except near the circular orbit. In view of these conditions, it is recommended that the reference trajectory be one which passes over the sun at a distance of one astronomical unit. Such a trajectory would have an eccentricity of 0.8 and a total ideal velocity requirement of approximately 17.2 Km/s.

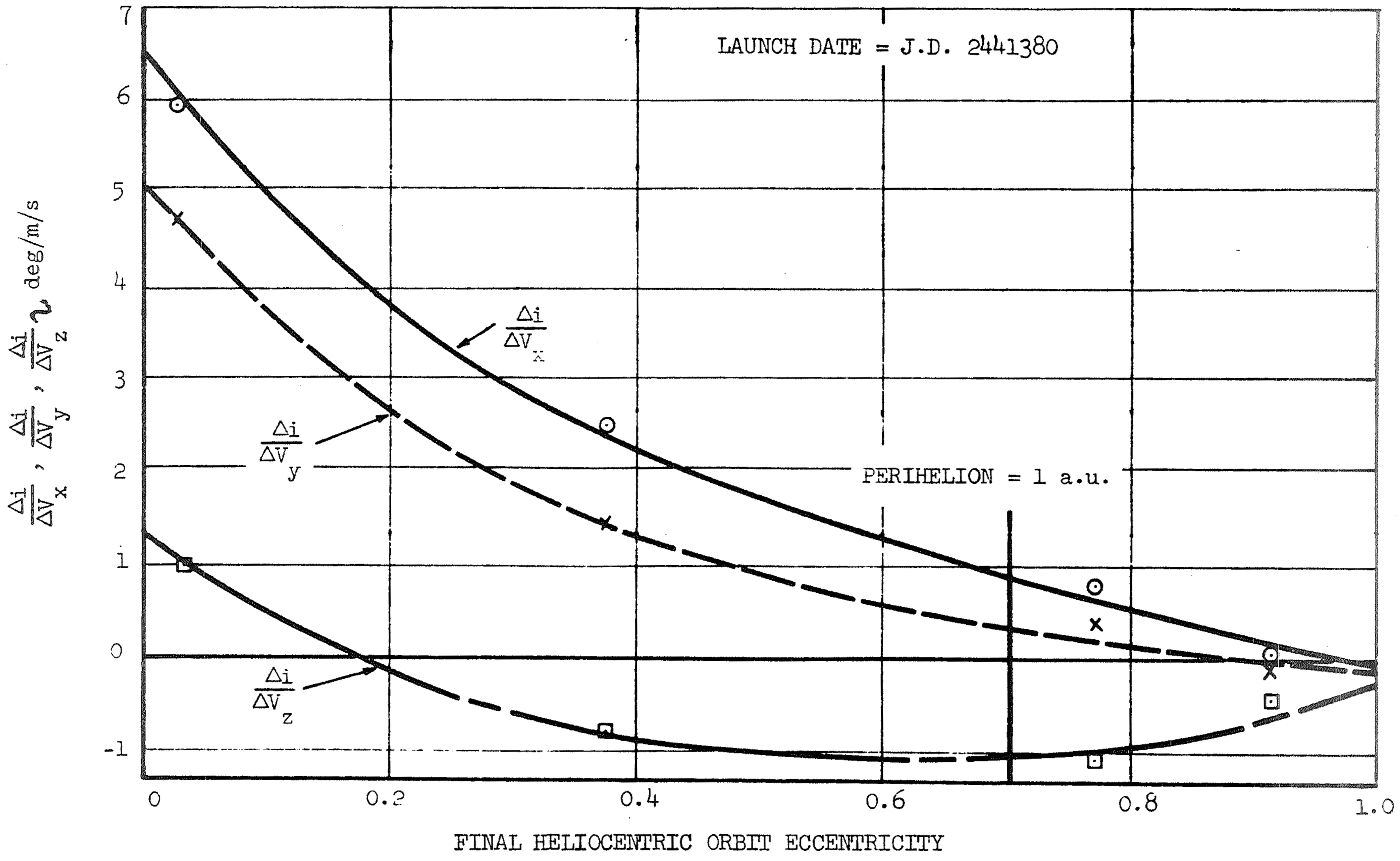

65-1254

Figure 10 Heliocentric Orbit Inclination Sensitivity to Injection Velocity Errors

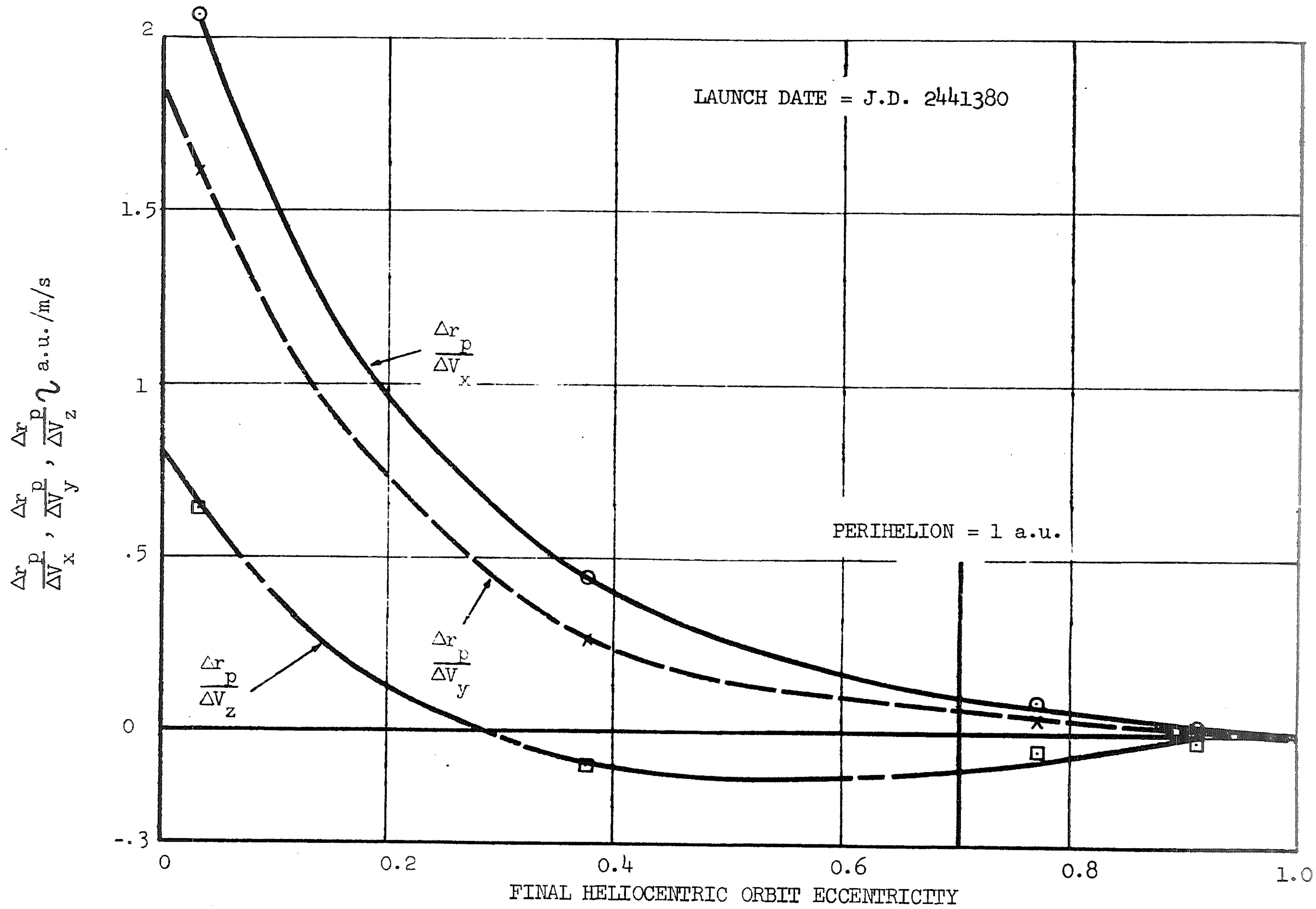

65-1252

Figure 11 Heliocentric Orbit Perhelion Sensitivity to Injection Velocity Errors

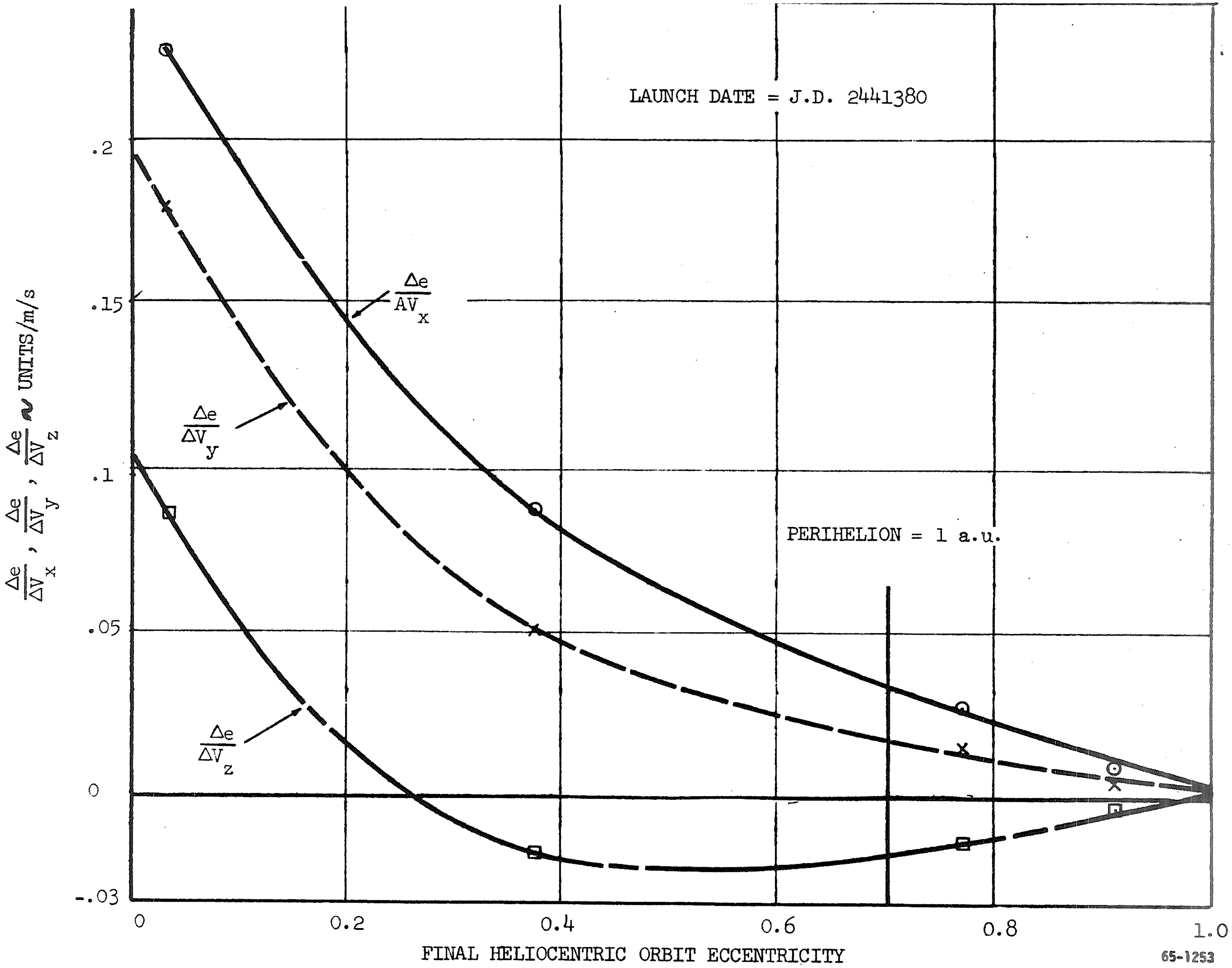

Figure 12 Heliocentric Orbit Eccentricity Sensitivity to Injection Velocity Errors

V. REFERENCES

1 Porter, R. F.; Luca, N. G.; and Edgecombe, D. S.; A Preliminary Study
of Jupiter Gravity Assisted Trajectories.
BMJ-NLVP-65-4
Battelle Memorial Institute, July 7, 1965.

2 Maxwell W. Hunter II, Future Unmanned Exploration of the Solar Systems
Astronautics and Aeronautics, Vol. No. 2, May 5, 1964.

APPENDIX

Mathematical Formulation of Problem

In the following discussion, it is assumed that the desired heliocentric trajectory lies in a plane normal to the ecliptic and has its aphelion at the point of exit from Jupiter's sphere of influence. The last condition is an approximation that is strictly true only when the point of exit lies in the ecliptic plane. The desired velocity at aphelion will be given and will range from zero to the circular orbit velocity of Jupiter (0 to 13.1 Km/s). These conditions fix the magnitude and direction of the velocity vectors relative to Jupiter at the point of exit.

$$\vec{V}_o = (0, V_j, V_a)$$

V_o is the magnitude of the exit velocity relative to Jupiter

V_a is the magnitude of the exit velocity relative to the Sun

V_j is the magnitude of Jupiter's velocity relative to the Sun

The velocity vector relative to Jupiter at entry to Jupiter's sphere of influence is of the following form:

$$\vec{V}_i = (\lambda V, \mu V + V_j, \nu V)$$

where V is the magnitude of the velocity vector relative to the sun and λ, μ and ν are its direction consines relative to Jupiter's coordinate system. For the analysis presented in this appendix it is assumed that Jupiter lies in the ecliptic plane. The coordinate system has its X axis lying along the vector to the sun, its Z axis normal to the ecliptic plane and its Y axis forming a right-handed system. The trajectory through Jupiter's sphere of influence is symmetrical, therefore, V_i must equal V_o. Equating the two and solving for V gives

$$V = -\mu V_j \pm [V_j^2 (\mu^2 - 1) + V_o^2]^{1/2}$$

If the trajectory from Earth is direct then μ is negative and only the plus sign is valid. If in addition

$$V_o = \bar{\alpha} V_j \qquad 1 \leq \bar{\alpha} \leq \sqrt{2}$$

then

$$V = V_j \left\{ -\mu + [\bar{\alpha}^2 + \mu^2 - 1]^{1/2} \right\}$$

Thus it is seen that the magnitude of the entry velocity relative to the sun is a function of Jupiter's velocity relative to the sun, the exit velocity relative to the sun and the y direction cosine of the entry velocity vector.

The two vectors $\vec{V}_i$ and $\vec{V}_o$ determine the plane of the transfer trajectory. The unit vector normal to this plane is

$$\vec{n} = \left[\frac{(-\mu+[\bar{\alpha}^2+\mu^2-1]^{1/2})(\nu-\mu(\bar{\alpha}^2-1)^{1/2})-(\bar{\alpha}^2-1)^{1/2}}{\bar{\alpha}^2 \sin \alpha}; \right.$$

$$\left. \frac{\lambda(\bar{\alpha}^2-1)^{1/2}(-\mu+[\bar{\alpha}^2+\mu^2-1]^{1/2})}{\bar{\alpha}^2 \sin \alpha}; \frac{-\lambda(-\mu+[\bar{\alpha}^2+\mu^2-1]^{1/2})}{\bar{\alpha}^2 \sin \alpha} \right]$$

where the turning angle α shown in Figure 4 is the angle formed by the two vectors. The angle α is given by the following equation:

$$\cos \alpha = \frac{1+(\mu+\nu[\bar{\alpha}^2-1]^{1/2})(-\mu+[\bar{\alpha}^2+\mu^2-1]^{1/2})}{\bar{\alpha}^2}$$

From a plot of α vs d/r_j, Figure 8, it is possible to determine the angle ξ between the velocity vector at entry relative to Jupiter and the position vector to the center of Jupiter.

$$\cos \xi = [1-(\frac{d}{R})^2]^{1/2}$$

where d, and R are as defined in Figure 4. The position of entry on the sphere of influence is then determined from a solution of the following equations:

$$\vec{n} \cdot \vec{R} = 0$$

$$\frac{\vec{R} \cdot \vec{V}}{RV} = -\cos \xi$$

$$\ell^2 + m^2 + n^2 = 1$$

where $\vec{R}$ is the position vector at entry with l, m, and n as direction cosines. The above equations are solved simultaneously for ℓ, m, and n. Thus, it is seen that the problem is completely determined except for the direction cosines of the entry velocity vector (λ, μ, ν).

The determination of the launch conditions for a given launch date that will give a specified heliocentric trajectory is an iterative process. With a given exit velocity and an assumed μ the magnitude of the entry velocity relative to the sun is computed. The hyperbolic excess velocity at Earth needed to achieve this velocity is determined from a plot such as Figure 5.

The patch conic program is used to compute a new value of μ. The calculation is repeated until the values of V and μ are compatible with the desired end conditions. The point of entry needed to achieve the desired heliocentric trajectory is then computed and compared with the point obtained from the patched conic program. The launch conditions are varied to hit the computed entry point and V and μ are calculated. The process is repeated until the magnitude, direction and point of entry are compatible with the desired end conditions.

GLOSSARY OF SYMBOLS

ΔV	Ideal velocity impulse required at Earth
e	Eccentricity
V_i	Velocity vector relative to Jupiter at entry into Jupiter's sphere of influence
V_o	Velocity vector relative to Jupiter at exit from Jupiter's sphere of influence
V_j	Jupiter's orbital velocity
V_∞	Hyperbolic excess velocity
α	Turning angle: angle between the velocity vectors entering and exiting from Jupiter's sphere of influence
d	Miss distance: the perpendicular distances from the center of Jupiter to the line defined by the velocity vector at entry to Jupiter's sphere of influence
ξ	The angle between the position vector and velocity vector at entry into Jupiter's sphere of influence relative to Jupiter's coordinate system
V_a	Velocity vector at exit from Jupiter's sphere of influence relative to the sun
r	Radius of Jupiter
r_j	Perijove
V	Velocity vector at entry into Jupiter's sphere of influence relative to the sun
λ, μ, ν	The direction cosines of V relative to Jupiter's coordinate system
R	The position vector at entry into Jupiter's sphere of influence relative to Jupiter's coordinate system
ℓ, m, n	The direction cosines of R
r_p	Perihelion
i	Inclination of final heliocentric orbital plane
ΔV_x, ΔV_y, ΔV_z	Injection velocity errors
J.D.	Julian date

APPENDIX B

NAVIGATION ANALYSIS

APPENDIX B

NAVIGATION ANALYSIS

A. Interplanetary Space Navigation

1. Mathematical Analysis

The Interplanetary Space Navigation (ISN) scheme is based upon the equations of motion of a point mass in a spherical coordinate system. Figure B-1 shows the orientation of the spherical coordinate frame ($R - \theta - \psi$) with respect to Cartesian inertial coordinate ($I_1 - I_2 - I_3$). The orientation of the orbital plane and the initial value of θ are defined by the assumed injection conditions. As the actual orbital plane is perturbed by the non-spherical gravity potentials and by the other bodies, the angle θ becomes only an approximation of the true range angle. For this reason, general definitions of the vehicle angular velocity

$$\omega_s = \left[\dot{\theta}^2 \cos^2\psi + \dot{\psi}^2 \right]^{1/2}$$

and range angle error

$$\Delta\theta_R = \frac{\Delta\dot{\theta} \; \dot{\theta} \cos^2\psi + \Delta\psi \dot{\psi}}{\omega_s}$$

are given here for use in the equations to follow.

The equations for the acceleration of a vehicle in spherical coordinates are

$$a_\theta = R\ddot{\theta} \cos\psi + 2\dot{\theta} (\dot{R} \cos\psi - R\dot{\psi} \sin\psi)$$

$$a_R = \ddot{R} - R\dot{\psi}^2 - R\dot{\theta}^2 \cos^2\psi$$

$$a\psi = R\ddot{\psi} + R\dot{\theta}^2 \sin\psi\cos\psi + 2\dot{R}\dot{\psi}$$

where the symbols θ, R, and ψ are as defined in Figure B-1 and the quantities a_θ, a_R, and $a\psi$ are linear accelerations in the θ, R, and ψ directions, respectively. In a form more suitable for tracking loop mechanization the above equations become

Page intentionally left blank

$$\ddot{\Theta} = \frac{g_{\Theta} + a_{m\Theta} + 2\dot{\Theta}\,(R\dot{\psi}\,\sin\psi - \dot{R}\,\cos\psi)}{R\,\cos\psi}$$

$$\ddot{R} = g_R + a_{MR} + R\,(\dot{\Theta}^2\,\cos^2\psi + \dot{\psi}^2)$$

$$\ddot{\psi} = \frac{g_{\psi} + a_{M\psi} - 2\dot{R}\dot{\psi} - R\dot{\Theta}^2\sin\psi\,\cos\psi}{R}$$

where a_Θ, a_R and a_ψ have been divided into their respective specific force ($a_{M\Theta}$, a_{MR}, $a_{M\psi}$) and gravitational (g_Θ, g_R, g_ψ) parts. The expressions for the gravitational terms depend on the sphere of influence within which the vehicle is moving. Oblateness terms of the central body are included when the vehicle is within the Earth's or Jupiter's sphere of influence. The standard expressions for N bodies are used with the number of bodies being governed by the sphere of influence.

In a purely inertial navigation system, these equations (or a similar set in Cartesian inertial coordinates) would be solved by open integration. Because of uncertainties in the gravity terms, measurement errors, and integration errors, the position tracking errors diverge with time. In the ISN concept observations of the line of sight to known planets relative to inertial space are used to bound these errors.

At the time an observation of a planet is taken, the output of the positioning tracking loop is used to compute the expected orientation of the line of sight of the observation. The difference between the actual observation and the expected line of sight are processed through a geometry relationship resulting in estimations of the errors $\Delta\Theta$ and $\Delta\psi$. As is shown in Figure B-2, these errors in Θ and ψ are filtered and fed back through the gains K_Θ, $K_{v\Theta}$, K_ψ, and $K_{v\psi}$ to bound the Θ and ψ loops and through K_R to bound the R loop. The purpose of the filter is to improve measurement noise attenuation for frequencies greater than orbit frequency. The filter is represented by the following equations

$$\Delta\Theta' = \frac{1}{\tau_1}\int_0^t (\Delta\Theta - \Delta\Theta')\,dt$$

$$\Delta\psi' = \frac{1}{\tau_2}\int_0^t (\Delta\psi - \Delta\psi')\,dt$$

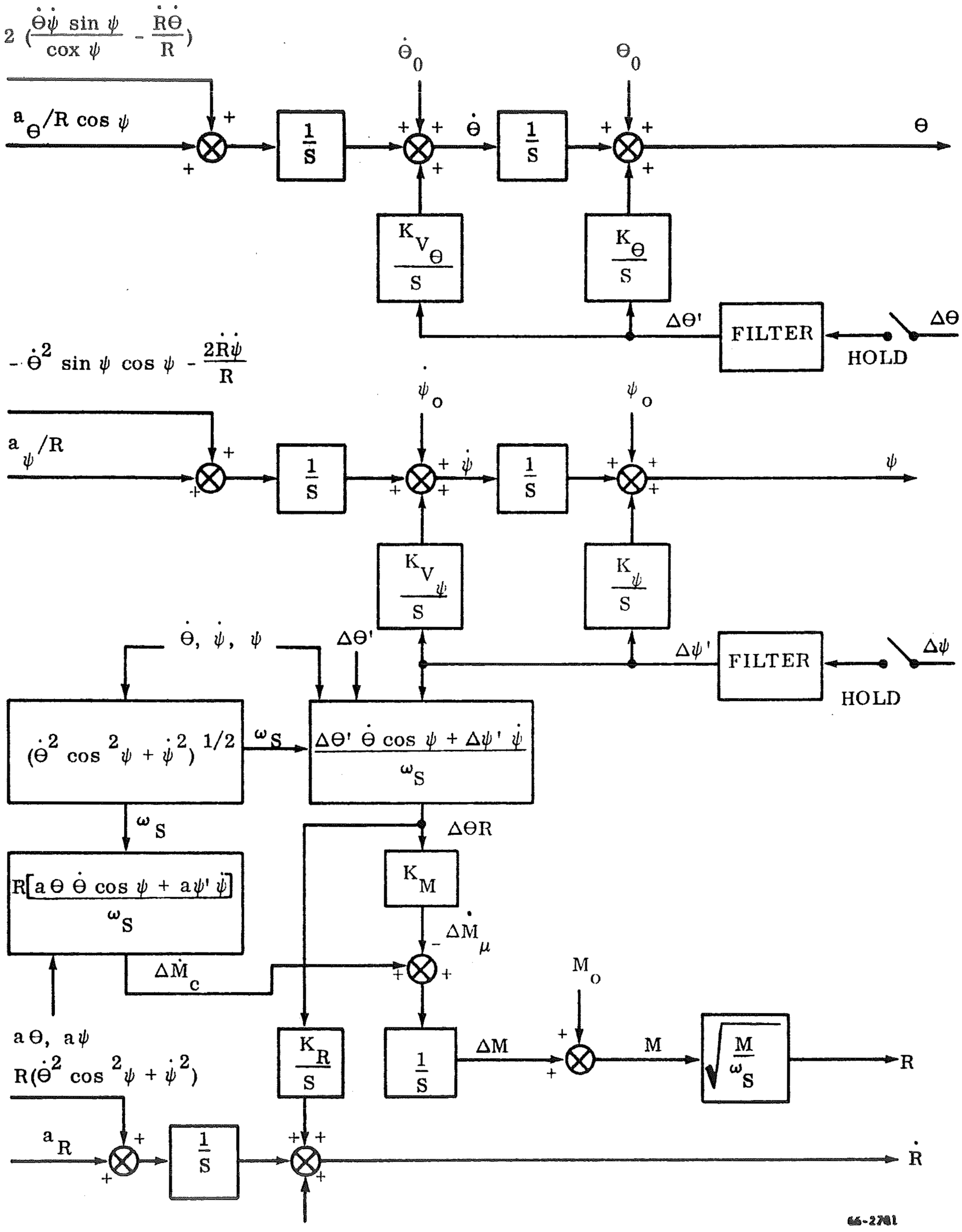
$2\left(\frac{\dot{\Theta}\dot{\psi}\sin\psi}{\cos\psi} - \frac{\dot{R}\dot{\Theta}}{R}\right)$
$a_\Theta/R\cos\psi$
$\dot{\Theta}_0$
Θ_0
$\frac{1}{S}$
$\dot{\Theta}$
Θ
$\frac{K_{V_\Theta}}{S}$
$\frac{K_\Theta}{S}$
$\Delta\Theta'$
FILTER
HOLD
$\Delta\Theta$
$-\dot{\Theta}^2\sin\psi\cos\psi - \frac{2\dot{R}\dot{\psi}}{R}$
a_ψ/R
$\dot{\psi}_o$
ψ_o
$\dot{\psi}$
ψ
$\frac{K_{V_\psi}}{S}$
$\frac{K_\psi}{S}$
$\Delta\psi'$
FILTER
HOLD
$\Delta\psi$
$\dot{\Theta}, \dot{\psi}, \psi$
$\Delta\Theta'$
$(\dot{\Theta}^2\cos^2\psi + \dot{\psi}^2)^{1/2}$
ω_S
$\frac{\Delta\Theta'\dot{\Theta}\cos\psi + \Delta\psi'\dot{\psi}}{\omega_S}$
$\Delta\Theta R$
ω_S
$\frac{R[a\Theta\dot{\Theta}\cos\psi + a\psi'\dot{\psi}]}{\omega_S}$
K_M
$\Delta\dot{M}_\mu$
$\Delta\dot{M}_c$
M_o
$a\Theta, a\psi$
$R(\dot{\Theta}^2\cos^2\psi + \dot{\psi}^2)$
$\frac{K_R}{S}$
ΔM
M
$\sqrt{\frac{M}{\omega_S}}$
R
a_R
$\dot{R}$
66-2781

Figure B-2 Interplanetary Space Navigation Loops where τ_1 and τ_2 are constants that determine the frequency above which attenuation of noise is reduced. At time $t = o$, $\Delta\Theta'$ and $\Delta\psi'$ are taken equal to $\Delta\Theta$ and $\Delta\psi$.

As shown in Figure B-2, $\ddot{R}$ is integrated once to obtain $\dot{R}$ which is used in calculating the coriolis terms in $\ddot{\Theta}$ and $\ddot{\psi}$. R itself is computed using the principle of constant angular momentum.

$$R = \left[\frac{M}{\omega_s}\right]^{1/2}$$

In order to correct for initial errors in the momentum, M, the feedback of $\Delta\Theta_R$ is introduced. It is based on the principle that when M is in error a corresponding lead or lag in Θ_R results for positive or negative values, respectively, of $M - M_{true}$. The situation is corrected by feeding back the integral of range angle error times a constant K_M.

In the presence of lateral perturbing forces or non-central gravity components, the principle of constant angular momentum does not hold, so that a momentum compensation must be applied to M. This compensation term ΔM_c is given by the following equation

$$\Delta M_c = \int_o^t \frac{R(a_\Theta \dot{\Theta} \cos\psi + a_\psi \dot{\psi})\, dt}{\omega_s}$$

The gains used in the ISN scheme are selected on the basis of a linear analysis of the equivalent two-body problem. The gain combinations are optimized based on the following requirements:

1) The system must be stable.

2) Initial condition error should be reduced to acceptable limits within less than one-quarter of the orbit.

Discussions of the dynamic analysis and gain selection are presented in the following paragraphs.

2. Dynamic Analysis

Ideally, the equations of motion used to compute the motion of the vehicle in the gravitational field associated with this mission would yield outputs of true position and velocity. These computations would require the exact initial conditions to start the computation. However, errors will be present, both in the initial conditions and in the modeling and computation process. Thus external navigational information available from observations is required to feed back corrections which bound the computation process. The equations model a dynamic situation, and their embodiment in the computer can be viewed as the computational analog of the motion of the bodies involved. All the model state variables appear as signal quantities at various points within the model.

The ISN uses angular measurements of the line of sight to available celestial bodies to estimate the angular orientation of the vehicle position vector relative to the computational frame of reference. This information is fed back to correct the angular orientation information of the mathematical model. In so doing, various information feedback paths, or loops, are determined from the indicated error point to points within the mathematical model. The selection of the feedback path and the gains to provide the dynamic compensation for each path constitute the design choices to be made in optimizing the ISN for a specific mission. It is convenient to use the techniques of feedback control theory in making this selection.

Fundamentally, the ISN performs the process of estimation of desired flight path parameters by processing information from on-board sensors. From the control design viewpoint it is possible to consider that the ISN performs the estimation by formulating a mathematical model of the orbital motion that causes the range angle output of the model to follow closely, or "track," the position vector as derived from the measurements. This tracking is accomplished in a closed loop manner so that the model output will follow the motion of the local vertical and bound the errors in estimation of the path. A functional block diagram illustrating this point of view is presented in Figure B-3 for the two-dimensional planar case. Ideally, the orbital model would be self-contained requiring only initial condition inputs and yielding outputs of computed vertical orientation, radial velocity, angular velocity of the vertical, and radius. In such an ideal situation no angular errors would be present and no information would be flowing into the model along the feedback paths. In the non-ideal case errors are present, and the tracking loop for correcting these errors is shown as the closed loop at the top of the figure. As far as their effect upon this tracking loop, the orbital equations become part of the compensation of the forward path of the loop. This permits one to use control theory to select compensation parameters so as to achieve specified performance. In the absence of noise, the time history of angular measurements supplies sufficient information to remove transient errors from this system so that angular position and velocity approach the true value. Similarly, by the relationship of orbital motion, the radius (or the magnitude of the vehicle position vector) also approaches the true value. The rate of change of radial velocity is fundamentally an expression of the

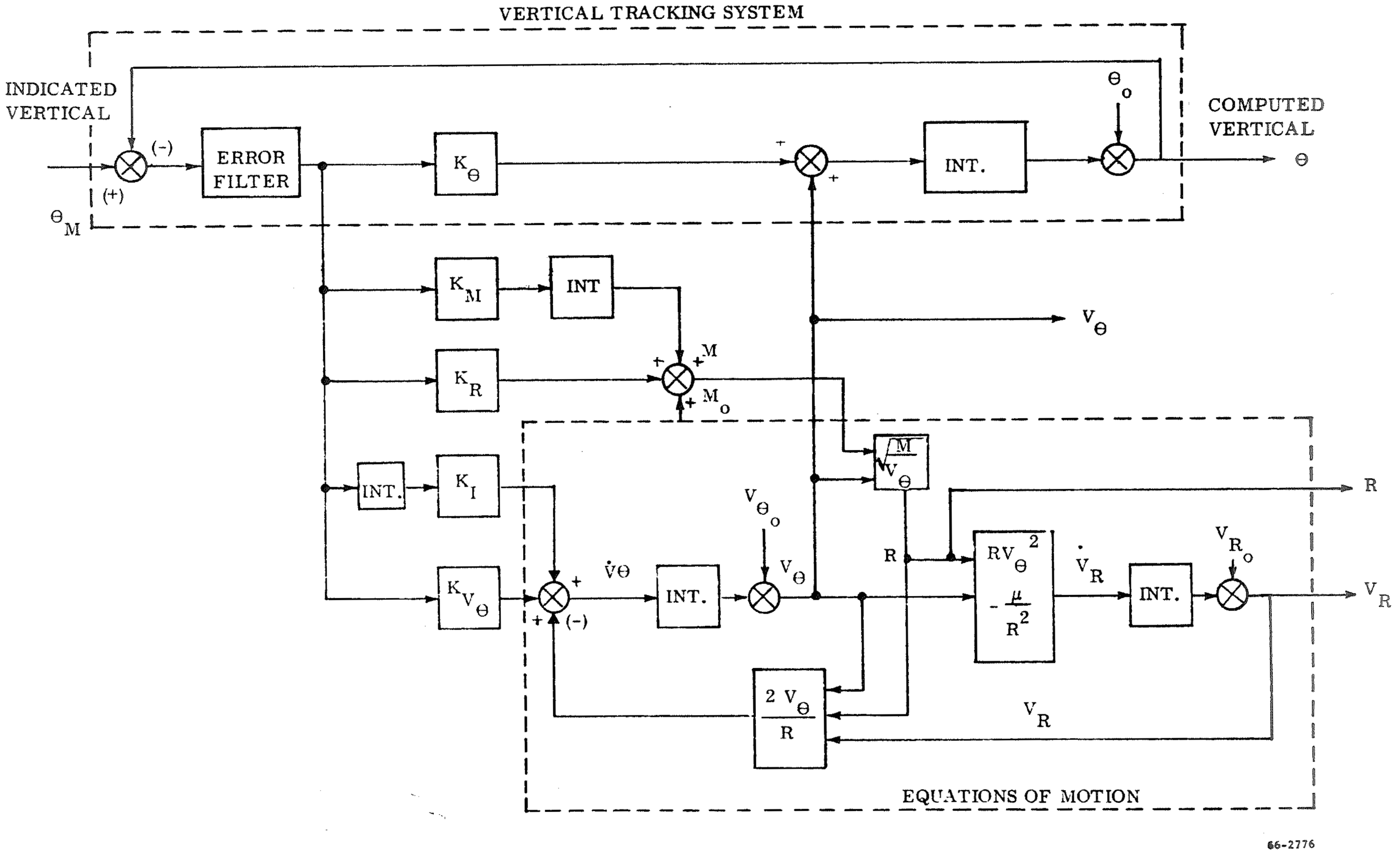
VERTICAL TRACKING SYSTEM
INDICATED VERTICAL
(-)
(+)
θM
ERROR FILTER
Kθ
+
+
INT.
θo
COMPUTED VERTICAL
θ
KM
INT
Vθ
KR
+
+M
+ Mo
√M/Vθ
R
INT.
KI
Vθo
R
RVθ²
- μ/R²
V̇R
INT.
VRo
KVθ
+
V̇θ
INT.
Vθ
VR
+
(-)
2 Vθ/R
VR
EQUATIONS OF MOTION
66-2776

Figure B-3 Interplanetary Space Navigation Control Loops angular momentum relationship of the orbit. As such, the radius (or position of the vehicle along the vertical) can be computed from the expression for angular momentum. In so doing, the errors associated with an open-loop integration of radial velocity to obtain radius can be avoided.

Viewed in this manner, the tracking system becomes a filter whose static and dynamic transmission characteristics can be specified and whose performance can be analyzed using all the techniques of standard control theory. The specifications of performance depend upon the form chosen for the model of the process as well as upon the mission requirements for transient and steady state accuracy. If the model assumes that the vehicle is in free fall motion about a central body whose gravitational field is described by the analytical model, the ideal filter would follow with no error all frequencies of motion of the indicated vertical up to and including orbital frequency and reject all frequency components above orbital frequency which arise from geometrical variations sensed by the vertical sensor. At the same time, initial condition errors should be eliminated as rapidly as possible. These two requirements conflict, so that one has to specify the compromise desired before the system parameters can be selected.

The critical frequency for orbital motion is, of course, the mean orbital frequency. To a first order approximation an elliptic orbit exhibits an angular velocity equal to a constant plus a sinusoidal term at orbital frequency. Thus, the filter should reproduce the orbital frequency term with identical amplitude and zero phase shift. Referring to Figure B-3, if one disregards the compensations, the upper portion of the block diagram represents a first order servo loop. If such a loop were to reproduce the orbital frequency term faithfully, the bandwidth would have to be high and there would be significant transmission of components of the indicated vertical at twice orbital frequency and above. The contribution that is made by the use of the equations of motion is to permit a reduction in the bandwidth of the tracking loop, while insuring unit amplitude ratio and zero phase shift at orbital frequency. It does this, as shown in the lower half of the figure, by essentially adding an undamped tuned oscillator which is automatically tuned to the frequency of the vehicle's orbit. In addition to performing the tuning function, the updating of momentum then appears as "integral control" added in parallel in the forward loop. The integral term converts the first order tracking system to second order and adds a closed-loop numerator zero to the transfer. Additional shaping of the frequency response is possible by adding compensation to the forward path of the loop.

The tuned system also results in the radius loop performing without error at orbital frequency. Ideally the radius computation would reject all other frequencies of the indicated vertical. The dynamics of the system are such that if a first order lag is used for compensation, the radius loop will cut off as $(\frac{\omega}{\Omega})$ for $\omega < \Omega$ and as $\frac{1}{(\omega/\Omega)}$ for $\omega > \Omega$, where Ω is orbital frequency, and ω is forcing frequency. Other compensations are feasible, of course.

3. Selection of ISN Gains

The motion of an orbiting vehicle is represented mathematically by a set of non-linear differential equations. In the ISN these equations are continually being integrated by the on-board computer with the information flowing as shown in Figure B-3. For nearly circular orbits, the analysis of the effects of measurements errors and inaccuracies in injection conditions can be achieved by a linearization of the equations considering small deviations from an equilibrium circular orbit. Comparison of time histories of vehicle motion using the circular linearized orbit equations with those using the non-linear set shows that for nearly circular orbits the differences between the two have negligible effect upon the choice of design parameters. For orbits of large eccentricity corresponding to the Jupiter mission, this same linearization is surprisingly effective in at least guiding the selection of gain values so that computer simulations can be made. In Figure B-3, the gain K_M is used to update errors in initial angular momentum, and the gain K_R adds lead compensation. This directly affects the computed value of radius which in turn modifies radial acceleration and through radial velocity changes the angular velocity. This angular momentum updating is most effective when a whole orbit can be averaged. However, when used over the portion of an orbit for which the radius is large, as in this application, this feedback to angular velocity is weak, and in the Jupiter Swing-by mission it was found to be simpler to use zero values of K_R and K_M and to add the integration term to the angular acceleration summation point, K_I.

The non-linear equations for the planar case then become those given by equation set (1).

$$\left.\begin{aligned}
\dot{\Theta} &= K_{\Theta}(\Theta_M - \Theta) + V_{\Theta} \\
\dot{V}_{\Theta} &= -\frac{2V_{\Theta}V_R}{R} + K_{V_{\Theta}}(\Theta_M - \Theta) + K_I\int(\Theta_M - \Theta)\,dt \\
\dot{V}_R &= RV_{\Theta}^2 - \frac{\mu}{R^2} \\
R &= \sqrt{\frac{M_o}{V_{\Theta}^2}}
\end{aligned}\right\} \qquad (1)$$

where Θ_M = local vertical measured by observations

Θ = computed local vertical

The linearized equations are linear differential equations in the deviation of the dependent variables from their nominal values. Using a circular orbit about a homogeneous spherical central body as the nominal path, the linear equations are

$$\left.\begin{aligned}
\Delta\dot{\theta} &= K_\theta(\Delta\theta_M - \Delta\theta) + \Delta V_\theta \\
\Delta\dot{V}_\theta &= -\frac{2V_{\theta_o}}{R_o}\Delta V_R + K_{V_\theta}(\Delta\theta_M - \Delta\theta) + K_I\int(\Delta\theta_M - \Delta\theta)\,dt \\
\Delta\dot{V}_R &= 2R_o V_\theta \Delta V_o + 3\theta_o^2 \, \Delta R \\
\Delta R &= -\frac{R_o}{2V_{\theta_o}}\Delta V_\theta
\end{aligned}\right\} \quad (2)$$

In equation set (2) no additional filtering of the measured vertical error information has been assumed. The linearized system of the Laplace transform of equation set (2) can be represented by the block diagram of Figure B-4. The forward path of this linearized tracking system can be considered to be the direct path through the gain K_θ in parallel with a compensation path. When this is done, the diagram is reduced to that of Figure B-5, and the presence of the undamped oscillator becomes more apparent.

The compensation can then be selected to provide a desired transient response for specified initial conditions which in this case are the injection errors at the start of the orbital journey. Considering the open-loop transfer function of the system, the two parallel paths combine to form the transfer function of equation (3).

$$G_{oL} = \frac{K_\theta}{V_{\theta_o}} \frac{\left[p^2 + \frac{K_{V_\theta}/V_{\theta_o}^2}{K_\theta/V_\theta}\,p + \left(1 + \frac{K_I/V_{\theta_o}^3}{K_\theta/V_{\theta_o}}\right)\right]}{p\left[p^2 + 1\right]} \quad (3)$$

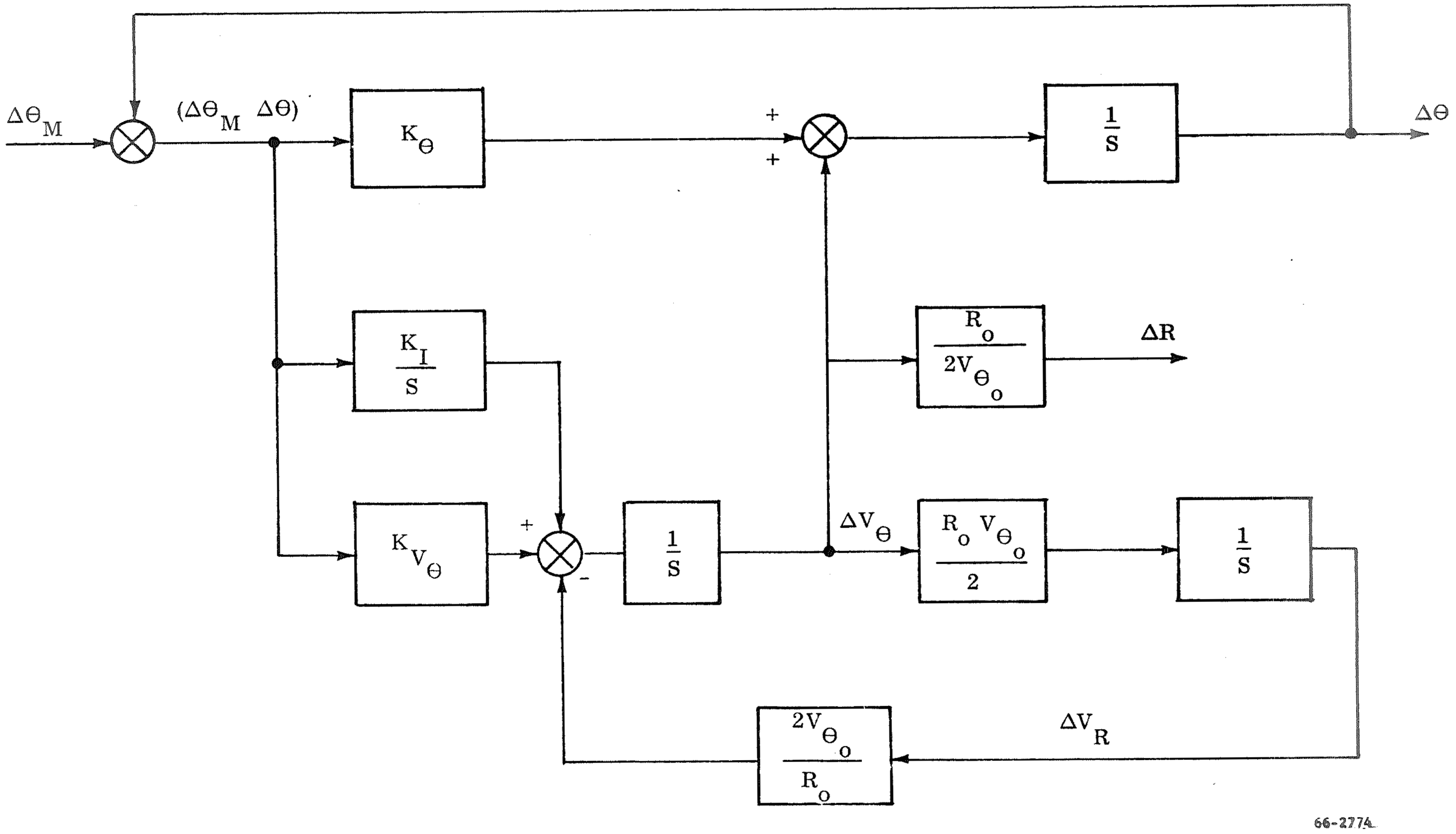
ΔΘM
(ΔΘM ΔΘ)
KΘ
+
+
1/S
ΔΘ
KI/S
Ro/2VΘo
ΔR
KVΘ
+
-
1/S
ΔVΘ
Ro VΘo/2
1/S
2VΘo/Ro
ΔVR
66-2774

Figure B-4 Linearized ISN Control Loops, Diagram I

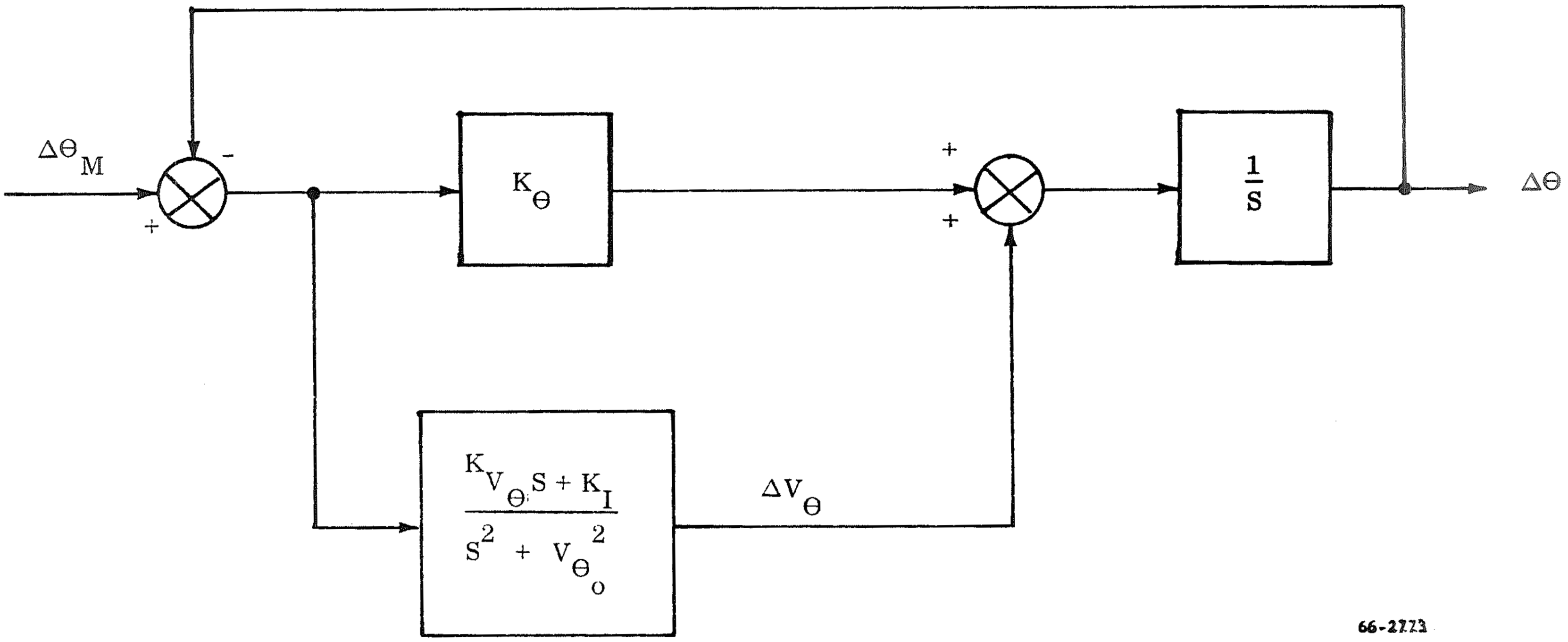
ΔΘ_M
+
-
K_Θ
+
+
1/S
ΔΘ
(K_{VΘ} S + K_I) / (S^2 + V_{Θo}^2)
ΔV_Θ
66-2773

Figure B-5 Linearized ISN Control Loops, Diagram II where the Laplace operator s has been non-dimensionalized by reference orbital frequency, i.e., $p = \frac{s}{V_{\theta_o}}$

This open-loop transfer function gives the pole-zero configuration of Figure B-6.

Equation 3 shows that the compensation zeros are complex and that the root locus gain is $\frac{K_\theta}{V_{\theta_o}}$. The ratio of K_{V_θ}/K_θ specifies the real part of the zeros and the ratio K_I/K_θ controls their natural frequency. The characteristic equation for the system is a cubic whose roots are given by equation (4).

$$p^3 + \frac{K_\theta}{V_{\theta_o}} p^2 + \left(1 + \frac{K_{V_\theta}}{V_{\theta_o}^2}\right) p + \left(\frac{K_\theta}{V_\theta} + \frac{K_I}{V_{\theta_o}^3}\right) = 0 \tag{4}$$

Equation (4) typically yields one real root and a pair of complex conjugate roots, and, correspondingly, the system exhibits a first order mode and a damped oscillatory mode of response.

These techniques and the previously described mathematical relationship of this Appendix were used in mechanizing and evaluating the ISN scheme as discussed in Section IV of this report (SCR 290-I).

B. Linear Optimum Filter Navigation Scheme

The Linear Optimum Filter (LOF) navigation scheme is based upon the equations of motion of a point mass in Cartesian inertial coordinate systems. The equations used in the simulation of the navigation scheme were the standard equations for n-bodies with oblateness terms of the central body included when the vehicle is within the sphere of influence of the Earth or Jupiter.

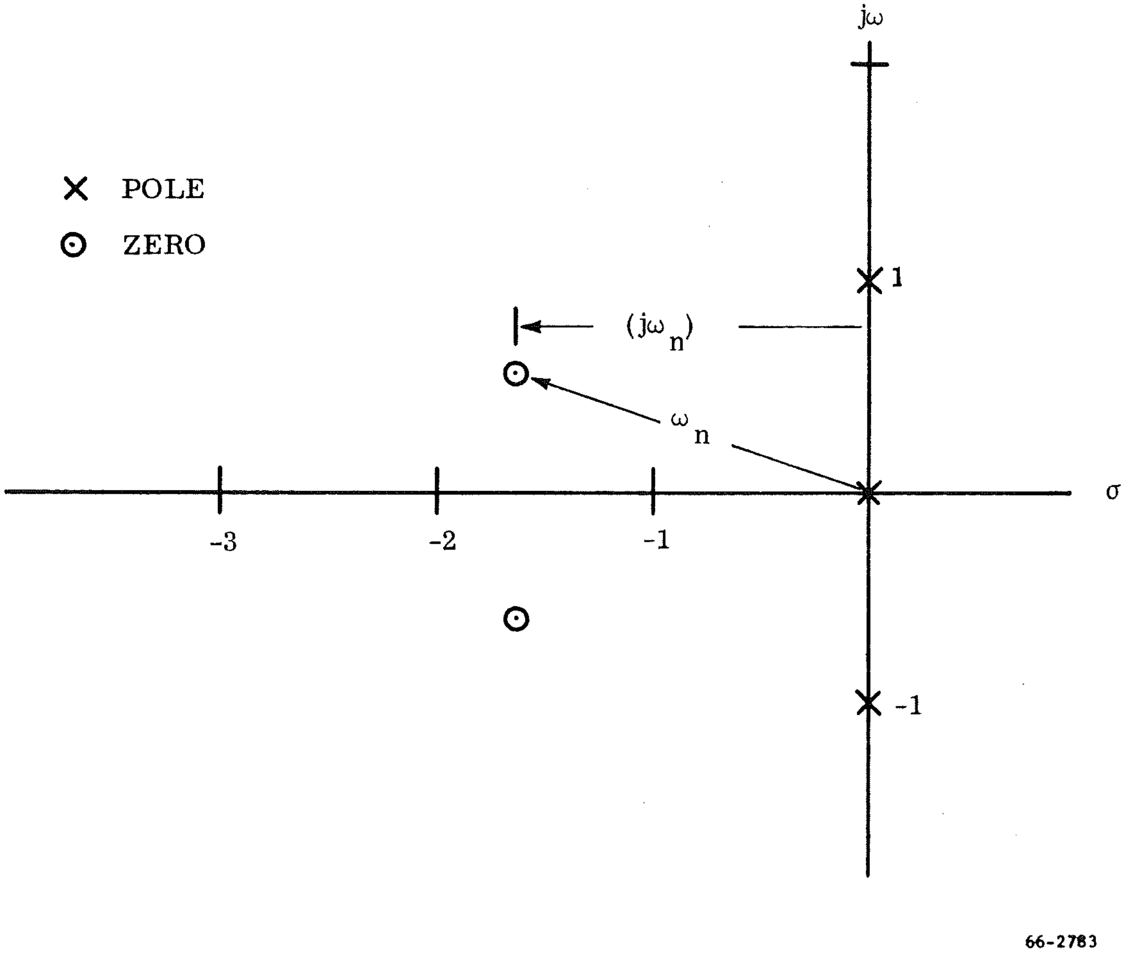
jω
× POLE
⊙ ZERO
1
$(j\omega_n)$
ω_n
σ
-3
-2
-1
-1
66-2783

Figure B-6 Open-Loop Pole-Zero Configuration

The equations of motion are integrated forward to the time of an observation at which time the state vector (the position and velocity) is updated using the following matrix equations

$$X_n = X'_n + K\delta A$$

Where X'_n is the state vector integrated forward from the last observation. δA is the difference between the measured and predicted observation noted by a subscript m and p, respectively. SA = $(\alpha_m - \alpha_p, \delta_m - \delta_p)$ where α and δ are the right ascension and declination in inertial space of the vector from the vehicle to the planet. The equations for α_p and δ_p are as follows

$$\alpha_p = \tan^{-1}\left[\frac{Y_p - Y}{X_p - X}\right]$$

$$\delta_p = \tan^{-1}\left[\frac{Z_p - Z}{\sqrt{(X_p - X)^2 + (Y_p - Y)^2}}\right]$$

where (X_p, Y_p, Z_p) are the coordinates of the planet being observed and (X, Y, Z) are the estimated coordinates of the vehicle. The measured values are obtained from an optical instrument which measures the line of sight of the planet relative to the inertial computational frame.

The weighting factor K is defined as follows:

$$K(t_n) = P(t_n) H^T(t_n) \left[H(t_n) P(t_n) H^T(t_n) + \phi(t_n)\right]^{-1}$$

where P is the covariance matrix of the uncertainty in the state vector, ϕ is the covariance matrix of the observational error, and H is the geometry matrix relating the state vector to the observations. The superscript T indicates the transpose.

The geometry matrix H is as follows:

$$H = \begin{bmatrix} \dfrac{Y_p - Y}{(X_p - X)^2 + (Y_p - Y)^2} & \dfrac{(X_p - X)(Z_p - Z)}{R_p^2 \sqrt{(X_p - X)^2 + (Y_p - Y)^2}} \\ \dfrac{-(X_p - X)}{(X_p - X)^2 + (Y_p - Y)^2} & \dfrac{(Y_p - Y)(Z_p - Z)}{R_p^2 \sqrt{(X_p - X)^2 + (Y_p - Y)^2}} \\ 0 & \dfrac{-\left[(X_p - X)^2 + (Y_p - Y)^2\right]}{R_p^2 \sqrt{(X_p - X)^2 + (Y_p - Y)^2}} \\ 0 & 0 \\ 0 & 0 \\ 0 & 0 \end{bmatrix}$$

where $R_p^2 = (X_p - X)^2 + (Y_p - Y)^2 + (Z_p - Z)^2$

The matrix $P(t_n)$ is the covariance matrix which has been extrapolated forward from the time of the last observation.

$$P(t_n) = \phi(t_n; t_{n-1}) \, P'(t_{n-1}) \, \phi^T(t_n; t_{n-1})$$

where $\phi(t_n, t_{n-1})$ is the transition matrix from the time of the n-1 observation to the time of the nth observation, and $P'(t_{n-1})$ is the covariance matrix updated after the n-1 st observation.

$$P' (t_{n-1}) = P (t_{n-1}) - K (t_{n-1}) H (t_{n-1}) P (t_{n-1})$$

The above mathematical relationships are employed in the mechanization and evaluation of the LOF scheme, as discussed in Section IV of this report (SCR 290-I).

APPENDIX C

GUIDANCE ANALYSIS

APPENDIX C

GUIDANCE ANALYSIS

A. Midcourse Guidance Scheme

The midcourse guidance scheme developed by United Aircraft is similar to current "perturbation" techniques in that both utilize linear theory expansions around a reference trajectory. The major difference in the scheme developed is that the reference trajectory is calculated on board the vehicle only as required; whereas in most current techniques a series of reference trajectories are precalculated on the ground and stored in the flight computers before launch. A mathematical description of the scheme is given below starting with a brief summary of linear theory.

Consider the non-linear equation of motion expressed in the form

$$\ddot{X} = F_1 (X, Y, Z)$$

$$\ddot{Y} = F_2 (X, Y, Z)$$

$$\ddot{Z} = F_3 (X, Y, Z)$$

The non-linear equations of motion may be expanded about a reference trajectory, i.e., a specific set of X(t), Y(t), and Z(t), in a Taylor series. After dropping all terms above first order in the expansion, the following differential equations are obtained.

$$\delta \ddot{X} = \frac{\partial F_1}{\partial X} \delta X + \frac{\partial F_1}{\partial Y} \delta Y + \frac{\partial F_1}{\partial Z} \delta Z$$

$$\delta \ddot{Y} = \frac{\partial F_2}{\partial X} \delta X + \frac{\partial F_2}{\partial Y} \delta Y + \frac{\partial F_2}{\partial Z} \delta Z$$

$$\delta \ddot{Z} = \frac{\partial F_3}{\partial X} \delta X + \frac{\partial F_3}{\partial Y} \delta Y + \frac{\partial F_3}{\partial Z} \delta Z$$

By defining the proper terms, the differential equations can be reduced to a set of first order differential equations

$$X_1 = \delta X \qquad X_4 = \delta \dot{X}$$

$$X_2 = \delta Y \qquad X_5 = \delta \dot{Y}$$

$$X_3 = \delta Z \qquad X_6 = \delta \dot{Z}$$

The equation then becomes (in matrix form)

$$\frac{dX}{dt} = [\,F(t)\,]\; X$$

$$[\,F(t)\,] = \begin{bmatrix} 0 & 0 & 0 & 1 & 0 & 0 \\ 0 & 0 & 0 & 0 & 1 & 0 \\ 0 & 0 & 0 & 0 & 0 & 1 \\ \frac{\partial F_1}{\partial X} & \frac{\partial F_1}{\partial Y} & \frac{\partial F_1}{\partial Z} & 0 & 0 & 0 \\ \frac{\partial F_2}{\partial X} & \frac{\partial F_2}{\partial Y} & \frac{\partial F_2}{\partial Z} & 0 & 0 & 0 \\ \frac{\partial F_3}{\partial X} & \frac{\partial F_3}{\partial Y} & \frac{\partial F_3}{\partial Z} & 0 & 0 & 0 \end{bmatrix}$$

The solutions of the above equation are of the form

$$X\,(t) = \phi\,(t,\ t_o)\; X\,(t_o)$$

where $X(t_o)$ is a vector initial condition at time t_o, $X(t)$ is the vector state at time t, and $\phi(t,\ t_o)$ is the transition matrix which relates the two. It can be seen from the above equation that if an initial condition of unity is put on X_1 at time t_o with all other components of X set to zero, then the time history of X is the first column of the $\phi(t, t_o)$ matrix. This is equivalent to introducing the proper initial conditions into the perturbation equations and integrating numerically. If this is done simultaneously for six sets of perturbation equations, with each set having a unit initial condition on one of the components of X and zero on all the other, all six columns of the transition matrix will be generated.

The midcourse guidance scheme uses the transition matrix in the following fashion. Prior to making a guidance correction, the equations of motion are integrated forward to the time, T, at which it is desired to be at a given point in space. Using this as the reference trajectory the transition matrix is calculated from the time of the guidance correction to time T. The calculated position at time T is compared with the desired position and the resulting X_{1T}, X_{2T}, and X_{3T} are substituted into the following equation

$$X_T = \phi(T, t_o)\, X_{to}$$

With $X_1 = X_2 = X_3 = 0$ the first three equations, of the six represented by the above matrix equation, can be solved for X_4, X_5, and X_6. Applying this velocity correction will result in a deviation from the reference trajectory at time T equal to X_{1T}, X_{2T}, and X_{3T}. The three simulation equations for X_4, X_5, and X_6 are given below.

$$\phi_{41} X_4 + \phi_{51} X_5 + \phi_{61} X_6 = X_{1T}$$

$$\phi_{42} X_4 + \phi_{52} X_5 + \phi_{62} X_6 = X_{2T}$$

$$\phi_{43} X_4 + \phi_{53} X_5 + \phi_{63} X_6 = X_{3T}$$

where ϕ_{ij} are the elements of the transition matrix $\phi(T_1\ t_o)$.

Solving the above equation for X_4, X_5, and X_6 gives

$$X_4 = D_1/D$$

$$X_5 = D_2/D$$

$$X_6 = D_3/D$$

where

$$D = \phi_{41} (\phi_{52} \phi_{63} - \phi_{53} \phi_{62}) + \phi_{42} (\phi_{53} \phi_{61} - \phi_{51} \phi_{63}) + \phi_{43} (\phi_{51} \phi_{62} - \phi_{52} \phi_{61})$$

$$D_1 = X_{1T} (\phi_{52} \phi_{63} - \phi_{53} \phi_{62}) + X_{2T} (\phi_{53} \phi_{61} - \phi_{51} \phi_{63}) + X_{3T} (\phi_{51} \phi_{62} - \phi_{52} \phi_{61})$$

$$D_2 = X_{1T} (\phi_{43} \phi_{62} - \phi_{42} \phi_{63}) + X_{2T} (\phi_{41} \phi_{63} - \phi_{43} \phi_{61}) + X_{3T} (\phi_{42} \phi_{61} - \phi_{41} \phi_{62})$$

$$D_3 = X_{1T} (\phi_{42} \phi_{53} - \phi_{43} \phi_{52}) + X_{2T} (\phi_{43} \phi_{51} - \phi_{41} \phi_{53}) + X_{3T} (\phi_{41} \phi_{52} - \phi_{42} \phi_{51})$$

This process is repeated each time a guidance correction is scheduled.

If the values of X_{1T}, X_{2T}, and X_{3T} are such that the assumptions on which the transition matrix is based are violated then a new reference trajectory is generated using the computed X_4, X_5, and X_6. This calculation is repeated until acceptable values of X_{1T}, X_{2T}, and X_{3T} are obtained. The guidance correction is then made using the accumulated velocity corrections.

B. Simplified Guidance Scheme

It was proposed as a part of the study that an investigation be made of a simple guidance scheme that applied a single correction at the entry into Jupiter's sphere of influence. The following paragraphs delineate the development of the equations for this scheme.

The analysis is based on the assumption that within Jupiter's sphere of influence the problem can be viewed as a two-body problem and that the desired exit velocity relative to the Sun should have a given magnitude, V_a, and be normal to the ecliptic plane. The coordinate system used is Jupiter centered with the X-axis directed toward the Sun, the Z-axis perpendicular to Jupiter's orbital plane, and the Y-axis forming a right-handed system. The exit velocity vector

$$V_e = (-\sin \omega \sin i V_a; V_j - \cos \omega \sin i V_a; \cos i V_a)$$

where V_j is the magnitude of Jupiter's orbital velocity and ω and i are the angle between the position vector of Jupiter and its line of nodes and the angle of inclination, respectively. The trajectory through Jupiter's sphere of influence is symmetrical; therefore the magnitude of the velocity of entry V_i must be equal to the velocity at exit V_e.

Thus: $$V_i = V_j [1 + \bar{\alpha}^2 - 2 \bar{\alpha} \cos \omega \sin i]^{1/2}$$

where $$\bar{\alpha} = V_a/V_j$$

The direction cosines of V_i (λ, μ, ν) must satisfy the following relationship:

$$n_1\lambda + n_2\mu + n_3\nu = 0 \qquad (1)$$

$$l\lambda + m\mu + n\nu = \cos \alpha \qquad (2)$$

$$r_1\lambda + r_2\mu + r_3\nu = -\cos \psi \qquad (3)$$

Where (n_1, n_2, n_3) are the direction cosines of the normal to the transfer plane, (l, m, n) are the direction cosines of the exit velocity vector, and (r_1, r_2, r_3) are the direction cosines of the position vector $\vec{R}$ at the point of entry into Jupiter's sphere of influence. α is the angle between $\vec{V}_i$ and $\vec{V}_e$ and is called the turning angle. ψ is the angle between $\vec{V}_i$ and $-\vec{R}$. Equation (1) represents the condition that V_i must be in the transfer plane. Equations (2) and (3) represent the fact that because of the dynamics of the problem, V_i must make certain angles with the position vector and the exit velocity vector.

Assuming that α and ψ are known, the above equations can be solved for λ, μ, and ν with the following results.

$$\begin{aligned}
\lambda &= \frac{\cos \alpha \, [n_3 r_2 - n_2 r_3] + \cos \psi \, [n_3 m - n_2 n]}{-\sin (\alpha - \psi)} \\
\mu &= \frac{\cos \alpha \, [n_1 r_3 - n_3 r_1] + \cos \psi \, [n_1 n - n_3 l]}{-\sin (\alpha - \psi)} \qquad (4) \\
\nu &= \frac{\cos \alpha \, [n_2 r_1 - n_1 r_2] + \cos \psi \, [n_2 l - n_1 m]}{-\sin (\alpha - \psi)}
\end{aligned}$$

The values of α and ψ are obtained from an iterative solution of the following equations:

$$\sin \psi = \frac{\operatorname{Cot} \frac{\alpha}{2}}{\frac{R}{\bar{\mu}} V_i^2 - 2} \qquad (5)$$

$$\alpha = \psi + \cos^{-1} [\, l\, r_1 + m\, r_2 + n\, r_3 \,] \qquad (6)$$

A value of α is assumed and substituted into equation (5). The resulting ψ is used in equation (6) to compute a new α and the process is repeated until it converges. The initial guess for α should be less than $\pi/2$ when r_2 is negative and greater than $\pi/2$ for r_2 positive. Equation (5) is derived from the properties of a hyperbolic trajectory, $\bar{\mu}$ is Jupiter's gravitational constant. Equation (6) comes from the dot product of the position vector and the exit velocity vector.

The above mathematical relationships were employed in the evaluation of the explicit on-board guidance schemes discussed in Section V of this report (SCR 290-I).